Modelling the heartwood profile of Douglas fir in France based on the stem profile and other tree dendrometric characteristics - insights from experimental sites and commercial log data

Antoine Billard, Frédéric Mothe, François Ningre, Julien Sainte-Marie, Marin Chaumet, Holger Wernsdörfer, Fleur Longuetaud

Modelling the heartwood profile of Douglas fir in France based on the stem profile and other tree dendrometric characteristics – insights from experimental sites and commercial log data

Antoine Billard[a], Frédéric Mothe[b], François Ningre[b], Julien Sainte-Marie[b], Marin Chaumet[c], Holger Wernsdörfer[b], Fleur Longuetaud[b,*]

[a] *Office National des Forêts, Direction Territoriale Seine-Nord, Boulevard de Constance, 77300 Fontainebleau, France*
[b] *SILVA, UMR1434, Université de Lorraine, AgroParisTech, INRAE, F-54000 Nancy, France*
[c] *FCBA, Pôle Biotechnologie Sylviculture Avancée, Equipe Sylviculture Avancée, Les Vaseix, 87430 Verneuil sur Vienne, France*

*Corresponding author
Email addresses: antoine.billard@onf.fr (Antoine Billard), frederic.mothe@ik.me (Frédéric Mothe), francois.ningre@inrae.fr (François Ningre), julien.sainte-marie@agroparistech.fr (Julien Sainte-Marie), marin.chaumet@fcba.fr (Marin Chaumet), holger.wernsdorfer@agroparistech.fr (Holger Wernsdörfer), fleur.longuetaud@inrae.fr (Fleur Longuetaud)

Abstract

Douglas fir (*Pseudotsuga menziesii* (Mirb.) Franco) is a softwood species that is becoming increasingly important in Europe. To improve the quality of products for certain specific outdoor uses, there is an interest in limiting the amount of sapwood, the non-durable part, and in enhancing the amount of heartwood.

The aim of this work was to develop a model of heartwood distribution in Douglas fir stems, taking tree dendrometric characteristics and silviculture into account. Several statistical models of varying complexity were developed, using sampling data from silvicultural experiments in France. Cross-validation and validation on an independent dataset of commercial logs demonstrated the good performance of the models.

Stem size at any height in the tree was the major predictor of the longitudinal heartwood profile. The other dendrometric characteristics of the trees had only minor effects, suggesting limited silvicultural control of heartwood formation.

Nevertheless, plausible model behaviour and interesting insights were found for two contrasting silvicultural scenarios, using a growth simulator. A more complete simulation study including additional wood quality criteria should be performed, in order to provide recommendations to forestry practice.

Keywords

Pseudotsuga menziesii; wood quality; longitudinal distribution; pipe model; sapwood; growth simulations

1. Introduction

Originating from North America, Douglas fir (*Pseudotsuga menziesii* (Mirb.) Franco) is a species that is becoming increasingly important in Europe, covering more than 800 000 hectares (Spiecker et al., 2019). Douglas fir has high productivity, desirable wood properties and is an interesting option for the future because it is less sensitive to drought than spruce (Nicolescu et al., 2023).

In France, it is the main species found in 440 000 hectares of forest, mainly in private forests. It became a major species after a massive planting in the second half of the 20^{th} century, given that the area planted with Douglas fir was estimated at only 4 000 hectares in 1937 (Sornay, 1937). France has even become Europe's leading producer of Douglas fir with 138 million cubic meters of standing volume, i.e. 5% of the total standing volume of French forests (IGN, 2023), and a high volume yield of 14.1 m^3/ha/year[1]. Every year, 4.4 million m^3 of Douglas fir are harvested[1].

Its very good mechanical properties (Zeidler et al., 2022) and the natural durability of its heartwood (Blohm et al., 2014; Humar et al., 2022) make the wood of Douglas fir suitable for construction or outdoor uses. Moreover, compared with other softwoods, Douglas fir also has a slower moisture regain rate when humidity conditions vary frequently, which may also explain its good durability (Pollet et al., 2018). In contrast, its sapwood is not naturally durable due to the low amount of extractives (Donaldson et al., 2019). On the other hand, if the wood is to be chemically treated, sapwood may be preferable, as it is more impregnable (Osborne, 2015). Therefore, the amount of sapwood, and its distribution within the stem, can strongly influence the choice of the sawing pattern and the material yield, depending on the type of products desired.

The amount and distribution of heartwood and sapwood in stems of Douglas fir are thus important criteria to guide silvicultural choices. Respective models should rely on dendrometric tree characteristics that can vary according to silvicultural scenarios applied in the field or generated using growth and yield simulators. Furthermore, the models should be in accordance with functional and theoretical knowledge.

From a functional point of view, sapwood is the newly formed xylem through which raw sap flows to transport water and minerals from roots to leaves. In the sapwood, the

[1]Portail OCRE - IFN (inventaires 2018-2022) `https://ocre-gp.ign.fr/ocre/`

specific conductivity decreases from the cambium to the heartwood boundary (Spicer and Gartner, 2001), until it stops completely and the cells die. At the same time, the chemical composition of the cell walls changes and sapwood turns into heartwood. For some species, like Douglas fir, this chemical change results in a colour change that makes the heartwood clearly visible. This coloured heartwood is more resistant to fungal and insect attacks due to the presence of extractives (Taylor et al., 2002). The time necessary to convert sapwood to heartwood depends strongly on the species (Hillis, 1987). For Douglas fir the change seems to begin at a cambial age of 8-9 years (Cardoso and Pereira, 2017).

The *pipe model* theory proposed by Shinozaki et al. (1964) may partly explain the amount and distribution of sapwood. It suggests that within the stem, the active area of the pipes (water columns) is proportional to the leaf area above that height. Based on this and an additional "branch thinning" theory, Aye et al. (2022) have recently proposed a process-based model of sapwood and heartwood profiles. Moreover, the pipe model has been widely used in process-based forest modelling. However, its general validity may be questioned (Lehnebach et al., 2018).

Nevertheless, from available theory, we would expect the amount of sapwood to increase with live-crown size, and the area of sapwood in the stem to be relatively constant between the crown base and the stem base at ground level. In turn, crown size depends on growing space as controlled through silviculture. Overall, this seems to be in accordance with literature results for Douglas fir. They suggest that the amount of sapwood increases as tree vitality, foliar mass or leaf area increase. Conversely, the amount of sapwood decreases as stand density increases. In particular, the (mostly interrelated) factors that influence the amount of sapwood or heartwood in Douglas fir are: tree age, height and diameter at breast height (D_{BH}) (McDowell et al., 2002; Chaumet, 2020a), tree vitality and health status (Maguire and Kanaskie, 2002; Weiskittel et al., 2006), the amount of foliage (Granier, 1981; Long et al., 1981), and genetics (Chaumet, 2020a).

Some of these factors are used in existing models to predict the amount of sapwood at 1.30 m of stem height (in terms of area, width or number of rings) (Grier and Waring, 1974; Kendall Snell and Brown, 1978; Waring et al., 1982; Weiskittel et al., 2006). However, few models of the longitudinal heartwood/sapwood distribution are available

in the literature for Douglas fir (Maguire and Batista, 1996; Osborne, 2015; Chaumet, 2020b). Particular attention has been paid to the latter type of models in this study, as it enables the entire commercial part of the stem to be characterised. The existing models are described in details and analysed in Section 2.4 and Appendix A1.

The overall objective of this work was to quantify the relationships between dendrometric variables and heartwood amount and distribution to propose a predictive statistical model for Douglas fir in France. According to the literature and our initial observations, the heartwood profile is relatively parallel to that of the stem under bark and its amount is highly correlated with the diameter of the stem (Cardoso and Pereira, 2017; Chaumet, 2020a). For this reason, in our approach we have chosen to model the amount of heartwood at a given height (rather than the sapwood), with the size of the cross-section at that height as the main driver. Dendrometric variables were modulated in particular by the stage of stand or tree development and stand density in our study. The specific objectives were:

- To evaluate the suitability of models from literature Maguire and Batista (1996), Maguire (2014) and Chaumet (2020b) based on data from experimental sites in France;
- To develop new models and evaluate their performance through comparison with literature models, cross-validation, and validation using an independent dataset;
- To evaluate the best-performing model for its sensitivity to silvicultural scenarios of contrasting stand densities, based on a growth and yield simulator.

Our analysis was guided by the following research questions:

- What is the heartwood/sapwood distribution in stems of Douglas fir? In particular, is the sapwood area relatively constant along the stem below the crown base, as suggested by the *pipe model* theory?
- What are the relationships between dendrometric variables and the amount of heartwood, and its distribution in stems of Douglas fir?
- What is the influence of stand density, as controlled through silviculture, on the quality of Douglas fir stems in terms of the proportion of heartwood and sapwood?

2. Materials and Methods

The abbreviations and units of the variables are summarised in the Appendix A2.

2.1. Calibration dataset

2.1.1. Study sites and sampling design

Eighty-six Douglas fir trees were sampled in four experimental sites in France: **Écouves**, **Grison**, **Quartier** and **Mélagues** (Table 1). The **Écouves** site was sampled twice (in 2010 and 2021), **Grison** and **Quartier** in 2014, and **Mélagues** in 2017. These experimental sites are part of two networks of silvicultural trials on Douglas fir in even-aged stands, one monitored by the French National Forestry Office (ONF) and the other belonging to the French data cooperative on forest growth known as "GIS Coop" (Bédéneau et al., 2001; Seynave et al., 2018). The aim of these experimental trials is to compare different and contrasting silvicultural scenarios (initial densities and thinning intensities). The selected sites for this study were all pure even-aged Douglas fir plantations aged between 23 and 74 years. In each site, we selected two or three experimental plots with various dynamics of stand density (Table 2), including a control (i.e., no silvicultural intervention). In each modality, 4 to 9 trees distributed across the entire diameter range were sampled to represent the different social statuses (Appendix A3). The most recent thinning was carried out 4 to 15 years before each sampling. The dominant heights (H_0) indicated that all the sites were located in stands of medium fertility for Douglas fir, i.e., $H_0 = 33$ m at 50 years (Angelier 2006). The sampling covered a wide range of initial planting densities from 2375 stems/ha to 341 stems/ha and diameters at breast height from 8 to 72 cm. A wide range of Relative Density Index (RDI) was also represented with values starting from 0.3 at the sampling selection date, where RDI is the ratio between the density per ha of a given stand with an average diameter D_g to the maximum theoretical density that a stand could hold with the same D_g (Reineke, 1933; Ningre et al., 2016). Overall, the sampled sites were representative of current and past silvicultural practices of Douglas fir plantations in France as well as in Europe (Nicolescu et al., 2023).

Table 1: Characteristics of the sites from the calibration dataset.

Site	Location	Altitude (m)	Installation date	Sampling date	Date of last thinning	Age of trees
Écouves_2010	48.510 N, 0.080 E	300	1965	2010	2000	63
Écouves_2021				2021	2010	74
Grison	46.492 N, 4.755 E	210	1991	2014	1999	44
Quartier	46.149 N, 2.767 E	630	1994	2014	2010	23
Mélagues	43.713 N, 3.058 E	800	1988	2017	2002	50

Table 2: Characteristics of the experimental plots from the calibration dataset at sampling date. All dendrometric variables are calculated on living trees before thinning when thinning occurs the year of sampling.

Site	Density treatment	Initial & final densities (tree.ha^{-1})		Thinning intensity	RDI ratio of last thinning	Basal area (m^2.ha^{-1})	Dominant height (m)	Dominant diameter (m)	Final RDI	Spacing factor	Number of sampled trees	DBH range of sampled trees (cm)	Plot area (ha)
Écouves_2010	high	2083	855	none	1	88.65	39.8	0.54	1.153	9.2	9	23-47	0.12
	medium	2083	433	moderate	0.84	70.68	41.3	0.57	0.812	12.5	9	24-52	
	low	2083	285	heavy	0.79	65.03	41.3	0.63	0.682	15.4	9	25-48	
Écouves_2021	high	2083	666	none	1	94.25	45.5	0.60	1.125	9.2	9	22-57	0.12
	medium	2083	197	moderate	0.75	63.43	46.5	0.71	0.607	16.5	6	43-62	
	low	2083	168	heavy	1	66.81	46.9	0.76	0.604	17.6	6	51-72	
Grison	high	1460	1045	none	0.92(*)	67.60	30.7	0.41	0.997	10.8	5	15-31	0.22
	medium	1200	446	moderate	0.68	45.50	28.7	0.44	0.592	17.7	5	23-41	0.22
	low	1110	167	heavy	0.7	31.90	29.2	0.53	0.351	28.5	5	32-44	0.21
Quartier	high	2375	2117	none	1	33.38	15.9	0.22	0.720	14.7	5	8-18	0.13
	medium	1071	494	moderate	0.56	16.43	16.0	0.26	0.290	30.2	5	12-23	0.17
	low	341	341	none	1	18.64	16.1	0.32	0.288	36.1	5	16-30	0.19
Mélagues	high	1119	733	none	1	73.55	36.5	0.49	0.963	10.9	4	21-43	0.11
	low	946	141	heavy	0.65	38.00	32.0	0.62	0.381	28.2	4	43-64	0.16

(*) RDI decrease due to windfalls in 1999

2.1.2. Field measurements

For each sampled tree, the following measurements were collected in the field: The circumference at breast height (used to calculate D_{BH}), the height of the lowest living whorl (with at least 3/4 of the branches being alive) assumed to correspond to the base of the living crown (H_{LC}) and the total tree height (H).

2.1.3. Calculating tree and stand variables

We used the monitoring measurements regularly carried out on all these experimental sites since their installation (Table 1) (i.e., circumference measurements for all trees and total height measurements for a sub-sample of trees) to calculate several stand-level variables that were tested as model inputs. These variables were calculated at the time

of sampling on living trees and before thinning if any. These were: basal area (G), H_0 (average height of the 100 largest trees in diameter per hectare), D_0 (quadratic mean of diameters for the 100 largest trees in diameter per hectare), RDI (see definition above), and the Spacing Factor (SF) of Hart-Becking (ratio of average distance between trees to dominant height). We also introduced a variable to characterize the intensity of the last thinning (RDI_{ratio}), calculated at that time as the ratio between the RDI after and the RDI before the thinning. RDI ratio values of 1 can be observed in low density plots, which generally involve heavy thinning or low planting density. This was the case at **Écouves_2021**, where the final density was already reached at the previous thinning at the age of 63, or at **Quartier**, where the plantation density was very low from the outset and did not require thinning. In addition to the stand data we calculated for each sampled tree its social status as the ratio of D_{BH} to D_0 and its slenderness (measure of stability and level of competition) as the ratio of H to D_{BH}

Finally, the candidate variables at tree level tested to build the models were : H, H_{LC}, L_{LC}, L_{LC}/H, D_{BH}, H/D_{BH}, age, RW, RW_5 and D_{BH}/D_0.

And the candidate variables at stand level tested to build the models were as follows: G, H_0, C_0, SF, RDI, RDI_{ratio} and final stand density.

2.1.4. Optical measurements at the laboratory

According to the protocol used during the sampling campaign, 11 to 15 wood discs were sampled at regular intervals along the stem of each tree, including one disc immediately below the base of the living crown and three other discs at three fixed heights: 0.3 m, 0.8 m and 1.3 m. For the two last campaigns, 15 discs per tree were sampled with three discs positioned at fixed heights at the bottom of the stem and the other 12 evenly distributed above.

Annual ring widths were measured along four orthogonal radii on each disc in the fresh state. For a given annual ring, its average width was calculated as the difference between the root mean square of its four outer radii and its four inner radii. For each tree, the following variables were calculated from breast height measurements only: The average ring width (RW) and the average width of the last five rings (RW_5) at the sampling date.

The radii of the disc (under-bark) and of the heartwood were also measured along the

four orthogonal radii on all the discs taken from a tree. The heartwood was delineated here based on the colour change observed between the coloured heartwood and the lighter sapwood. Measurements of heartwood radius were performed in the fresh state except for **Grison** and **Quartier**, which were measured in the air-dry state. In the latter cases, heartwood radius in the fresh state was estimated by multiplying the measured radius by the ratio between fresh and dry under-bark disc radii. We assume here that the shrinkage is radially homogeneous. This constitutes a source of error, but in our view it is largely acceptable. For each disc, the average radii of the disc under-bark (R_{UB}) and of the heartwood (R_{HW}) were calculated as the root mean square of the four respective radii.

Stem profiles including the distribution of heartwood and sapwood are given for each tree in the sample in the Appendix A4.

2.2. Validation dataset

The **TreeTrace_Douglas** dataset (`https://doi.org/10.15454/YUNEGL`) was used to validate the models. This dataset includes measurements on 52 butt logs (approximately 12.5 m long) from 52 Douglas fir stems at four unidentified sites, named A, B, C and D, in the Bourgogne-Franche-Comté Region of France (Longuetaud et al., 2022). The average number of growth rings counted at the base of the butt logs (used to approximate the age of the trees) was 52, 53, 52 and 58 for sites A, B, C and D, respectively. Each butt log was cut into three shorter logs (approximately four metres long) allowing four discs to be sampled per tree, located between the shorter logs and at both ends of the butt log, i.e. 208 discs in total. Optical measurements of ring widths, heartwood radius and under-bark disc radius were made on each disc along four orthogonal radii in the same manner as for the calibration dataset.

As the logs were sampled from a sawmill log yard, tree related data, in particular diameter at breast height and tree height, were not measured. Breast height position along the butt logs was estimated assuming that the bottom of the logs was 30 cm above ground level. D_{BH} was therefore estimated by linear interpolation of the diameters of the two lowest discs located approximately at 0.3 m and 4.5 m. This is a potential source of error, but even when measurements are taken on standing trees, the accuracy of the diameter measurement at 1.30 m is not guaranteed and errors are always possible. D_{BH} distribution is shown in Appendix A5. The ratio of H to D_{BH} (*slenderness*) was

estimated from the slenderness measured over the first 12 metres of the log by fitting a linear regression on the calibration dataset (see details in Appendix A6) and by using the fit to predict *slenderness* on the validation dataset. The other variables, especially crown variables, could not be estimated for this data set. Appendix A7 shows how these four sites compare with those in the calibration set (Section 2.1) and also with the simulations (Section 2.3).

2.3. Use of the model to predict the quantity of heartwood at the output of a growth simulator

2.3.1. The growth simulator used: SimCoP

The simulations were carried out using the SimCoP simulator, initially developed by Ottorini (1991, 1995) to evaluate and define silvicultural scenarios (initial density, thinning, pruning) for pure and even-aged Douglas fir stands. SimCoP is a distance-dependent tree model whose construction principles are inspired by the work of Mitchell (1975a,b). Since 2011, SimCoP has been implemented in the Capsis forest growth simulation platform (Dufour-Kowalski et al., 2012).

At the start of the growth process (SimCoP always starts at the seed stage), each tree is assigned a height growth potential, the value of which depends on site fertility and is modified by crown competition. Each tree thus has its own vigour (ratio between the height of the tree and the dominant height of the stand) derived from a normal distribution. Growth in height determines the lateral expansion of the crown, with the constraint that the crowns of neighbouring trees do not interpenetrate. The resulting dimensions of the crown, in particular the effective foliar volume depicting photosynthetic efficiency and needle retention, are then used to assess the increase in bole volume. Finally, this increase is distributed along the bole in such a manner as to ensure that the annual ring area follows Pressler's law (Lehnebach et al., 2018). In comparison with empirical growth and yield models, SimCoP can be considered as a semi-functional model due to its biologically explicit representation of tree development and growth. We therefore expect that SimCoP can be used to evaluate a wide range of silvicultural scenarios reflecting various growth conditions.

SimCoP has different sources of randomness: Initial seed vigour, the mortality model (selection of trees to be removed) (Ningre et al., 2016) and the thinning algorithm (se-

lection of trees to thin). Thus, for a given silvicultural scenario, 50 simulation runs were performed to take account of the stochasticity of the model and the resulting variability of the model outputs.

The thinning algorithm is based on a fraction of trees to be harvested, by diameter class of the simulated distribution. These fractions change for each thinning operation. In accordance with current silvicultural practices (Nicolescu et al., 2023), the algorithm results in thinning being carried out mainly from above, especially the first ones.

The SimCoP simulator can be used to build trees with a known growth history. The stacking of growth rings is available, as well as the final shape acquired by the stem over time (taper). The characteristics of the crown are also known. It was therefore possible to reconstruct the variables to be used as inputs to our heartwood models.

2.3.2. Case studies

We tested two contrasted silvicultural scenarios: One without intervention to maximise competition between trees with only natural mortality and one with heavy thinning. We chose an initial planting density of 1111 stems/ha (3 m $\times$ 3 m grid), well representative of current planting densities in France. The scenario with heavy thinning is based on a decrease in the number of stems, as proposed in the Douglas fir silviculture guide (Sardin, 2013). It corresponds to a target RDI around 0.45, which means that the stand is approximately maintained at 45% of their maximum stem density. Furthermore, the thinning algorithm implemented leads to G and RDI dynamics that are fully consistent with the simulations proposed by the French National Forest Office (ONF) for Douglas fir silviculture in France (Fournier et al., 2022). A common rotation period of 55 years was set for the final cut.

The dominant height growth, which drives tree and stand growth, corresponds to the second-class fertility curve (33 m at 50 years according to Angelier (2006)). For the heavy thinning scenario, five thinning operations were carried out during the rotation period. For SimCoP simulations we set a plot size of 60 m $\times$ 60 m. The density per hectare at the final cut at 55 years was 219 for the heavy thinning scenario and 823 for the scenario without intervention. Further information on the simulation of the two scenarios can be found in the Appendix A8. In terms of initial and final densities, the two scenarios with and without interventions were quite close to **Mélagues** stands with low and high final

densities, respectively. D_{BH} distribution for each scenario is shown in Appendix A5.

2.4. Statistical modelling

Statistical analyses and modelling were carried out with R software (R Core Team, 2021) using mainly packages `stats`, `nlme` (Pinheiro and Bates, 2000; Pinheiro et al., 2017) and `minpack.lm` (Elzhov et al., 2016). The `lm` function was used to fit linear regressions and study slopes when testing the *pipe-model* theory. The `nlme` function was used to fit the mixed models. The `pairs` function was used to visualize the relationships between parameters and candidate variables.

2.4.1. Models from the literature

The model of Maguire and Batista (1996) allows to predict sapwood area at a given height h in the stem. It is described in Appendix A1.1. Firstly, the sapwood area at breast height is predicted as a function of D_{BH}, H and L_{LC}/H. Secondly, the sapwood area profile along the stem is modelled from the sapwood area at breast height using a variable exponent model as proposed by Kozak (1988). The exponent of this model depends on h/H, H, L_{LC}, D_{BH}/H and L_{LC}/H. In our implementation, heartwood radius was therefore obtained through sapwood area and R_{UB}.

The model of Maguire (2014) allows to predict heartwood diameter at a given height h in the stem from D_{BH}, H, L_{LC}, D_{BH}/H and L_{LC}/H. It is described in Appendix A1.2.

Chaumet (2020b) has proposed two models to predict the rate of heartwood on the radius or diameter of the cross-section (Appendix A1.3). The first takes the age of the tree as input as well as the ratio between the diameter of the cross-section and the D_{BH} in the form of a polynomial of degree 3. The second does not take the age as input to the model, but the ratio between the diameter of the section and the D_{BH} in the form of a polynomial of degree 3 (as in the model with age) and H/D_{BH} as well as the under-bark diameter of the cross-section (i.e., $2 \times R_{UB}$).

2.4.2. New modelling approach

At first approach, Fig. 1 shows an excellent correlation between R_{HW} and R_{UB}, whatever the height in the stem. A simple linear regression explained 98% of R_{HW}

variability and that is the reason why we have chosen to build our model based on this relationship.

When analysed in more detail, tree by tree, the variation of R_{HW} with R_{UB} was similar to a growth curve with a horizontal segment starting at 0 until heartwood appears, then an almost linear portion, and finally an inflection for the larger discs (Appendix A9). After testing several equations from growth models (Zeide, 1993), a segmented model starting with a horizontal segment followed by a Chapman-Richards growth function was used to model this relationship (Equation (1)):

$$R_{HW} = \begin{cases} 0 & \text{if } R_{UB} \leq R_0 \\ a\left(1 - e^{(-b(R_{UB} - R_0))}\right)^c & \text{if } R_{UB} > R_0 \end{cases} \qquad (1)$$
$$R_0 = e^s$$

where a, b, c and s are model parameters to be fitted.

For the smallest cross-sections of the stem, there is no heartwood, then from a certain diameter in the stem, the heartwood appears. This threshold is modelled by R_0 which represents here the radius of the stem cross-section (R_{UB}) from which the heartwood appears and which must be strictly positive. We set $R_0 = e^s$ to guarantee this condition.

Then, to build the model and test the effect of other variables, we followed the approach proposed by Pinheiro and Bates (2006): We started with a mixed-effect model with no explanatory variable other than R_{UB}, and we used plots of the estimated tree random effects versus the candidate tree or stand variables to identify the relationships of interest to be modelled. The model was thus built step by step by modelling one by one some parameters (starting with a, b, c and s) according to the candidate variables. This step-by-step procedure resulted in Models (A) to (D) (detailed below), ranging from the least complex to the most complex (i.e., containing the largest number of explanatory variables). The Akaike Information Criterion (AIC) was used to select the best model at each step of the process. The step-by-step construction of the model is illustrated in Appendix A10. Analyses of residuals were also performed to help selecting the relevant variables.

To avoid convergence problems due to too many parameters to adjust, a diagonal

positive-definite matrix was used by specifying `pdDiag` in the nlme function. To build the model, the calibration dataset containing 1241 observations from 86 sample trees was used.

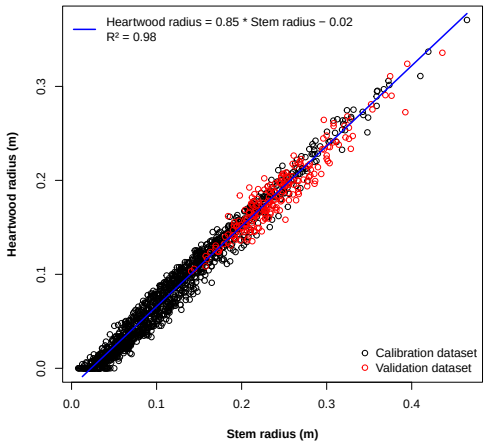

Figure 1: Average heartwood radius (R_{HW}) as a function of the average under-bark stem radius (R_{UB}). On the plot there are several points per tree representing the different measurement heights along the stem.

Model (A). Parameters a and b were found to vary clearly with D_{BH}, but not in the same way, allowing to propose the following equations in addition to Equation (1) as Model (A):

$$\begin{aligned} a &= a_1 + D_{BH}^{a_2} \\ b &= b_1 + b_2 \cdot D_{BH} \end{aligned} \tag{A}$$

where a_1, a_2, b_1, b_2, c and s are model parameters.

Model (B). By fitting mixed models with tree random effects on the parameters of Model (A), a better estimate of a could be obtained by using RW_5 in addition to D_{BH}, leading to the following equations in addition to Equation (1) as Model (B):

$$\begin{aligned} a &= a_1 + D_{BH}^{a_2} + a_3 \cdot RW_5 \\ b &= b_1 + b_2 \cdot D_{BH} \end{aligned} \tag{B}$$

where a_1, a_2, a_3, b_1, b_2, c and s are model parameters.

The use of RW instead of RW_5 gave about the same results.

Model (C). By fitting mixed models with tree random effects on the parameters of Model (B), parameter c appeared to depend on the ratio of H to D_{BH}, leading to the following equations in addition to Equation (1) as Model (C):

$$\begin{aligned} a &= a_1 + D_{BH}^{a_2} + a_3 \cdot RW_5 \\ b &= b_1 + b_2 \cdot D_{BH} \\ c &= c_1 + c_2 \cdot H/D_{BH} \end{aligned} \tag{C}$$

where a_1, a_2, a_3, b_1, b_2, c_1, c_2 and s are model parameters.

This model, which takes three tree-level variables as input, has been implemented in the SimCoP growth simulator.

Model (D). Finally, parameter s was found to vary in relation with the length of the living crown (L_{LC}), leading to the following equations in addition to Equation (1) as Model (D):

$$\begin{aligned} a &= a_1 + D_{BH}^{a_2} + a_3 \cdot RW_5 \\ b &= b_1 + b_2 \cdot D_{BH} \\ c &= c_1 + c_2 \cdot H/D_{BH} \\ s &= s_1 + s_2 \cdot L_{LC} \end{aligned} \tag{D}$$

where a_1, a_2, a_3, b_1, b_2, c_1, c_2, s_1 and s_2 are model parameters.

3. Results

3.1. Validity of the pipe-model theory on our data

Variations in sapwood area and width between 1.30 m and the base of the crown were studied. Linear regressions were fitted of sapwood area and then sapwood width as a function of height in the stem (keeping only measurements in this part of the stem). There was therefore one slope value and its associated p-value per tree. The slopes obtained are shown in Appendix A11 in boxplots by site and density treatment. The slopes for the sapwood area varied between about -35.8 and -0.2 cm^2/m. The slopes for

the sapwood width varied between about -0.3 and 0.2 cm/m and remained around 0, with no clear tendency to be positive or negative. For sapwood area, 84.5% of the trees had a negative slope significantly different from 0, while for sapwood width, only 13.1% of the trees had a slope significantly different from 0, four being negative and seven being positive (for two young trees the p-values could not be calculated because the number of observations between 1.30 m and the base of the crown was too low). On average, for the trees in the calibration dataset, the area of sapwood decreased by 49% between 1.30 m and the base of the crown. Hence, the sapwood area was not constant under the crown, but the sapwood width was much more stable.

3.2. Models from the literature

The model of Maguire and Batista (1996) with 9 parameters fitted on our calibration dataset (by 10-fold cross-validations; Section 3.4) performed well with an average RMSE of 10 mm and an average relative RMSE of 12.2% (Table 3).

The model of Maguire (2014) with 10 parameters gave slightly poorer results on our data with an average RMSE of 11 mm and a average relative RMSE of 13.5% (Table 3).

3.3. Adjustment of new models

Analysis of our data showed that the heartwood radius at a given height essentially depended on the stem radius at that same height (Fig. 1). The radius or diameter of the stem was therefore the most important factor to take into account to correctly predict the amount of heartwood at any height in the tree. This was followed by D_{BH}, RW_5, H/D_{BH} and L_{LC} as the model became more complex.

The five models of increasing complexity (Equation (1), Models (A) to (D)) were fitted to the calibration dataset. The AIC, which was the criterion used to select the variables and models, is given in Table 4. The parameters of the models are also given in Table 4.

According to the linear regression of Fig. 1, the heartwood began to appear when the stem reached a diameter under bark of 4.6 cm on average. From the fitted models, the diameter at which the heartwood appeared (calculated from the estimated value of R_0) varied from 1.8 to 5.1 cm, depending on the model (Equation (1) to Model (C)). In

Model (D), the parameter regulating this diameter varied according to L_{LC} (the larger L_{LC} is, the larger the diameter of the section at which the heartwood appears is).

Depending on the model, heartwood begins to appear when the under-bark diameter of the stem reaches around 1.8 to 2.7 cm (values obtained for Models (A) and (C), respectively, from the parameter s and Equation (1) ; Table 4). Model (D) shows that the value at which heartwood begins to appear increases with the length of the living crown.

3.4. Cross-validation

The average of the results of 1000 10-fold cross-validations was used to evaluate and compare the proposed models with each other (Table 3). The RMSE for predicting R_{HW} varied from 10.2 mm to 6.4 mm depending on the complexity of the model, corresponding to relative RMSE between 12.27 and 7.70 %. We observe a clear reduction in RMSE for the **Quartier** and **Mélagues** sites with the addition of the variable RW_5 in Model (B) (Fig. 2). Then, by further increasing the number of parameters, the gain in RMSE was relatively small.

Table 3: Comparison of the different models by 10-fold cross-validations on the calibration dataset. The values in the table are averages obtained from 1000 cross-validations.

Model	p	RMSE (m)	Relative RMSE (%)	Bias (m)	R^2
Maguire and Batista (1996)	9	1.0049e-02	12.21	1.7483e-04	0.98
Maguire (2014) in Osborne (2015)	10	1.1214e-02	13.52	-3.9849e-04	0.97
Chaumet (2020b) with age	6	6.9309e-03	8.36	1.6924e-04	0.99
Chaumet (2020b) without age	7	7.6190e-03	9.19	5.9601e-04	0.99
Equation (1)	4	1.0179e-02	12.27	-1.2517e-04	0.98
(A)	6	8.8231e-03	10.64	4.1320e-05	0.98
(B)	7	7.1201e-03	8.59	5.7839e-05	0.99
(C)	8	6.8019e-03	8.20	1.3800e-06	0.99
(D)	9	6.3882e-03	7.70	-1.3066e-04	0.99

3.5. Validation on an independent dataset

Equation (1) and Models (A), (B) and (C) were applied to the 208 observations from the 52 trees of the validation dataset **TreeTrace_Douglas** (Fig. 3 and Appendix A12).

Table 4: Estimated parameters and their standard deviation in brackets for the total calibration dataset ($n = 1241$). p is the number of parameters. The AIC and RMSE are also given.

Model	p	a or $a1$	$a2$	$a3$	b or $b1$	$b2$	c or $c1$	$c2$	s or $s1$	$s2$	AIC	RMSE (m)
Equation (1)	4	1.3704e+00	–	–	7.6826e-01	–	1.0538e+00	–	-3.6702e+00	–	-7895.65	1.00e-02
		(4.4239e-01)	–	–	(3.0940e-01)	–	(4.0350e-02)	–	(6.7626e-02)	–		
(A)	6	2.5261e-01	3.2880e+00	–	1.0652e+01	-9.8774e+00	2.0542e+00	–	-4.6989e+00	–	-8272.885	8.59e-03
		(1.1825e-02)	(6.0060e-02)	–	(6.8626e-01)	(7.3918e-01)	(9.4744e-02)	–	(2.0576e-01)	–		
(B)	7	2.7436e-01	3.0276e+00	-1.4572e+01	1.0745e+01	-1.0044e+01	2.0487e+00	–	-4.6689e+00	–	-8843.71	6.82e-03
		(1.0044e-02)	(4.2542e-02)	(7.2523e-01)	(5.4235e-01)	(5.8800e-01)	(7.3738e-02)	–	(1.5638e-01)	–		
(C)	8	2.5880e-01	2.9777e+00	-9.3168e+00	1.0417e+01	-9.6691e+00	2.2180e+00	-3.2765e-03	-4.3156e+00	–	-8953.942	6.51e-03
		(9.0526e-03)	(4.1165e-02)	(7.6384e-01)	(5.1718e-01)	(5.5956e-01)	(7.7879e-02)	(3.2458e-04)	(9.9501e-02)	–		
(D)	9	2.7698e-01	2.7653e+00	-8.7760e+00	8.4150e+00	-7.7407e+00	1.7279e+00	-1.8914e-03	-4.2977e+00	4.5625e-02	-9130.068	6.06e-03
		(1.1775e-02)	(4.5886e-02)	(8.1018e-01)	(5.4183e-01)	(5.8225e-01)	(6.1717e-02)	(2.3990e-04)	(7.3349e-02)	(3.0613e-03)		

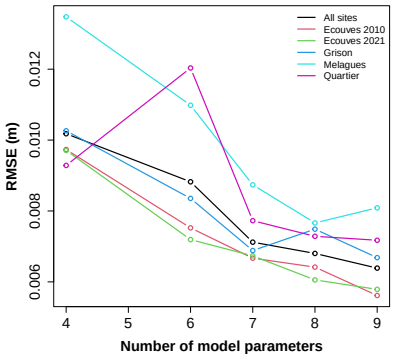

Figure 2: Evolution of the RMSE of R_{HW} as a function of the number of model parameters. The values presented are those obtained by 1000 10-fold cross-validations on the calibration dataset. The 4-parameter model corresponds to Equation (1). The 6-, 7-, 8- and 9-parameter models were obtained when adding the variables D_{BH} (Model (A)), RW_5 (Model (B)), H/D_{BH} (Model (C)) and L_{LC} (Model (D)), respectively.

Model (D) could not be tested because it required tree crown length (L_{LC}), which was not available in our validation dataset. Equation (1) and Models (A), (B) and (C) gave equivalent results (Table 5), meaning that using D_{BH}, RW_5 or H/D_{BH} did not improve the predictions for this dataset and did not degrade them much either. The RMSE for predicting R_{HW} varied from 13 mm to 15 mm depending on the complexity of the model, corresponding to relative RMSE between 7 and 8 %. The relative RMSE was lower than for the calibration dataset because the trees in the validation dataset were larger on average. In the validation dataset, these three variables showed a much lower variability

than in the calibration dataset and this is probably why their use in the models did not change the predictions very much. The trees of the validation dataset came from the log yard of a sawmill and had all reached exploitable breast height diameters and therefore showed little variability in their D_{BH}. They have also all grown relatively quickly compared with the trees of our calibration dataset, which was made up of trees from experimental plots with varying growth conditions. The coefficients of variation of D_{BH} were 41% and 13% for the calibration and validation datasets, respectively, for RW_5 they were 63% and 32%, respectively, and for H/D_{BH} they were 25% and 16%, respectively. And, D_{BH} and RW_5 presented rather high values compared to those of the calibration dataset (Appendix A7).

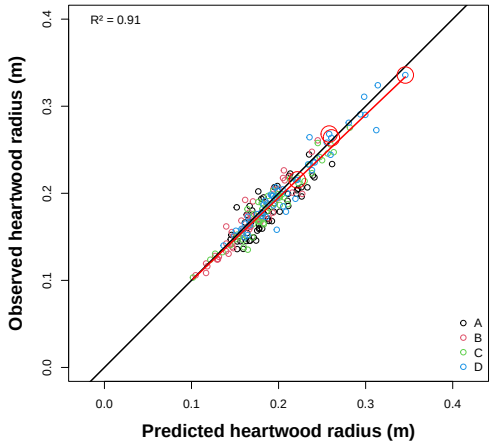

Figure 3: Observed values as a function of predicted values for heartwood radius modelled with Equation (1) for trees in the validation set. One point represents one height level for a given tree. The $y = x$ line is shown in black and the linear regression of the scatter plot in red. The points circled in red represent the largest tree in the dataset ($D_{BH} = 0.81$ m) which is outside the validity limit of the model in terms of D_{BH} and under-bark stem radius (R_{UB}). The results obtained for Models (A), (B) and (C) are given in Appendix A12.

3.6. Sensitivity analysis of the model

A sensitivity analysis of the models is presented in Fig. 4 for Models (A) and (B) and in Appendix A13 for Models (C) and (D). For each variable in the models, we look at the predictions by varying its values between $\mu - 1.5 \times \sigma$ and $\mu + 1.5 \times \sigma$, with μ and σ

Table 5: Comparison of the performance of the different models for predicting heartwood radius on the validation dataset.

Model	p	RMSE (m)	Relative RMSE (%)	Bias (m)	R^2
Chaumet (2020b) with age	6	1.4109e-02	7.62	-4.3884e-03	0.90
Chaumet (2020b) without age	7	1.8962e-02	10.24	9.6845e-03	0.89
Equation (1)	4	1.3354e-02	7.21	4.4942e-03	0.91
(A)	6	1.4520e-02	7.84	2.6065e-03	0.89
(B)	7	1.5390e-02	8.31	-5.9155e-03	0.88
(C)	8	1.4968e-02	8.08	-1.2135e-03	0.87

the mean and standard deviation of the corresponding variable, respectively, as observed in the calibration dataset. For D_{BH}, μ was 36 cm, and for RW_5, μ was 2.3 mm.

Figure 4 shows that Models (A) and (B) predict a greater amount of heartwood for trees with the lowest D_{BH} compared to the prediction for similar stem sections of larger trees. However, in this case, these small sections can be located as well at the bottom of trees with a small D_{BH} as at a higher level in trees with larger D_{BH}.

Figure 4 on the right shows that trees with a lower RW_5 tend to have more heartwood on the stem section whatever the height in the tree.

3.7. Use of the model in a growth simulator

To calculate the amount of heartwood here, we used Model (C), which was the most complete model that could be straightforwardly used with SimCop. Indeed, it does not include a crown size variable (unlike Model (D)), because the definition of the crown base in SimCoP, linked to the size of the crown, is probably not perfectly equivalent to the field measurement used for the calibration dataset (Appendix A7). Appendix A14 illustrates the variability of two of the input variables of Model (C) for the two simulated scenarios. The graph shows the difference in values of these two variables per diameter class between the two scenarios (i.e., lower H/D_{BH} and higher RW_5 for the scenario with heavy thinning compared to the one without intervention) and also a greater variability for the scenario with heavy thinning.

Table 6 summarizes the results of the two scenarios simulated with the SimCoP growth simulator. The total stem volume of living trees did not vary drastically in the

simulations, with 721 m^3/ha for the scenario without intervention and 759 m^3/ha for the heavy thinning scenario when including the volume of final cut and thinnings.

The total volume of wood larger than 14 cm in diameter (corresponding to commercial volume) was also relatively similar between the two scenarios with 37 m^3/ha more for the heavy thinning scenario. Contrary to previous volumes, the volume of heartwood was 9 m^3/ha higher in the trees from the scenario without intervention.

Figure 5 shows the relation between the proportion of heartwood in volume and the commercial volume of the stem (i.e., above 14 cm in diameter) for the simulated trees from the two scenarios. Overall, trees from thinning operations (in red), which were younger, had a lower proportion of heartwood (generally much lower than 50%) and a much larger variability than trees from final cuts. The greatest variability was observed for trees with a volume of less than about 1 m^3, which were more numerous in the first thinning operations. The proportion of heartwood in final-cut trees (in blue and green) was high for the smallest trees (< 1 m^3), then decreased, reaching a minimum for trees of around 1.5 m^3 before increasing steadily to a maximum for trees of around 4 m^3, after which a decline appears to begin. These trends observed for the trees from the final cut were similar for the two scenarios, with a slightly and rather constant difference between them, but with greater variability in the proportions of heartwood for the scenario with thinning. On average, this proportion ranged from 49% for the dynamic scenario to 53% for the scenario without intervention (see Table 6).

In the scenario with thinning, the final cut logically included trees with larger diameters than in the control plot (without intervention), but in insufficient numbers to achieve a comparable volume of heartwood (Fig. 6 and 7). Considering also the trees that were thinned, the total volume of heartwood produced was relatively equivalent between the two scenarios, excluding dead trees.

The noticeable decrease in heartwood proportion observed in the largest trees in volume (> 4 m^3), i.e. beyond the calibration data, was significantly more pronounced for the final cut of the dynamic scenario (green curve in Fig. 5). This result is also visible in Fig. 7, where the volume of heartwood appears to stabilize beyond 70 cm in D_{BH}, leading to a decrease in its proportion.

Table 6: Growth simulations. Number of trees (excluding dead trees), total above ground volume, volume of wood above 14 cm in diameter (i.e., commercial volume) and volume of heartwood in the commercial part of the stem predicted by Model (C) in harvested trees for the two scenarios studied. The differences between the total number of trees harvested and the initial density of 1111 stems/ha correspond to dead trees.

Scenario		Number of trees (stems/ha)	Stem volume (m^3/ha)	Volume > 14 cm (m^3/ha)	Heartwood volume (m^3/ha)
Without intervention	Final cut	823	721	655	348
With thinning	Thinnings	866	294	244	106
	Final cut	219	465	447	233
	Total	*1086*	*759*	*692*	*339*

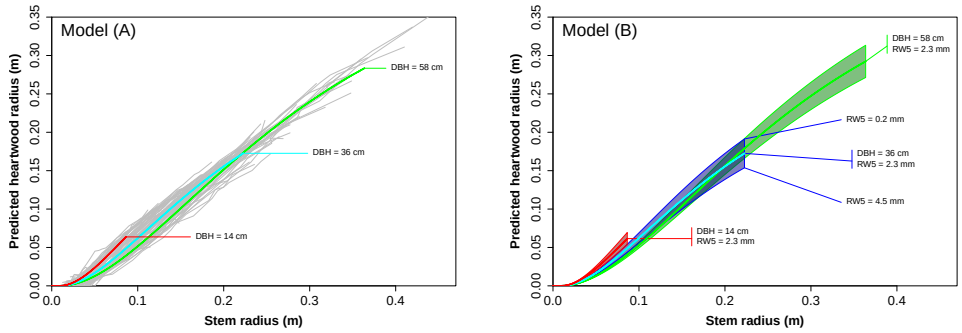

Figure 4: Heartwood radius (R_{HW}) predicted by Models (A) and (B) in relation with stem radius (R_{UB}) and different values of D_{BH} and RW_5. The gray curves in the figure on the left show the values observed on the 86 trees from the calibration dataset. The range of variation of each variable was set to the mean value $\pm$ 1.5 times the standard deviation (here for D_{BH} on the left and for D_{BH} and RW_5 on the right). The mean values of D_{BH} and RW_5 measured on the calibration dataset were respectively: 36 cm and 2.3 mm. The D_{BH} varies between 14 cm and 58 cm (on the left), and for each D_{BH} value, RW_5 varies from 0.2 mm to 4.5 mm (on the right). Stem radius at ground level was estimated by 1.25 times half of D_{BH}.

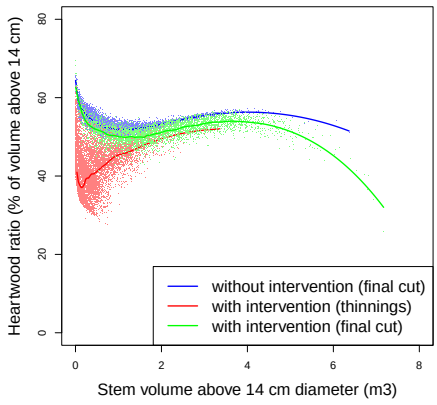

Figure 5: Heartwood ratios predicted by the Model (C) as a function of stem volume above 14 cm in diameter obtained for the two contrasted scenarios from growth simulations: Trees harvested during thinning operations in red ("with intervention" scenario), trees harvested at final cut in green ("with intervention" scenario) or blue ("without intervention" scenario). Each dot represents a tree from one of the 50 simulations. Solid lines show Loess smoothing.

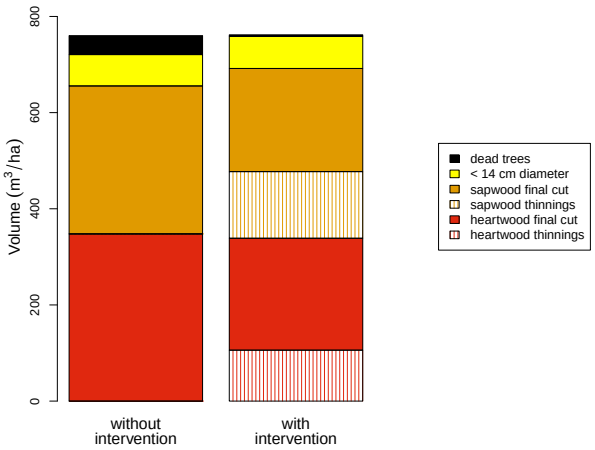

Figure 6: Heartwood/sapwood volumes predicted by the Model (C) from growth simulations for both scenarios: Volumes of dead trees, volumes of stem below 14 cm in diameter, volumes of sapwood and heartwood collected during thinning operations and at the final cuts.

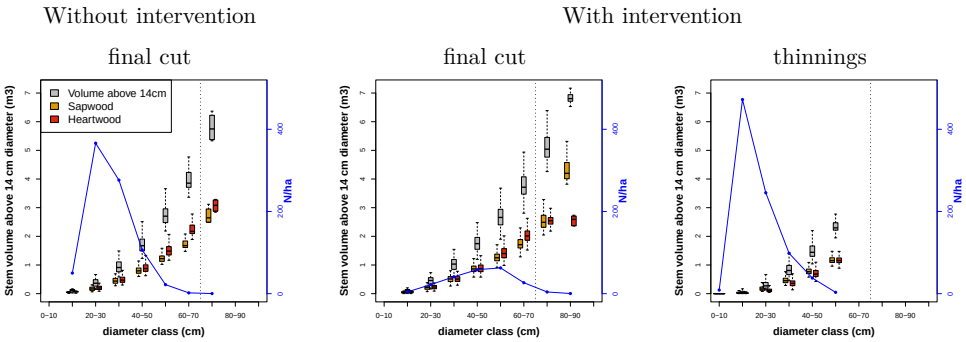

Figure 7: Heartwood/sapwood volumes predicted by the Model (C) from growth simulations for each diameter class and both scenarios: Boxplots of the total stem volume above 14 cm in diameter (grey), sapwood volume (orange) and heartwood volume (red) collected during thinning operations and final cuts. The blue line corresponds to the number of stems per hectare.

4. Discussion

4.1. Pipe model theory

The "pipe model" theory (Shinozaki et al., 1964) suggests that the area of active pipes at any height in the stem is proportional to the foliage area above that height. Consequently, the conductive sapwood area below the crown base should be more or less constant. This was not the case for our Douglas fir data. Rather, the sapwood width was approximately constant below the crown base, as also shown by Longuetaud et al. (2006) for Norway spruce. If the width of the sapwood is constant, its area is generally not, due to the more or less pronounced taper of the stem. Both sapwood width and area can only be constant below the crown base when the stem is cylindrical. Accordingly, from our data we could observe that sapwood area was least variable along the stem (i.e., with a slope near 0) in the high density stands (Appendix A11), whatever the site, i.e., for silvicultural treatments resulting in the most cylindrical stems. Overall, sapwood area clearly decreased by an average of 49% between the height of 1.30 m and the base of the crown. Such a decrease was also observed for Douglas fir by Waring et al. (1982) who reported a value of 36%, and by Hein et al. (2008) for young trees (24-34 years of age).

However, the "pipe model" refers to active pipes, which may not represent the entire area of the visible sapwood measured in our study. To our knowledge, methods are lacking that would allow converting a visible sapwood area (whose limit is defined on the basis of the colouration of the heartwood) into a truly conductive area. Rust (1999) compared several methods of measuring the sapwood/heartwood boundary in Scots pine and concluded that X-rays can detect sapwood based on its water content as the "conductive zone" of the trunk, whereas the staining method detects an additional transition zone that is relatively dry but chemically unaltered. A Master's thesis (Billard, 2017) based on our data compared the positioning of this boundary based on a change in colour (coloured heartwood vs light sapwood) and a change in water content (X-rays). The results presented in Appendix A15 show that the radius of the heartwood (if considered here as a dry, non-conductive area) is underestimated by an average of approximately 4 mm when using the colour difference method and therefore that the two methods generally correspond well, with the exception of this slight shift.

Nevertheless, the limited validity of the "pipe model" theory has already been revealed

for many other species and reported in the review by Lehnebach et al. (2018). In the lack of a consistent theory, the development of statistical models for the distribution of sapwood and heartwood becomes even more important.

4.2. Modelling of the longitudinal heartwood profile

Our models and those available in literature differ with respect to (1) the predicted variable of heartwood or sapwood size, (2) the way the longitudinal profile of heartwood or sapwood is depicted, and (3) the further tree- or stand-level explanatory variables. Sapwood area and heartwood diameter as a function of height in the tree are modelled by Maguire and Batista (1996) and Maguire (2014), respectively. Models by Chaumet (2020b) predict the ratio of heartwood diameter to stem diameter, where the heartwood profile is related to the longitudinal variation in stem size (stem diameter divided by D_{BH}) rather than height, similar to our approach. In turn, the best-performing of the two models by Chaumet (2020b) relies on tree age as further explanatory variable, suggesting an effect of ontogeny. By contrast, in our models, variables related to tree vigour, social status and growth dynamics as controlled through silviculture (D_{BH}, RW_5, H/D_{BH} and L_{LC}) provided better predictions than age. This was in accordance with the models by Maguire and Batista (1996) and Maguire (2014). The latter models rely on D_{BH}, as our Models (A) to (D), and on crown size as our Model (D). Crown size, and other proxies of tree vitality, are known to be linked to the quantity of sapwood (e.g., Grier and Waring (1974) for Douglas fir). Moreover, the predictors of our models were consistent with the main explanatory variables for sapwood thickness in Douglas fir found by Smith et al. (1966): Stem-section diameter, growth in the last decade, D_{BH} and crown related variables.

Referring to these relationships, our modelling approach suggested a clear hierarchical order. We found a very strong relationship between stem radius and heartwood radius at any height in the stem, which accounted for 98% of the variation (Fig. 1; Table 3). This suggests that heartwood formation was mainly determined by stem development, whatever the growth conditions (low to high stand densities; Table 2) and tree ages (23-74 years; Table 1) of our experimental sites. Nevertheless, introducing D_{BH} and RW_5 as further predictors clearly reduced RMSE from about 12.3 to 8.6% (Equation (1) and Model (B) in Table 3). The introduction of RW_5 especially allowed to reduce RMSE

for the **Quartier** site (corresponding to the change from 6 to 7 model parameters in Fig. 2) with the youngest trees of our calibration dataset (Table 1). We would therefore recommend using at least the 7-parameter Model (B), while Models (C) and (D), with H/D_{BH} and L_{LC}, only provided marginal improvements.

However, crown morphology (e.g., L_{LC} in our Model (D)) can be an important proxy for a larger assessment of wood quality, especially in complex stands for which limited knowledge is available in this respect (Pretzsch and Rais, 2016). In turn, tree age as a predictor is usually not available for complex, uneven-aged stands. This may limit the use of age-related models such as the one by Chaumet (2020b), which otherwise provided good results, comparable to ours. Another aspect is that the effect of age is sometimes difficult to dissociate from the site effect in experiments conducted in even-aged stands such as ours (see Table 1), and this can potentially affect the correct consideration of the age effect in models. In an industrial context, height in the tree may not be available, which would limit the use of models by Maguire and Batista (1996) and Maguire (2014). In this respect, our Equation (1) has the advantage of relying only on log radius (or diameter) and its longitudinal variation, which can commonly be assessed in sawmills. Evaluation of our models based on an independent dataset suggested that using Equation (1) alone may be sufficient to some extent, especially if logs come from trees with little variation in D_{BH} and radial growth (Section 3.5).

Moreover, this evaluation suggested good performance of our models even at the limit of their validity range (Fig. 3 and Appendix A12). Indeed, trees from the validation dataset had relatively large diameters and high growth rates compared to those from the calibration dataset (Section 3.5). However, a more detailed analysis of Model (A) (with only D_{BH} as input variable) showed a questionable reduction in the amount of heartwood for large trees above about 75 cm D_{BH} (Appendix A16). This is likely due to a lack of large trees in our calibration dataset, which was otherwise quite suitable for model development given its wide range of variations in the candidate input variables (Table 2). Thus, we recommend using Models (A) to (D) with caution when trees exceed 75 cm D_{BH}. Acquiring data for larger trees would likely allow to extend the scope of application of our models, by improving parameter estimation and possibly model formulation.

4.3. Effects of silviculture on heartwood and sapwood quantities

Despite of the strong relationship between heartwood radius and stem radius, statistical model performance was improved to some extend by introducing further predictors (D_{BH} and RW_5, and to a lesser extent H/D_{BH} and L_{LC}), as discussed above. These predictors are influenced by growth conditions as controlled through silviculture. Thus, the simulation analysis with SimCoP should show to what extend this influence finally propagated on the quantities of heartwood and sapwood, after an entire silvicultural schedule (production cycle) of 55 years. For the reasons given above, we focus here on simulation results for trees less than 75 cm D_{BH}.

Concerning the heartwood ratio at the final cut, two stems of the same commercial volume had on average a slightly lower heartwood ratio for the scenario with intervention than for that without intervention (Fig. 5). This was in accordance with results by Chaumet (2020b), who also found small differences in heartwood ratio for two silvicultural scenarios that were quite similar to those we have explored. However, for young Douglas firs (24-34 years of age), Hein et al. (2008) did not find any statistically significant differences in sapwood area percentage between trees growing under contrasted initial stand densities (100, 200 and 1200 stems $\cdot$ ha^{-1}).

Interestingly, for each of our two scenarios, the heartwood ratio at the final cut firstly decreased and then increased with increasing commercial stem volume (Fig. 5). This model behaviour may also reflect effects of competition: Trees of low social status (i.e., low commercial volume) had a low sapwood ratio (high heartwood ratio) associated with low tree vitality; Trees of high social status (i.e., high commercial volume) are supposed to have more sapwood associated with higher tree vitality and growth, and they also produced more heartwood due to their big stem size, resulting in a high heartwood ratio; Trees of intermediate social status would form the turning point of this relationship. Note that beyond about 4 m^3 of commercial volume, trees pass the model validity limit of about 75 cm D_{BH} (see Fig. 7 for the relationship between commercial volume and D_{BH} class).

The thinned trees in Fig. 5 showed a similar pattern than those of the final cut, but with clearly lower heartwood ratios. Thinned trees reached a given commercial volume more rapidly as they were younger, implying higher vitality and related sapwood ratio

(lower heartwood ratio).

From a silvicultural point of view, the scenarios with and without intervention had similar total volume for production of exploitable stems (Table 6; Fig. 6). On the one hand, the scenario with intervention produced trees with an overall slightly lower heartwood ratio at the final cut (Fig. 5). Furthermore, at the final cut, the bigger trees of 60-70 cm D_{BH} (and to a lesser extent those of 50-60 D_{BH}) had similar sapwood volume but somewhat lower heartwood volume in the scenario with intervention (Fig. 7). This may be explained by the last thinning before the final cut, resulting in a change in RW_5 compared to the scenario without intervention. On the other hand, the scenario with intervention resulted in a higher number of big trees of 60-70 cm D_{BH} and in a lower number of smaller trees of 40-50 cm D_{BH} at the final cut (Fig. 7). The former had a higher heartwood ratio than the latter, due to the increase in heartwood ratio between about 1.5 m^3 and 4 m^3 of commercial volume (Fig. 5).

Overall, these results suggested a plausible behaviour of our heartwood model in the simulation analysis, with insights into the effects of silviculture through the explanatory variables selected (D_{BH}, RW_5 and H/D_{BH}).

In the French context, sawmills equipped with chipper canter technology, aiming at mass-production of timber from medium-sized logs, do not always distinguish between heartwood and sapwood. In contrast, companies using band-saws can respond to specific orders of sapwood-free timber from big logs of overall high quality. Given our results, a silvicultural strategy for the production of high-quality, large Douglas fir trees may be: To grow them not too fast at the beginning in order to limit the quantity of juvenile wood and branch size (Barrette et al., 2023), then to accelerate growth to limit rotation length and related risks (storms, diseases, insect attacks), and to slow it down towards the end. Thus, the quantity of heartwood during the last years of the production cycle may be optimised (effect of RW_5). We would expect the changes in growth rate to have little impact on wood density as another important quality criterion. Indeed, there is only a moderate relationship between ring width and wood density in Douglas fir (Fabris, 2000). However, a more complete simulation study should be performed in order to provide final recommendations to forestry practice, considering several contrasted silvicultural scenarios and additional wood quality criteria. To this end, our heartwood models may

contribute to the development of simulation tools that link tree growth, wood properties and product characteristics of Douglas fir (e.g., Poschenrieder et al., 2016).

5. Conclusion

In this study, models of various degrees of complexity were developed to predict the amount of heartwood and its longitudinal distribution in Douglas fir stems in France. The amount of heartwood at a given height depended essentially on stem size (i.e., diameter of the stem cross-section at that height and D_{BH}), and to a lesser extent on tree growth dynamics. Validation on completely independent data, with trees whose characteristics were at the limit of validity in relation to our calibration set, showed that the models performed well. However, it seems reasonable, at this stage, not to use these models for trees with a diameter at breast height greater than 75 cm. One of the proposed models was implemented in a Douglas fir growth-quality simulator (Model (C) taking D_{BH}, RW_5 and H/D_{BH} as inputs). Simulations were carried out for two contrasting silvicultural scenarios. They suggested overall small differences in heartwood amount. Nevertheless, plausible model behaviour and interesting insights for silvicultural management were found. A more complete simulation study should be performed in order to provide final recommendations to forestry practice, considering several contrasted silvicultural scenarios and additional wood quality criteria. For a valid application of the models on larger trees, the calibration set should be completed in this sense. It would be interesting to test the developed models on other independent data that exhibit greater variability in diameters and growth rates in order to better assess the added value of the different input variables.

Acknowledgements:

Many thanks to Charline Mola, Adeline Motz, Frédéric Bordat, Vincent Rousselet, Adrien Contini, Jean Ladier and Daniel Rittié for their precious help in this experiment (sampling in the field and measurements in the laboratory). Thanks to Francis Colin as coordinator of the ExtraFor_Est project, from which some of the data was collected. We would also like to thank Salomé Fournier and Christine Deleuze from the ONF for their careful review and advice.

SILVA laboratory is supported by a grant overseen by the French National Research Agency (ANR) as part of the "Investissements d'Avenir" program (ANR-11-LABX-0002-01, Lab of Excellence ARBRE). Some of the data used in this work was collected as part of the joint Modelfor 2012–2015 project between INRAE and ONF. Another part of the data was collected as part of the ExtraFor_Est project and Antoine Billard's thesis funded by ADEME and the Grand Est Region. We thank the "GIS Coopérative de données" (GIS Coop) supported by ONF, INRAE, FCBA and CNPF-IDF for the management of some of the studied sites. We are in particular grateful to GIS Coop Douglas and to the French Ministry of Agriculture and Forest for GIS Coop financial support.

References

Angelier, A., 2006. Guide des sylvicultures pour le douglas : de nouvelles courbes de fertilité adaptées. Rendez-Vous Techniques 11, 7–12.

Aye, T.N., Brännström, Å., Carlsson, L., 2022. Prediction of tree sapwood and heartwood profiles using pipe model and branch thinning theory. Tree Physiology 42, 2174–2185.

Barrette, J., Achim, A., Auty, D., 2023. Impact of intensive forest management practices on wood quality from conifers: literature review and reflection on future challenges. Current Forestry Reports 9, 101–130.

Billard, A., 2017. Modélisation de la distribution de l'aubier chez le Douglas. Master's thesis. M2 FAGE, Université de Lorraine.

Blohm, J.H., Melcher, E., Lenz, M.T., Koch, G., Schmitt, U., 2014. Natural durability of Douglas fir (Pseudotsuga menziesii [Mirb.] Franco) heartwood grown in southern Germany. Wood Material Science & Engineering 9, 186–191. doi:10.1080/17480272.2014.903296.

Bédéneau, M., Sindou, C., Ruchaud, F., Bailly, A., Crémière, L., 2001. Un partenariat scientifique original : La coopérative de données sur la croissance des arbres et peuplements forestiers. Revue forestière française LIII, 171–177.

Cardoso, S., Pereira, H., 2017. Characterization of Douglas-fir grown in Portugal: heartwood, sapwood, bark, ring width and taper. European Journal of Forest Research 136, 597–607.

Chaumet, M., 2020a. Douglas fir heartwood determinism – between silviculture and genetics. FCBA INFO .

Chaumet, M., 2020b. Rapport final : Modélisation du profil de duramen du douglas. Technical Report. FCBA. URL: https://www.fcba.fr/wp-content/uploads/2024/06/Rapport-final-DURAMEN-modelisation-diffusion.pdf.

Donaldson, L.A., Singh, A., Raymond, L., Stefan, H., Schmitt, U., 2019. Extractive distribution in Pseudotsuga menziesii: effects on cell wall porosity in sapwood and heartwood. IAWA Journal 40, 721 – 740. doi:10.1163/22941932-40190248.

706 Dufour-Kowalski, S., Courbaud, B., Dreyfus, P., Meredieu, C., De Coligny, F., 2012. Capsis: an open
707 software framework and community for forest growth modelling. Annals of forest science 69, 221–233.
708 Elzhov, T.V., Mullen, K.M., Spiess, A.N., Bolker, B., Mullen, M.K.M., Suggests, M., 2016. Package 'min-
709 pack. lm'. Title R Interface Levenberg-Marquardt Nonlinear Least-Sq. Algorithm Found MINPACK
710 Plus Support Bounds .
711 Fabris, S., 2000. Influence of cambial ageing, initial spacing, stem taper and growth rate on the wood
712 quality of three coastal conifers. Ph.D. thesis. University of British Columbia.
713 Fournier, S., Sardin, T., Dreyfus, P., Francois, D., Mandret, X., Simeoni, M., Renaud, J.P., Akroume, E.,
714 Bouvet, A., Berthelot, A., et al., 2022. Dendrometric data from the silvicultural scenarios developed
715 by office national des forêts (onf) in france: a tool for applied research and carbon storage estimates.
716 Annals of Forest Science 79, 48.
717 Granier, A., 1981. Etude des relations entre la section du bois d'aubier et la masse foliaire chez le
718 Douglas (Pseudotsuga menziesii Mirb. Franco). Annales des Sciences Forestières 38, 503–512.
719 Grier, C.C., Waring, R.H., 1974. Conifer foliage mass related to sapwood area. Forest Science 20,
720 205–206.
721 Hein, S., Weiskittel, A.R., Kohnle, U., 2008. Effect of wide spacing on tree growth, branch and sapwood
722 properties of young Douglas-fir [Pseudotsuga menziesii (Mirb.) Franco] in south-western Germany.
723 European Journal of Forest Research 127, 481–493.
724 Hillis, W.E., 1987. Heartwood and tree exudates. volume 4. Springer, Berlin.
725 Humar, M., Vek, V., Oven, P., Lesar, B., Kržišnik, D., Keržič, E., Hočevar, M., Brus, R., 2022. Durability
726 and moisture dynamics of douglas-fir wood from Slovenia. Frontiers in plant science 13, 860734.
727 IGN, 2023. Mémento – Edition 2023. Institut national de l'information géographique et forestière.
728 Saint-Mandé, France. URL: https://inventaire-forestier.ign.fr/IMG/pdf/memento_2023.pdf.
729 Kendall Snell, J.A., Brown, J.K., 1978. Comparison of tree biomass estimators–dbh and sapwood area.
730 Forest Science 24, 455–457.
731 Kozak, A., 1988. A variable-exponent taper equation. Canadian Journal of Forest Research 18, 1363–
732 1368.
733 Lehnebach, R., Beyer, R., Letort, V., Heuret, P., 2018. The pipe model theory half a century on: a
734 review. Annals of botany 121, 773–795.
735 Long, J.N., Smith, F.W., Scott, D.R., 1981. The role of douglas-fir stem sapwood and heartwood in the
736 mechanical and physiological support of crowns and development of stem form. Canadian Journal of
737 Forest Research 11, 459–464.
738 Longuetaud, F., Mothe, F., Leban, J.M., Mäkelä, A., 2006. Picea abies sapwood width: variations within
739 and between trees. Scandinavian Journal of Forest Research 21, 41–53.
740 Longuetaud, F., Pot, G., Mothe, F., Barthelemy, A., Decelle, R., Delconte, F., Ge, X., Guillaume,
741 G., Mancini, T., Ravoajanahary, T., et al., 2022. Traceability and quality assessment of Douglas
742 fir (Pseudotsuga menziesii (Mirb.) Franco) logs: the TreeTrace_Douglas database. Annals of Forest
743 Science 79, 1–21.
744 Maguire, D.A., 2014. Models for the height and shape of the heartwood core in Douglas-fir. Technical

Report. CIPS 2013 Annual Report. Center for Intensive Planted-forest Silviculture, College of Forestry, Oregon State University, Corvallis, OR, USA.

Maguire, D.A., Batista, J.L., 1996. Sapwood taper models and implied sapwood volume and foliage profiles for coastal Douglas-fir. Canadian Journal of Forest Research 26, 849–863.

Maguire, D.A., Kanaskie, A., 2002. The ratio of live crown length to sapwood area as a measure of crown sparseness. Forest Science 48, 93–100.

McDowell, N., Barnard, H., Bond, B., Hinckley, T., Hubbard, R., Ishii, H., Köstner, B., Magnani, F., Marshall, J., Meinzer, F., Phillips, N., Ryan, M., Whitehead, D., 2002. The relationship between tree height and leaf area: sapwood area ratio. Oecologia 132, 12–20.

Mitchell, K.J., 1975a. Dynamics and simulated yield of Douglas-fir. For. Sci. Monogr. 17, 1–39.

Mitchell, K.J., 1975b. Stand description and growth simulation from low-level stereo photos of tree crowns. Journal of Forestry 73, 12–45.

Nicolescu, V.N., Mason, W.L., Bastien, J.C., Vor, T., Petkova, K., Podrázskỳ, V., Đodan, M., Perić, S., La Porta, N., Brus, R., et al., 2023. Douglas-fir (Pseudotsuga menziesii (Mirb.) Franco) in Europe: an overview of management practices. Journal of Forestry Research , 1–18.

Ningre, F., Ottorini, J.M., Le Goff, N., 2016. Trajectoires d'autoéclaircie du Douglas (Pseudotsuga menziesii) en France. Revue forestière française 68, 323–343.

Osborne, N.L., 2015. Simulating wood properties in the context of a growth and yield model for planted Douglas-fir.

Ottorini, J., 1991. Growth and development of individual Douglas-fir in stands for applications to simulation in silviculture 48, 651–666.

Ottorini, J., 1995. Simulation et sylviculture du douglas. Revue forestière française XLVII, 97–105.

Pinheiro, J., Bates, D., 2006. Mixed-effects models in S and S-PLUS. Springer science & business media.

Pinheiro, J., Bates, D., DebRoy, S., Sarkar, D., Heisterkamp, S., Van Willigen, B., Maintainer, R., 2017. Package 'nlme'. Linear and nonlinear mixed effects models, version 3, 274.

Pinheiro, J.C., Bates, D.M., 2000. Mixed-effects models in S and S-PLUS. Springer.

Pollet, C., Henin, J.M., Hébert, J., Jourez, B., 2018. Impact de la vitesse de croissance sur les propriétés technologiques du bois de douglas. Forêt.Nature 146, 60–72.

Poschenrieder, W., Rais, A., van de Kuilen, J.W.G., Pretzsch, H., 2016. Modelling sawn timber volume and strength development at the individual tree level–essential model features by the example of douglas fir. Silva Fennica 50.

Pretzsch, H., Rais, A., 2016. Wood quality in complex forests versus even-aged monocultures: review and perspectives. Wood science and technology 50, 845–880.

R Core Team, 2021. R: A Language and environment for statistical computing. R Foundation for Statistical Computing. Vienna, Austria. URL: `https://www.R-project.org/`.

Reineke, L.H., 1933. Perfecting a stand-density index for even-aged forest. Journal of agricultural research 46, 627–638.

Rust, S., 1999. Comparison of three methods for determining the conductive xylem area of scots pine (pinus sylvestris). Forestry 72, 103–108.

784 Sardin, T., 2013. Douglasaies françaises, référentiels sylvicoles, fr correctif 2013. Les guides de sylvicul-
785 ture , 53.
786 Seynave, I., Bailly, A., Balandier, P., Bontemps, J.D., Cailly, P., Cordonnier, T., Deleuze, C., Dhôte,
787 J.F., Ginisty, C., Lebourgeois, F., et al., 2018. GIS Coop: networks of silvicultural trials for supporting
788 forest management under changing environment. Annals of Forest Science 75, 1–20.
789 Shinozaki, K., Yoda, K., Hozumi, K., Kira, T., 1964. A quantitative analysis of plant form-the pipe
790 model theory: I. basic analyses. Japanese Journal of ecology 14, 97–105.
791 Smith, J., Walters, J., Wellwood, R., 1966. Variation in sapwood thickness of Douglas-fir in relation to
792 tree and section characteristics. Forest Science 12, 97–103.
793 Sornay, J., 1937. Les peuplements de Douglas en France. Bulletin de la Société forestière de Franche-
794 Comté , 198–214.
795 Spicer, R., Gartner, B., 2001. The effects of cambial age and position within the stem on specific
796 conductivity in Douglas-fir (Pseudotsuga menziesii) sapwood. Trees 15, 222–229.
797 Spiecker, H., Lindner, M., Schuler, J., 2019. Douglas-fir – an option for Europe. EFI What Science Can
798 Tell Us 9.
799 Taylor, A.M., Gartner, B.L., Morrell, J.J., 2002. Heartwood formation and natural durability – a review.
800 Wood and Fiber Science 34, 587–611.
801 Waring, R.H., Schroeder, P.E., Oren, R., 1982. Application of the pipe model theory to predict canopy
802 leaf area. Canadian Journal of Forest Research 12, 556–560.
803 Weiskittel, A.R., Maguire, D.A., Garber, S.M., Kanaskie, A., 2006. Influence of Swiss needle cast on
804 foliage age-class structure and vertical foliage distribution in Douglas-fir plantations in north coastal
805 Oregon. Canadian Journal of Forest Research 36, 1497–1508.
806 Zeide, B., 1993. Analysis of growth equations. Forest science 39, 594–616.
807 Zeidler, A., Borůvka, V., Černý, J., Baláš, M., 2022. Douglas-fir outperforms most commercial european
808 softwoods. Industrial Crops and Products 181, 114828. URL: https://www.sciencedirect.com/
809 science/article/pii/S0926669022003119, doi:https://doi.org/10.1016/j.indcrop.2022.114828.

List of Tables

List of Figures

Appendices

Modelling the heartwood profile of Douglas fir in France based on the stem profile and other tree dendrometric characteristics – insights from experimental sites and commercial log data

UMR Silva
Université de Lorraine, AgroParisTech, INRAE, Silva, 54000 Nancy, France

Contents

APPENDIX A1

Models from the literature

A1.1 Model of Maguire and Batista (1996)

The model of Maguire and Batista (1996) is as follows. A first model allows to predict the sapwood surface at breast height:

$$S_{SWBH} = \frac{\pi}{4}(b_1 D_{BH})^2 \cdot \left(1 - \exp\left(-b_2 \frac{L_{LC}}{H}\right)\right)^{(b_3 H)}$$

The sapwood surface profile can then be predicted using the variable exponent model proposed by Kozak (1988):

$$Z = \frac{h}{H}, \qquad p = \frac{H_{BH}}{H}, \qquad X = \frac{1 - \sqrt{Z}}{1 - \sqrt{p}}$$

$$C = k_1 Z + k_2 \sqrt{Z} + k_3 \frac{D_{BH}}{H} + k_4 L_{LC} + k_5 \frac{L_{LC}}{H} + k_6 (H - L_{LC})$$

$$S_{SW} = S_{SWBH} \cdot X^C \tag{A1.1}$$

where h is the height of the disc, H_{BH} the breast height (1.37 m for Maguire and Batista (1996) and 1.30 m in our case), H is the total tree height, L_{LC} the length of the living crown, S_{SWBH} the surface of sapwood at breast height, S_{SW} the surface of sapwood at height h, D_{BH} is the diameter at 1.30 m and b_1, b_2, b_3, k_1, k_2, k_3, k_4, k_5 and k_6 are fixed-effect parameters.

In order to estimate the mean heartwood radius (R_{HW}) with the sapwood surface model of Maguire and Batista (1996) the following equation was used:

$$R_{HW} = \sqrt{R_{UB}^2 - \frac{S_{SW}}{\pi}} \tag{A1.2}$$

The model was tested after refitting on our calibration dataset. The fitting can be performed directly using Eq. (A1.2) or using Eq. (A1.1) then applying Eq. (A1.2) on the predicted results. The first method, which gives a better estimation of R_{HW}, was used here.

A1.2 Model of Maguire (2014)

The model of Maguire (2014), as described by Osborne (2015), can be summarized as follows:

$$H_{HW} = \frac{H}{1 + \exp(k_1 + k_2 \cdot \log(\frac{L_{LC}}{H}) + k_3 \cdot \log(L_{LC}) + k_4 \cdot \frac{H}{D_{BH}}}$$

$$D_{HWBH} = k_5 \cdot D_{BH}^{k_6 \cdot H + k_7 \cdot \log(\frac{L_{LC}}{H}) + k_8 \cdot \log(L_{LC})}$$

$$X = \frac{h - h_0}{H_{HW} - h_0} \qquad K = \frac{0.5 \cdot H_{CB} - h_0}{H_{HW} - h_0} \qquad Z = \frac{K - X}{K - 1} \qquad W = \frac{X - 1}{K - 1}$$

$$I_1 = \begin{cases} 0 & \text{if } K \leq 0 \text{ or } (K > 0 \text{ and } X \leq K) \\ 1 & \text{otherwise} \end{cases} \qquad I_2 = \begin{cases} 0 & \text{if } K \leq 0 \\ 1 & \text{otherwise} \end{cases}$$

$$Y_1 = I_2 \cdot (X + I_1 \cdot (W \cdot (1 + Z) - 1)) - (X - 1) \cdot (X - I_2 \cdot X)$$
$$Y_2 = I_2 \cdot (X + I_1 \cdot (W \cdot (X + K \cdot Z) - X) - (X - 1) \cdot (X - I_2 \cdot X))$$
$$Y_3 = I_2 \cdot \left(X^2 + I_1 \cdot (K \cdot W \cdot (2 \cdot X - K + K \cdot Z) - X^2)\right)$$

$$R_{HW} = \frac{D_{HWBH}}{2} \cdot \left(1 - X + Y_1 + \left(k_9 \cdot \exp\left(\frac{D_{BH}}{H}\right)\right) \cdot Y_2 + \left(k_{10} \cdot \exp\left(\frac{H}{D_{BH}}\right)\right) \cdot Y_3\right)$$

A1.3 Models of Chaumet (2020b)

Chaumet (2020b) proposed two formulas for modeling diameter heartwood ratio, with and without using tree age. Both models are based on a diameter ratio R_D used in the form of a polynomial of degree 3 in the models and calculated as follows:

$$R_D = \frac{d_{OB}}{D_{BH}} \times 100 \tag{A1.3}$$

- The model including tree age is as follows:

$$Ratio_{HW} = a + b \cdot R_D + c \cdot R_D^2 + d \cdot R_D^3 + e \cdot \frac{R_D}{age} + f \cdot \frac{R_D^2}{age} \tag{A1.4}$$

  where d_{OB} is the over-bark stem diameter at a given height, age the tree age, and a, b, c, d, e, and f are parameters.

- The model without tree age is as follows:

$$Ratio_{HW} = a + b \cdot R_D + c \cdot R_D^2 + d \cdot R_D^3 + e \cdot \frac{H}{D_{BH}} + f \cdot D_{UB} + g \cdot R_D \cdot D_{UB} \tag{A1.5}$$

  where D_{UB} is the under-bark stem diameter at a given height and a, b, c, d, e, f and g are parameters.

In our case, since over bark diameter was not measured, R_D was computed as the ratio of under-bark diameter to over-bark diameter at breast height:

$$R_D = \frac{D_{UB}}{D_{BH}} \times 100$$

The models were readjusted using our calibration set. The heartwood radius was then calculated as the product of $Ratio_{HW}$ by under-bark radius (R_{UB}).

APPENDIX A2

List of abbreviations used in the article

Table A2.1: Dendrometric variables used in the article.

Abbreviation	Unit	Meaning	Scale
D_g	m	Average diameter of a stand	
D_0	m	Dominant diameter	stand
C_0	m	Dominant circumference	
H_0	m	Dominant height	
RDI	without	Relative Density Index	
RDI_{ratio}	without	Ratio between RDI after and RDI before the last thinning	
G	m^2/ha	Basal area	
SF	%	Spacing factor of Hart-Becking	
D_{BH}	m	Diameter at 1.30 m	
H	m	Total tree height	
H_{LC}	m	Height to the base of the living crown	
L_{LC}	m	Length of the living crown	tree l
RW	m	Average ring width at breast height	
RW_5	m	Average ring width of the five last growth years at breast height	
h	m	Height in the stem of a disc	
R_{UB}	m	Average under-bark stem radius at a given height	disc l
R_{HW}	m	Average heartwood radius at a given height	

APPENDIX A3

Additional informations on the forests and trees sampled

Tables A3.1 and A3.2 shows the usual dendrometric variables for each tree of the calibration dataset.

Table A3.1: Mean tree measurements in **Écouves** forest. D_{BH} is the diameter at breast height, D_0 the average diameter of the dominant trees, H the total tree height, H_{LC} the height of the base of the living crown, H_{LLB} the height of the lowest living branch, L_{LC} the length of the living crown, RW_5 the average ring width of the five last rings at breast height. NA means not available.

Forest	Density treatment	Tree ID	Age (year)	D_{BH} (m)	H (m)	H_{LC} (m)	H_{LLB} (m)	L_{LC} (m)	RW_5 (m)	D_{BH}/D_0
Écouves_2010	high	E10	63	0.23	31.0	24.9	22.1	6.1	0.0002	0.48
		E11	63	0.43	40.3	28.9	26.1	11.4	0.0029	0.91
		E12	63	0.30	35.3	26.2	26.2	9.1	0.0010	0.63
		E13	63	0.33	36.5	27.6	26.5	9.0	0.0014	0.70
		E14	63	0.38	38.0	25.5	23.0	12.5	0.0024	0.76
		E15	63	0.28	31.8	24.0	21.5	7.8	0.0006	0.59
		E16	63	0.30	37.7	27.3	26.0	10.4	0.0015	0.61
		E17	63	0.47	37.5	28.8	25.9	8.7	0.0030	0.95
		E18	63	0.29	32.6	25.1	24.5	7.5	0.0005	0.59
	medium	E01	63	0.52	40.8	28.0	26.1	12.8	0.0046	1.01
		E02	63	0.24	31.2	22.8	17.9	8.4	0.0003	0.46
		E03	63	0.41	39.1	27.7	26.0	11.4	0.0036	0.78
		E04	63	0.50	40.6	25.2	24.2	15.4	0.0035	0.99
		E05	63	0.28	35.6	24.6	23.5	10.9	0.0010	0.55
		E06	63	0.35	40.0	27.5	26.3	12.6	0.0018	0.66
		E07	63	0.33	36.9	29.6	26.2	7.3	0.0014	0.64
		E08	63	0.46	41.7	25.0	24.3	16.7	0.0026	0.91
		E09	63	0.26	33.0	25.1	25.1	7.9	0.0008	0.48
	low	E19	63	0.28	33.6	24.9	23.2	8.7	0.0007	0.50
		E20	63	0.25	32.3	22.9	19.1	9.3	0.0004	0.46
		E21	63	0.45	40.7	25.6	23.7	15.1	0.0019	0.85
		E22	63	0.35	39.2	24.7	21.6	14.6	0.0018	0.61
		E23	63	0.35	35.5	22.4	19.8	13.1	0.0015	0.63
		E24	63	0.48	40.1	25.5	24.6	14.6	0.0025	0.86
		E25	63	0.47	39.6	24.7	23.0	14.9	0.0030	0.83
		E26	63	0.41	38.5	26.0	25.1	12.6	0.0027	0.72
		E27	63	0.41	39.5	27.8	26.6	11.8	0.0021	0.73
Écouves_2021	high	A5-38	74	0.36	40.7	30.9	26.3	9.8	0.0036	0.65
		A5-75	74	0.45	43.7	29.4	22.9	14.3	0.0020	0.85
		A5-86	74	0.41	44.1	30.2	29.1	13.8	0.0019	0.77
		A5-88	74	0.48	46.4	32.4	30.8	14.0	0.0020	0.91
		A5-109	74	0.53	41.8	30.4	27.3	11.4	0.0019	0.97
		A5-116	74	0.30	39.3	30.1	29.2	9.2	0.0005	0.54
		A5-139	74	0.24	36.9	33.9	32.7	3.0	0.0001	0.45
		A5-142	74	0.22	35.1	31.8	27.6	3.4	0.0000	0.42
		A5-168	74	0.57	46.2	31.8	30.5	14.4	0.0029	1.15
	medium	C7-57	74	0.43	41.5	30.2	25.1	11.3	0.0029	0.67
		C7-86	74	0.61	45.1	29.6	26.5	15.6	0.0033	0.99
		C7-90	74	0.52	44.6	29.3	26.8	15.3	0.0026	0.84
		C12-54	74	0.50	42.2	29.2	NA	13.0	0.0025	0.80
		C12-116	74	0.43	41.0	35.5	NA	5.5	0.0018	0.68
		C12-150	74	0.62	46.2	29.0	27.6	17.2	0.0043	0.96
	low	D6-19	74	0.51	45.1	29.2	26.9	15.9	0.0022	0.75
		D6-57	74	0.63	47.0	30.9	26.6	16.1	0.0021	0.93
		D6-85	74	0.72	46.8	30.5	26.0	16.2	0.0033	1.13
		D10-36	74	0.72	50.8	32.1	25.4	18.7	0.0039	1.04
		D10-61	74	0.57	45.9	31.9	23.8	14.1	0.0023	0.85
		D10-67	74	0.64	46.1	27.6	24.2	18.4	0.0024	0.97

Table A3.2: Mean tree measurements in **Grison**, **Quartier** and **Mélagues** forests. D_{BH} is the diameter at breast height, D_0 the average diameter of the dominant trees, H the total tree height, H_{LC} the height of the base of the living crown, H_{LLB} the height of the lowest living branch, L_{LC} the length of the living crown, RW_5 the average ring width of the five last rings at breast height.

Forest	Thinning intensity	Tree ID	Age (year)	D_{BH} (m)	H (m)	H_{LC} (m)	H_{LLB} (m)	L_{LC} (m)	RW_5 (m)	D_{BH} $/D_0$
Grison	high	GT1	44	0.15	19.8	17.2	15.2	2.5	0.0000	0.38
		GT2	44	0.21	22.1	17.9	17.6	4.2	0.0001	0.54
		GT3	44	0.23	27.8	19.5	18.9	8.3	0.0017	0.63
		GT4	44	0.29	26.0	20.6	16.5	5.4	0.0020	0.75
		GT5	44	0.31	27.0	18.3	17.6	8.7	0.0021	0.85
	medium	GI1	44	0.23	21.6	16.6	15.2	5.0	0.0008	0.58
		GI2	44	0.27	22.9	15.0	11.0	7.9	0.0018	0.67
		GI3	44	0.28	25.0	10.4	10.4	14.6	0.0027	0.72
		GI4	44	0.34	25.7	13.2	13.0	12.5	0.0034	0.82
		GI5	44	0.41	27.9	13.0	11.9	14.9	0.0041	1.01
	low	GD1	44	0.32	25.3	15.6	4.3	9.7	0.0024	0.67
		GD2	44	0.38	28.2	18.2	16.6	10.0	0.0024	0.79
		GD3	44	0.40	30.3	14.2	11.0	16.1	0.0038	0.82
		GD4	44	0.42	29.3	12.9	12.7	16.4	0.0038	0.87
		GD5	44	0.44	28.8	14.7	12.7	14.1	0.0040	0.93
Quartier	high	QT1	23	0.08	11.0	5.3	4.5	5.7	0.0004	0.40
		QT2	23	0.11	12.3	5.3	4.5	6.9	0.0016	0.55
		QT3	23	0.13	12.7	8.6	4.7	4.1	0.0004	0.63
		QT4	23	0.14	13.8	7.2	6.2	6.6	0.0014	0.69
		QT5	23	0.18	14.7	6.2	5.3	8.4	0.0021	0.92
	medium	QI1	23	0.12	11.4	3.7	2.2	7.7	0.0014	0.48
		QI2	23	0.14	14.3	4.1	3.3	10.2	0.0030	0.60
		QI3	23	0.17	14.4	4.7	3.0	9.8	0.0027	0.71
		QI4	23	0.19	15.6	4.3	2.6	11.3	0.0049	0.79
		QI5	23	0.23	17.8	4.6	3.3	13.2	0.0063	0.98
	low	QD1	23	0.16	10.2	1.9	1.1	8.3	0.0027	0.55
		QD2	23	0.20	13.9	3.9	1.6	10.0	0.0048	0.69
		QD3	23	0.24	12.6	2.8	1.9	9.8	0.0053	0.80
		QD4	23	0.24	13.9	2.7	1.0	11.2	0.0066	0.86
		QD5	23	0.30	14.7	4.4	2.3	10.3	0.0053	0.98
Mélagues	high	D5	50	0.21	27.2	24.1	17.8	3.1	0.0000	0.48
		D6	50	0.43	31.8	20.6	18.9	11.2	0.0022	0.98
		D7	50	0.29	30.6	20.4	18.1	10.3	0.0010	0.68
		D8	50	0.29	31.2	19.1	17.6	12.1	0.0010	0.65
	low	D1	50	0.51	30.7	13.9	11.1	16.8	0.0038	0.92
		D2	50	0.43	34.1	14.0	10.4	20.1	0.0031	0.75
		D3	50	0.47	26.6	10.5	8.2	16.1	0.0036	0.85
		D4	50	0.64	33.6	12.2	8.9	21.4	0.0039	1.06

APPENDIX A4

Under-bark stem radius and heartwood radius profiles for each tree of the calibration dataset

The following graphics show the patterns of heartwood (red) and sapwood (yellow) for each tree in the calibration dataset. The title of each page indicates the dataset (Écouves_2010, Écouves_2021, Grison, Quartier, Mélagues) and the density treatment (low, medium, high). Tree names are given in the top-right corner of each individual plot. The green lines represents the base of the living crown (solid line) and the lowest living branch (dotted line).

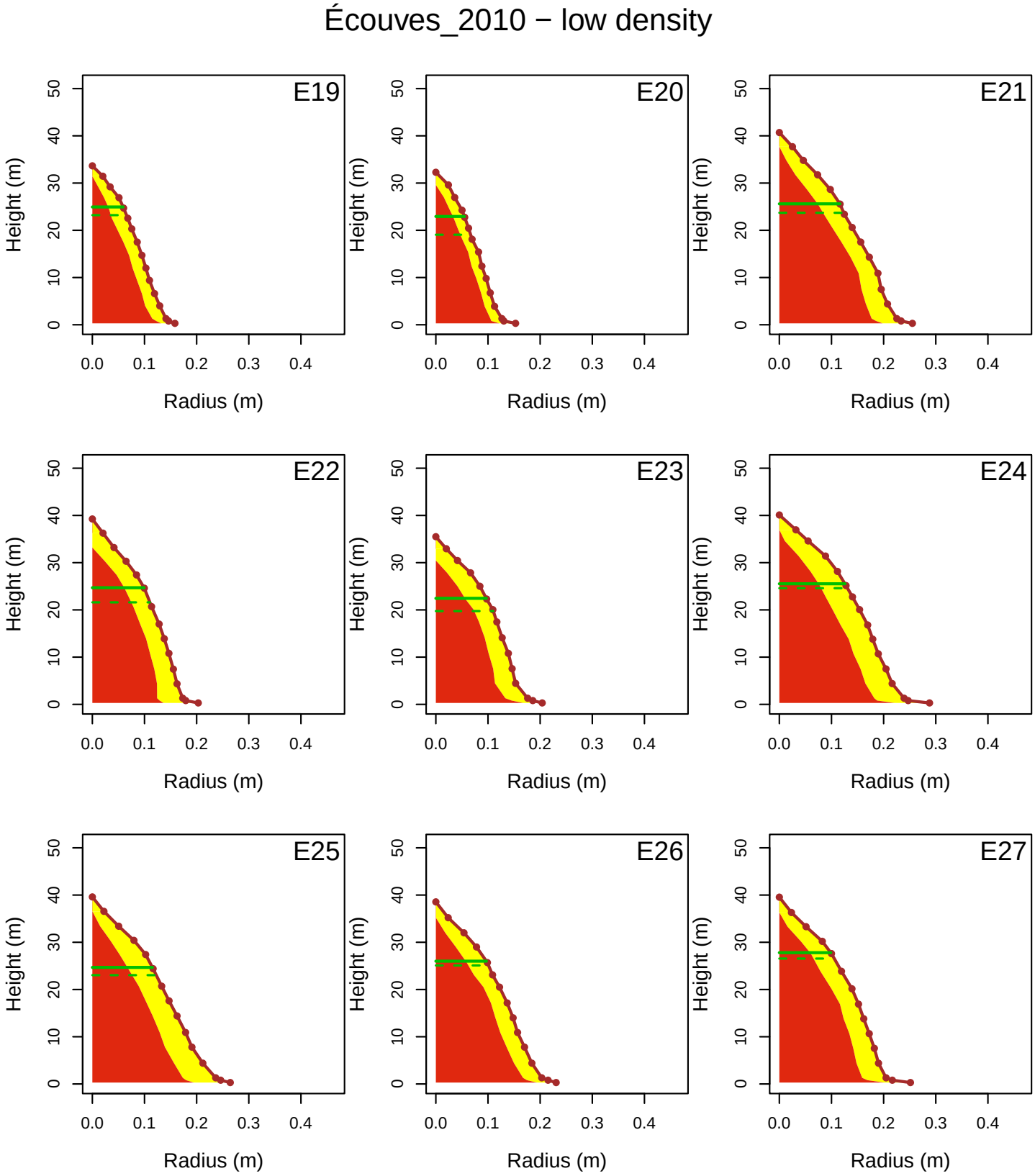

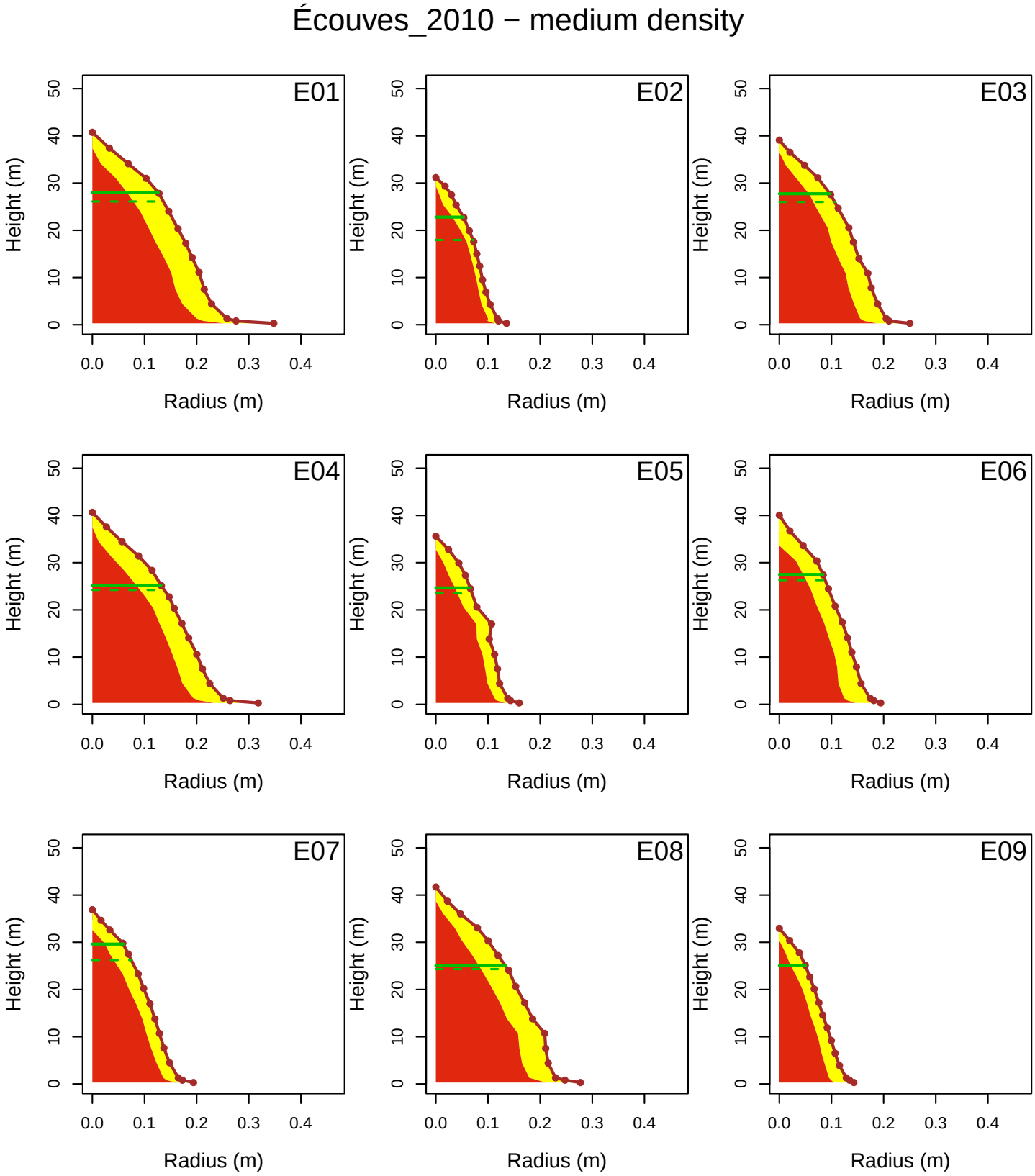

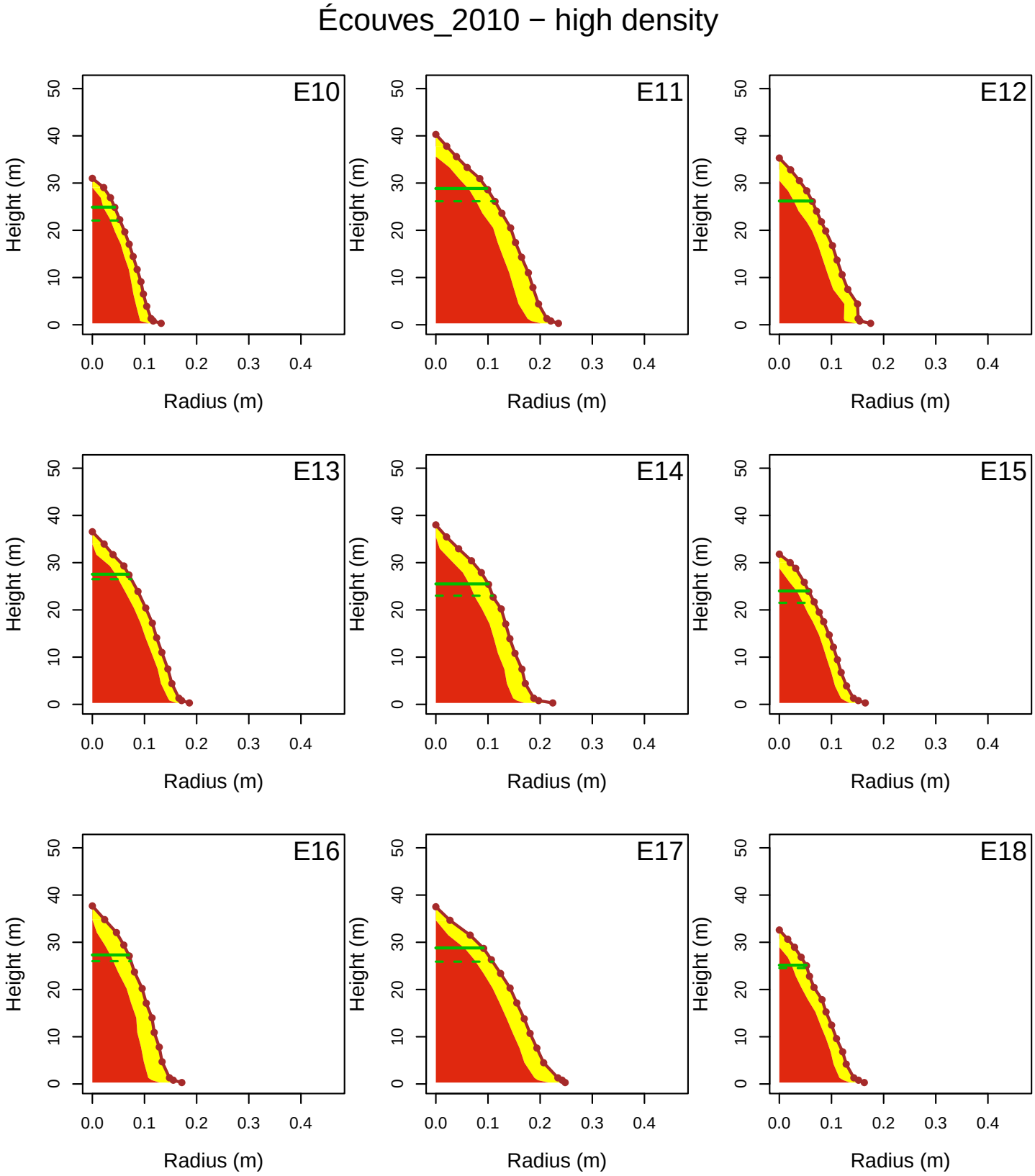

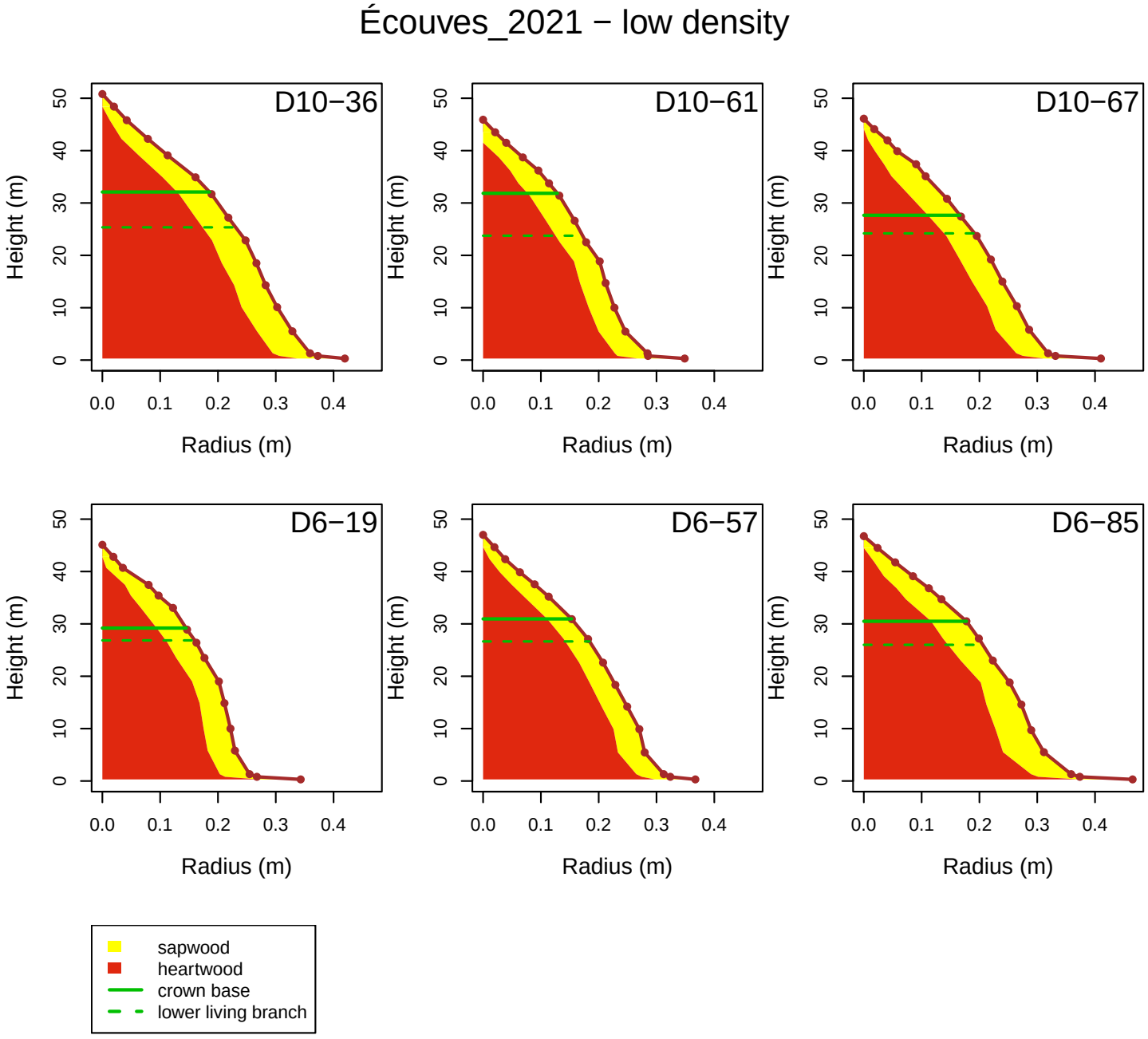

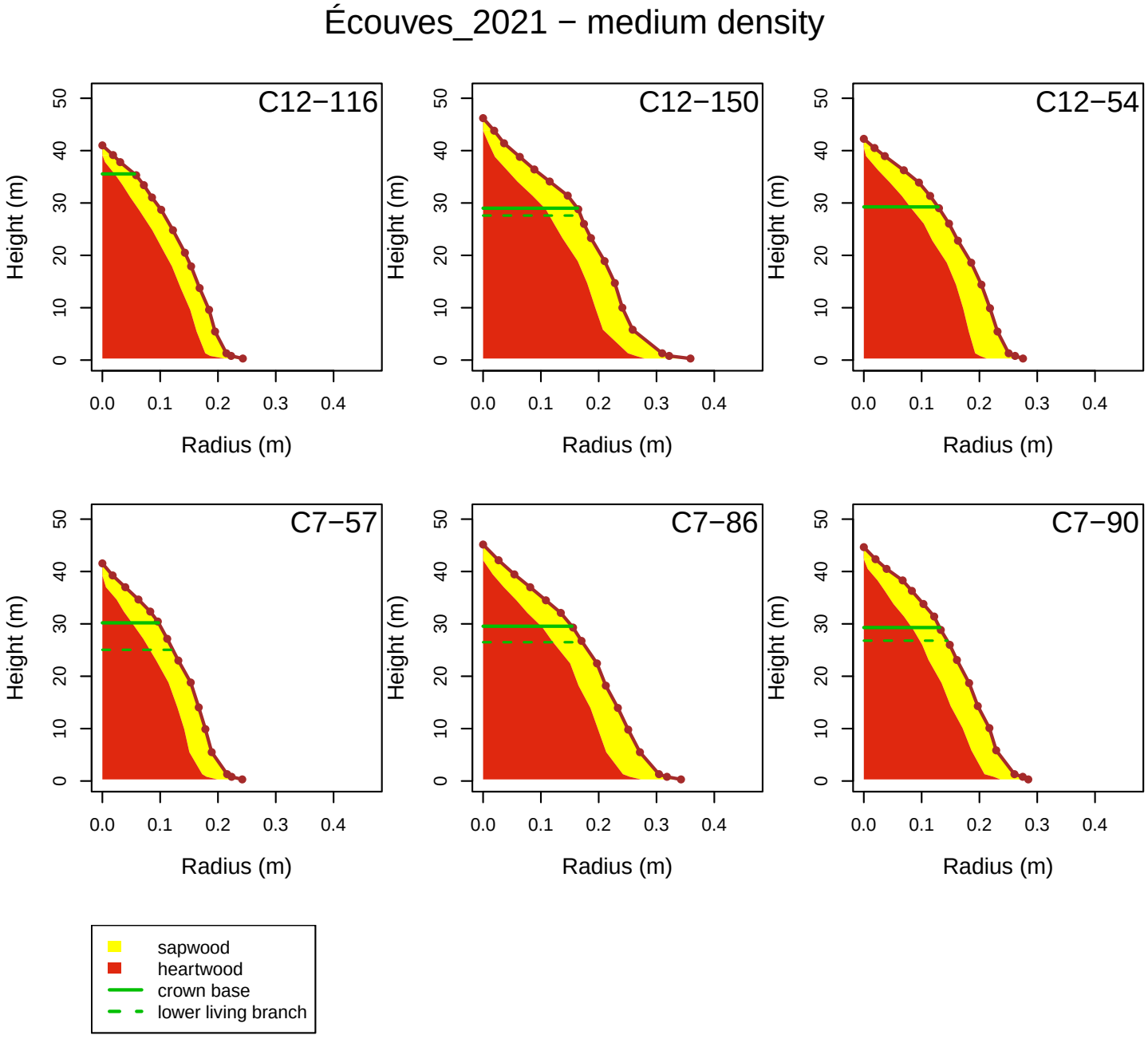

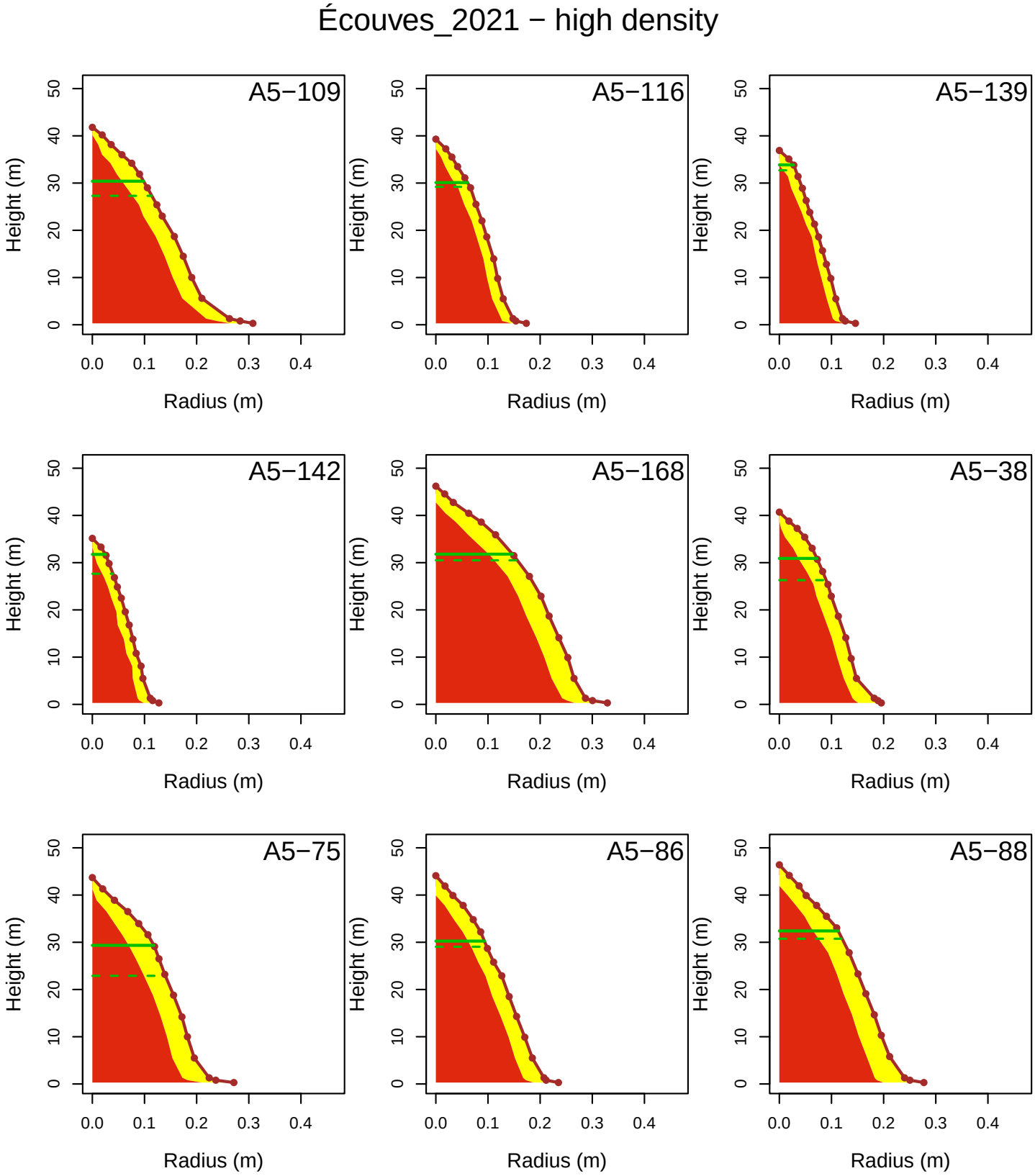

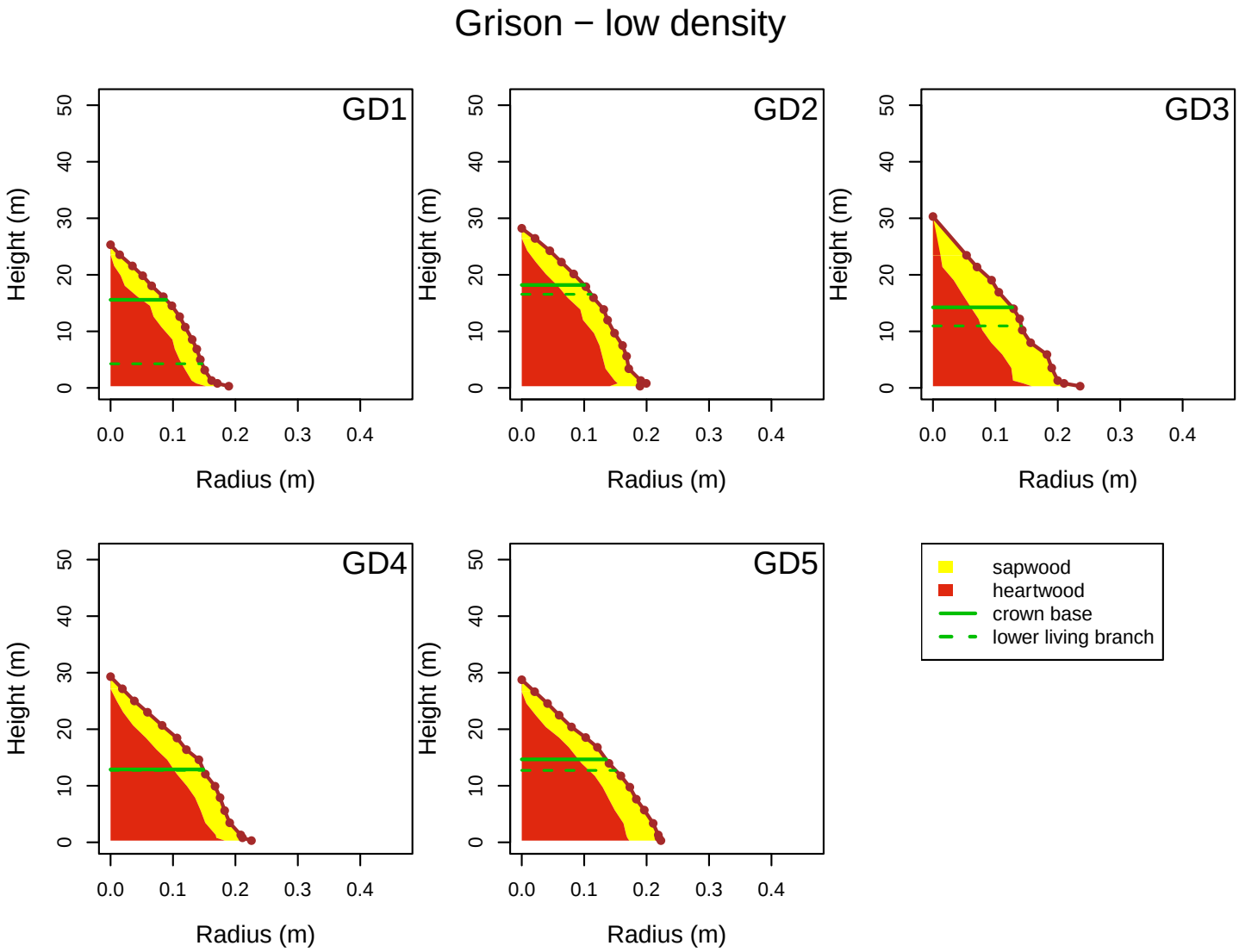

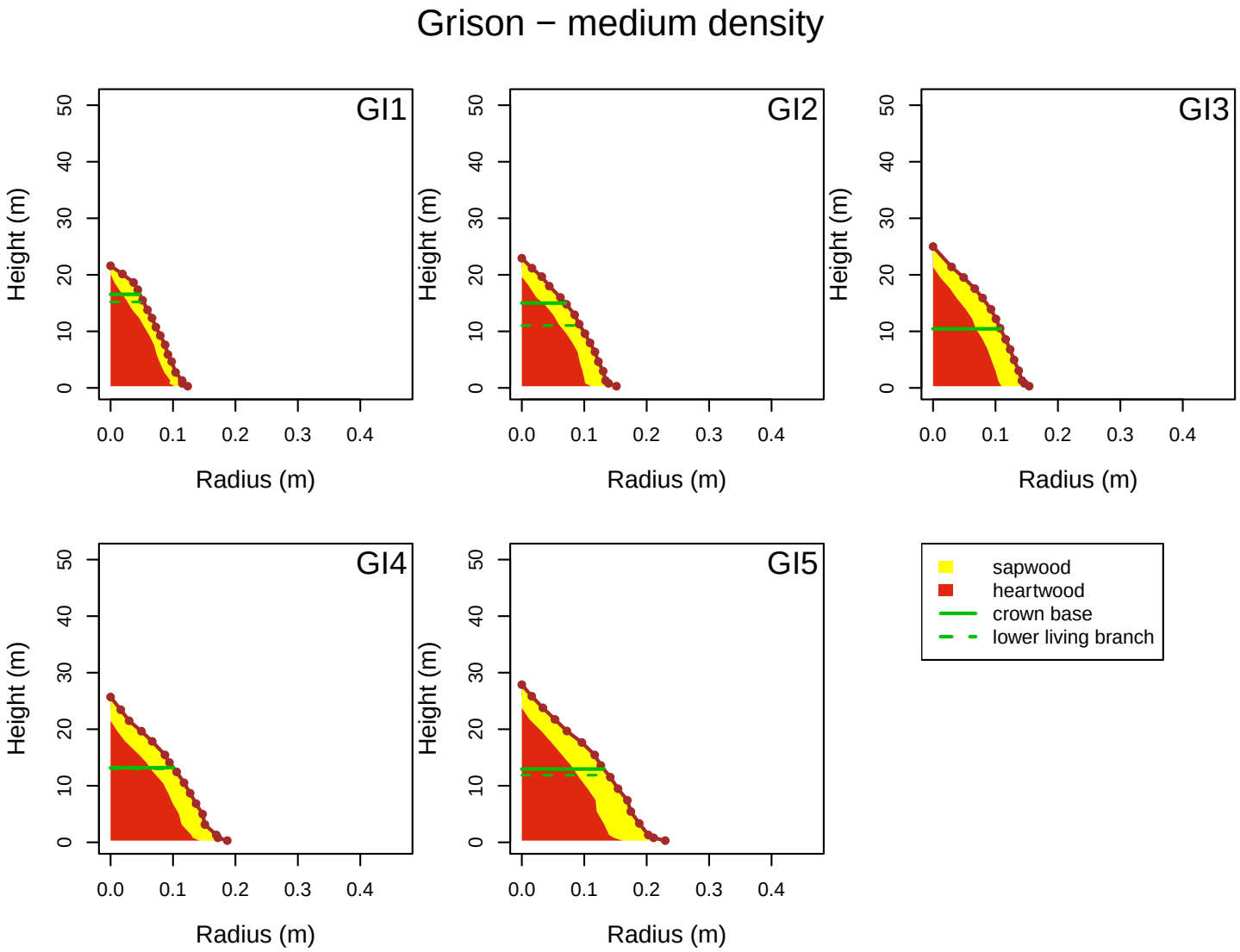

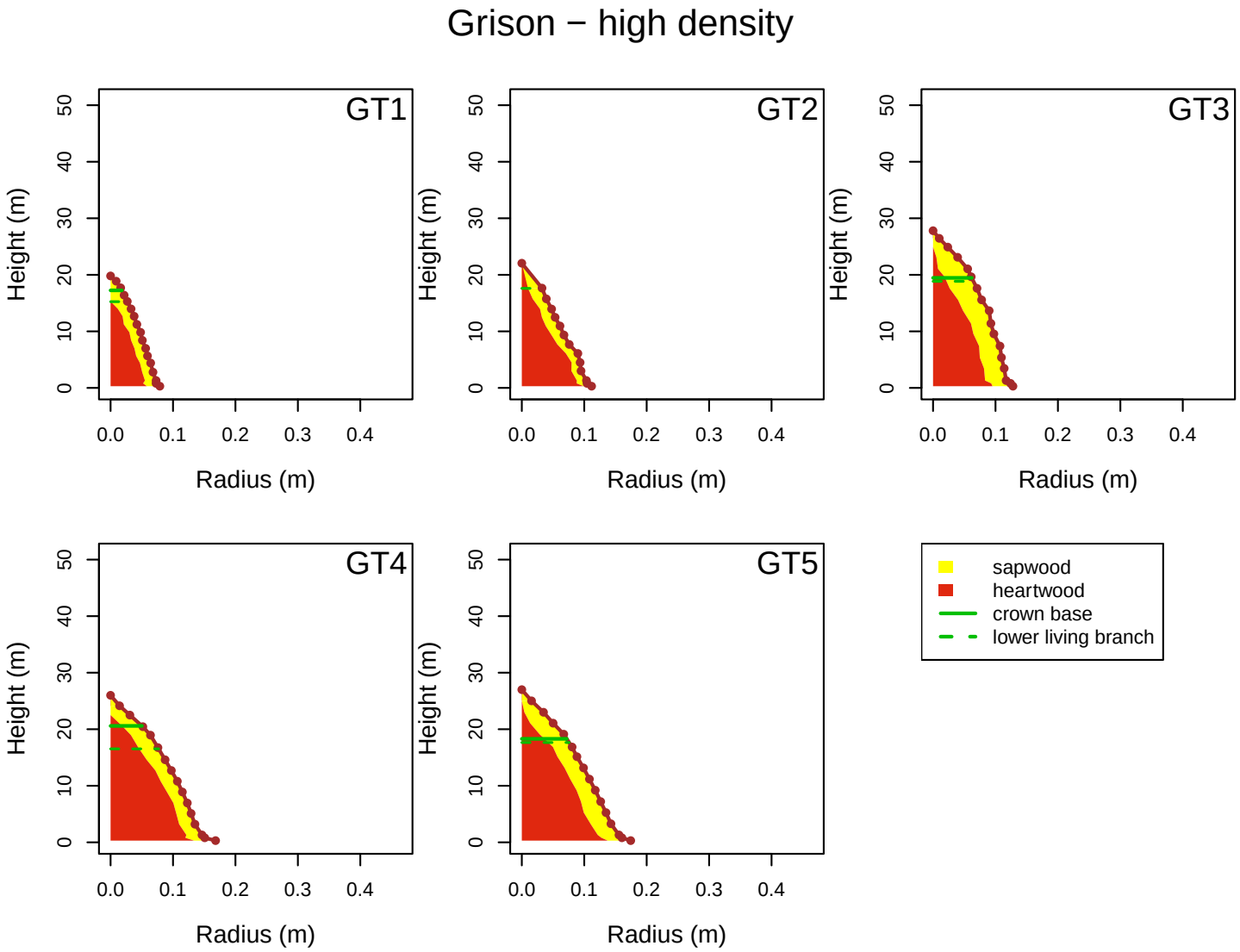

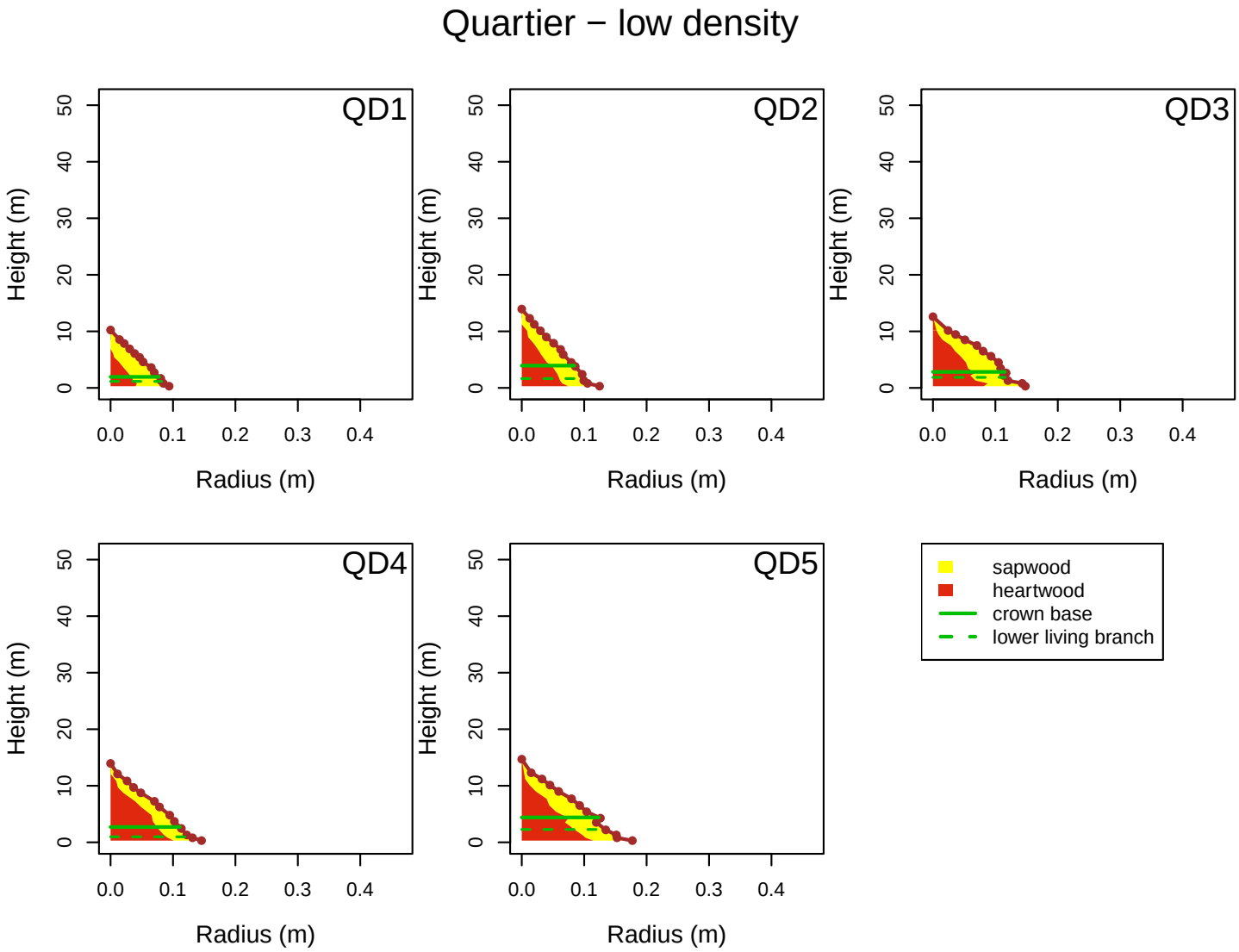

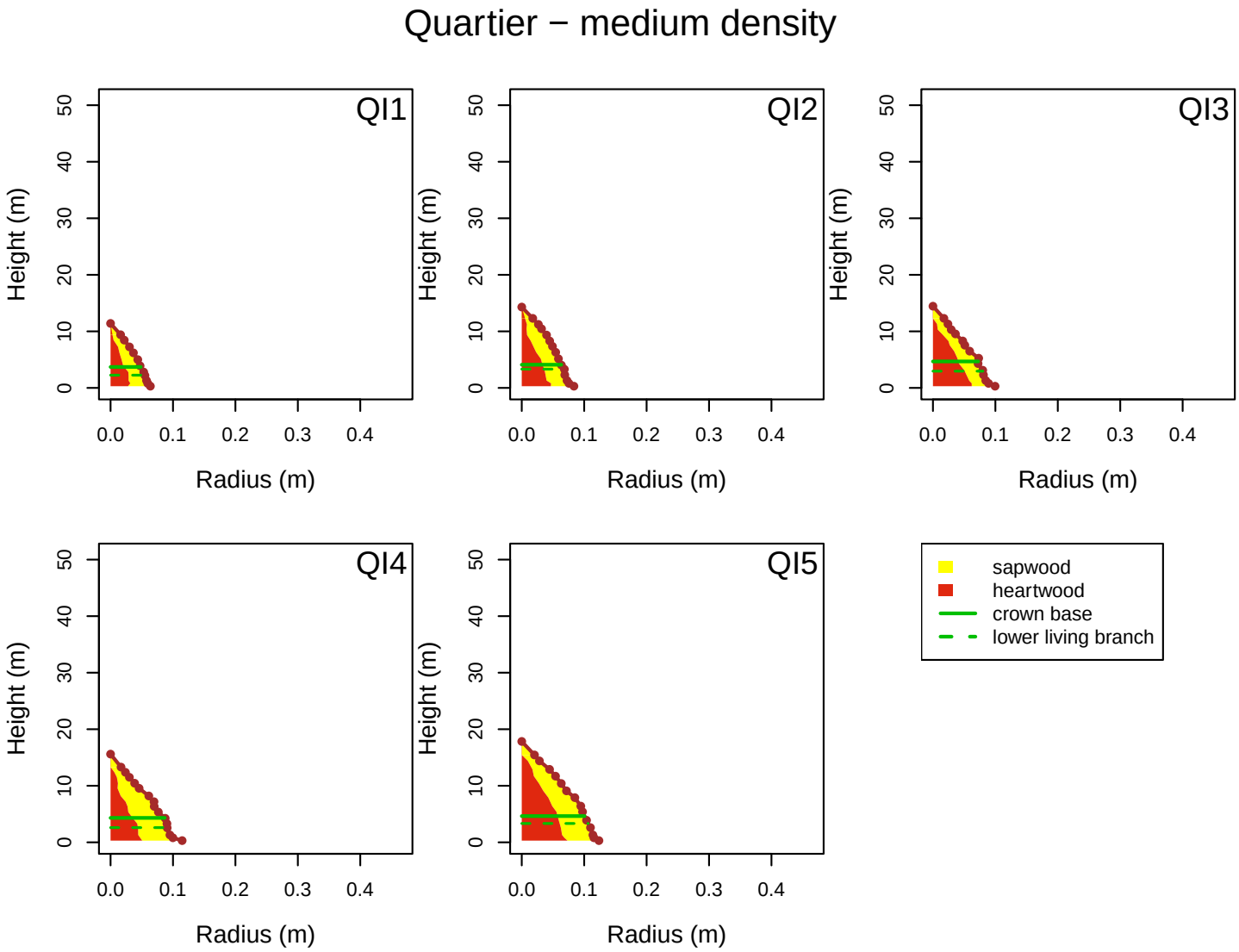

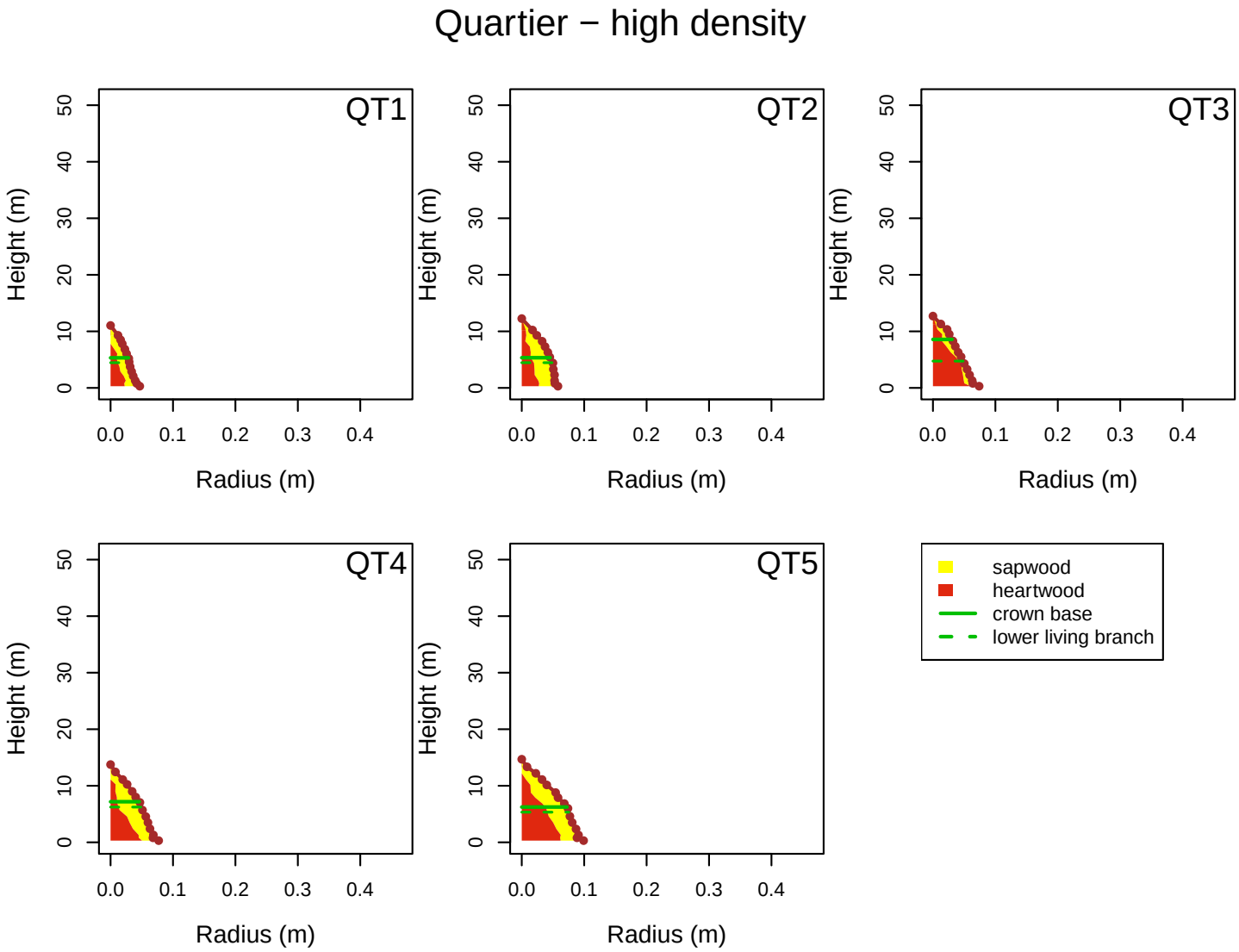

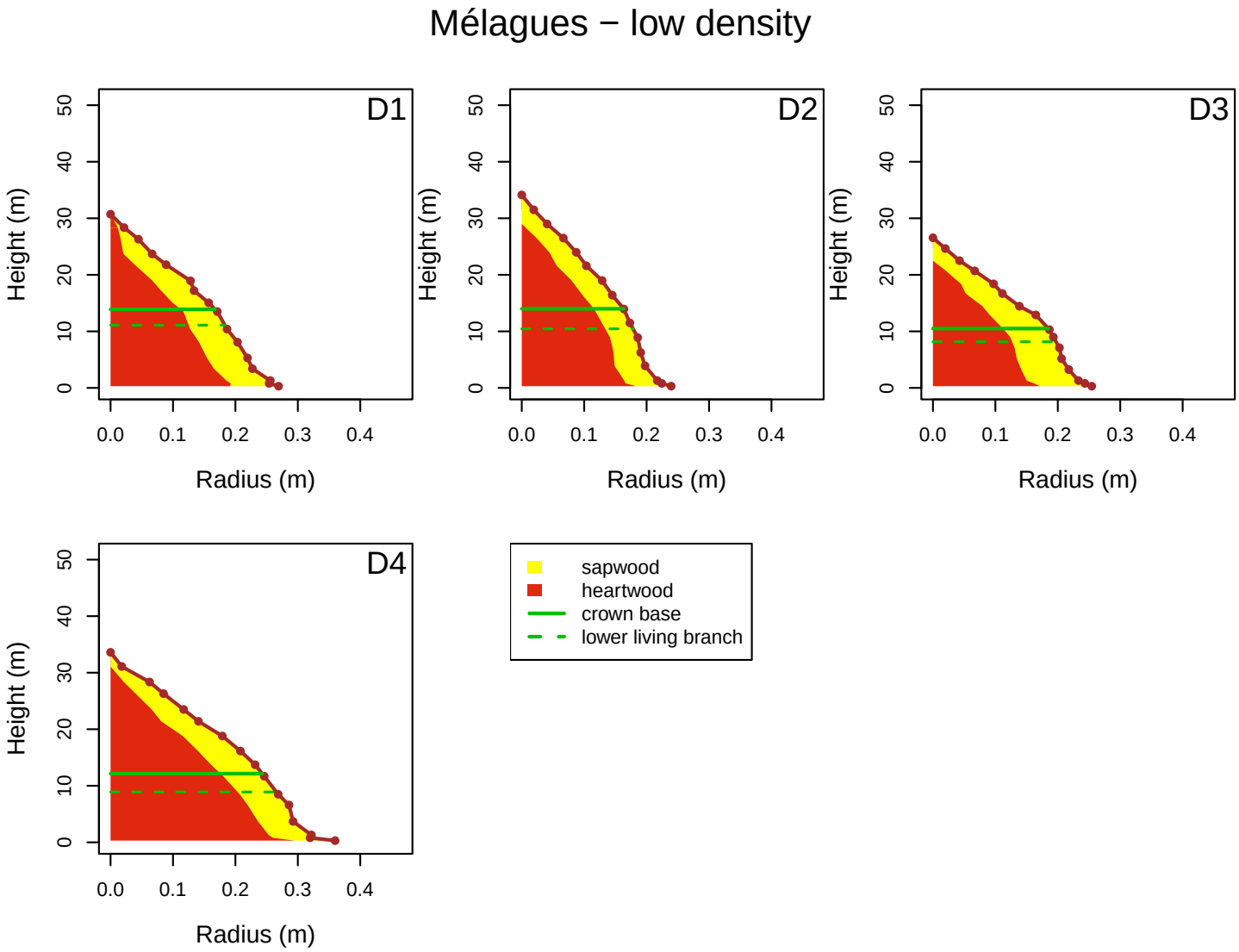

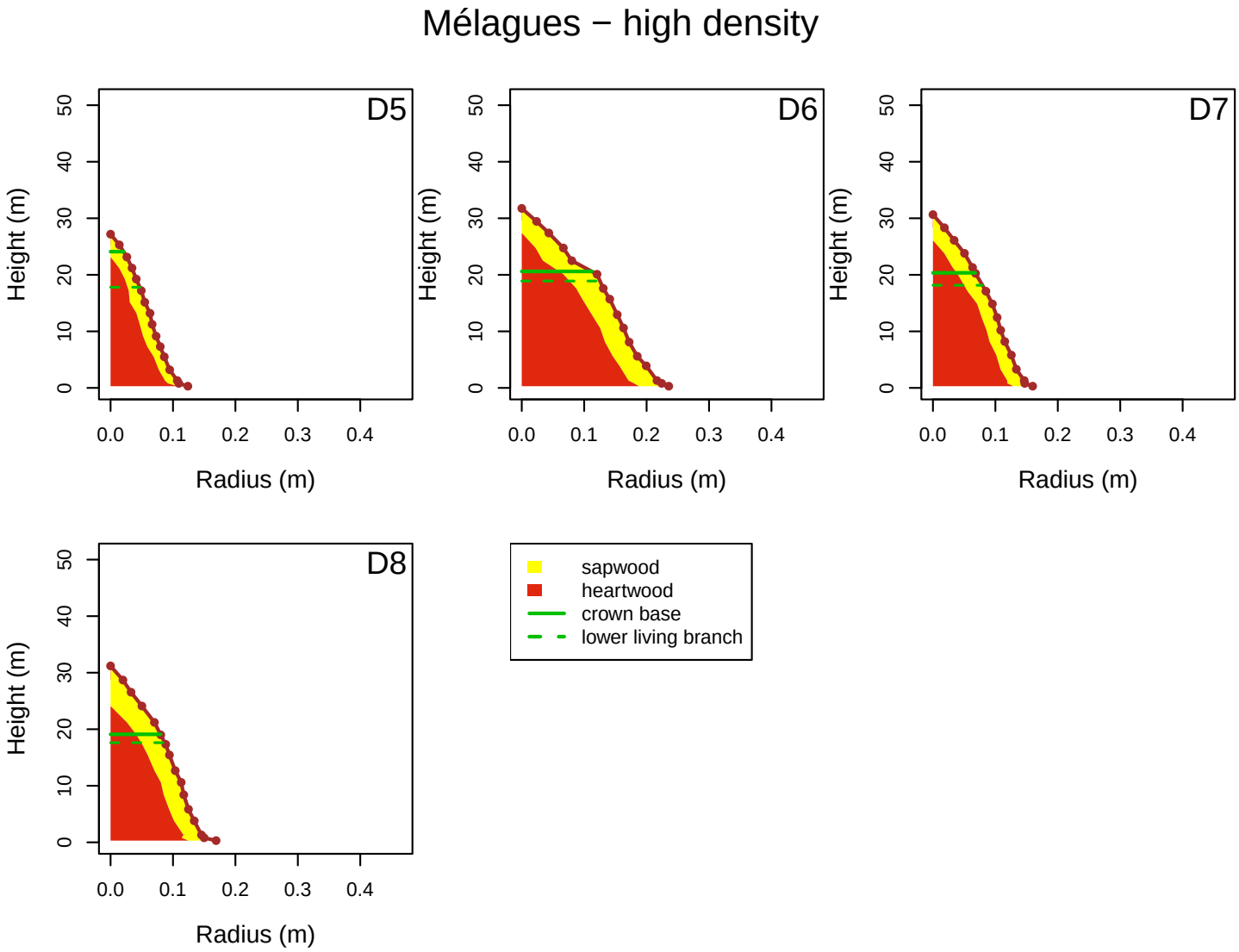

APPENDIX A5

DBH distributions for the different datasets

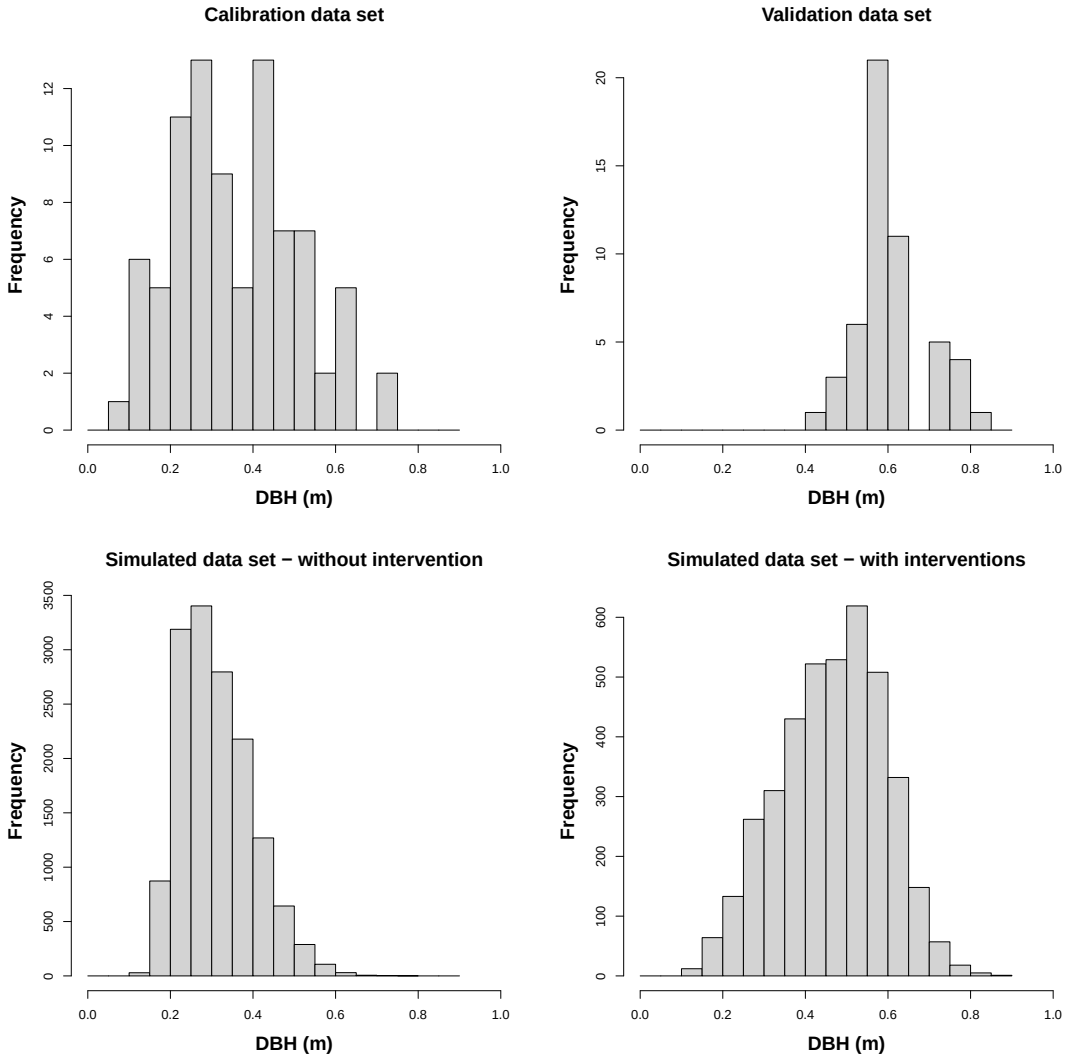

Figure A5.1: Diameter distributions at 1.30 m for trees in the different data sets: calibration set, validation set and simulated data with the two scenarios, without and with interventions. For the simulated data, the trees from the 50 different simulations are shown together.

APPENDIX A6

Estimation of slenderness for trees in the **TreeTrace_Douglas** validation dataset

For trees in the **TreeTrace_Douglas** validation dataset, the *slenderness* (H/D_{BH}) was estimated from the $slenderness_{12}$ by fitting a linear regression on trees from the calibration dataset.

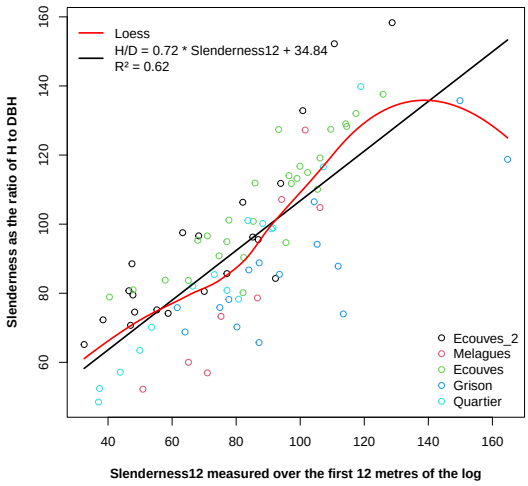

Figure A6.1: Ratio of H to D_{BH} (*slenderness*) as a function of the slenderness measured over the first 12 metres of the log ($slenderness_{12}$).

APPENDIX A7

Variability of candidate explanatory variables between sites and between silvicultural modalities within sites

For SimCop simulations, only the final cut trees for the 50 simulations are shown, i.e. 14 815 trees for the treatment without intervention and 3950 for the treatment with intervention.

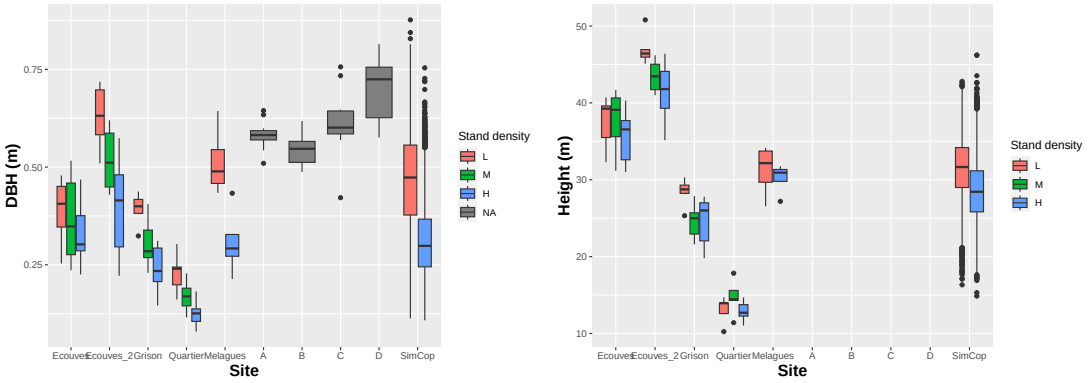

Figure A7.1: Variability of tree size: Diameter at breast height (D_{BH}) (on the left) and total tree height (H) (on the right). Tree height was not available for the **TreeTrace_Douglas** validation dataset (sites A, B, C and D) that involved logs measured on a log yard.

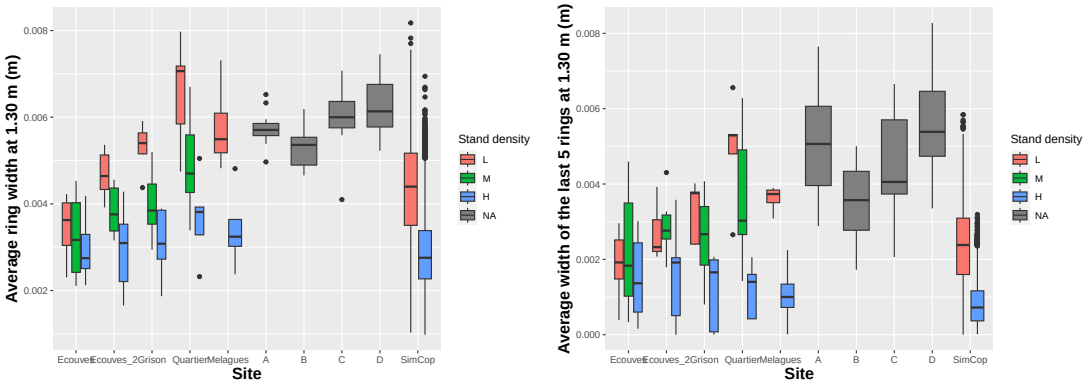

Figure A7.2: Variability of radial growth: Average ring width (RW) (on the left) and average width of the last five rings (RW_5) (on the right).

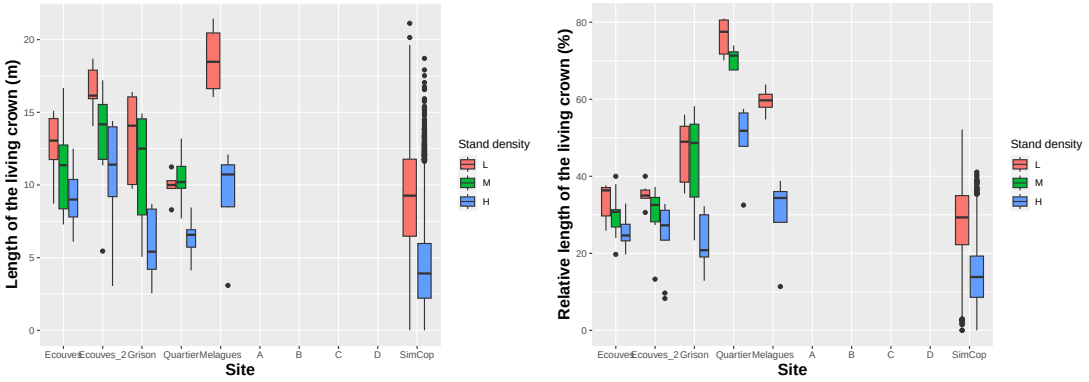

Figure A7.3: Variability of crown size: Length of the living crown (L_{LC}) (on the left) and relative length of the living crown (on the right). Crown length was not available for the **TreeTrace_Douglas** validation dataset (sites A, B, C and D) that involved logs measured on a log yard.

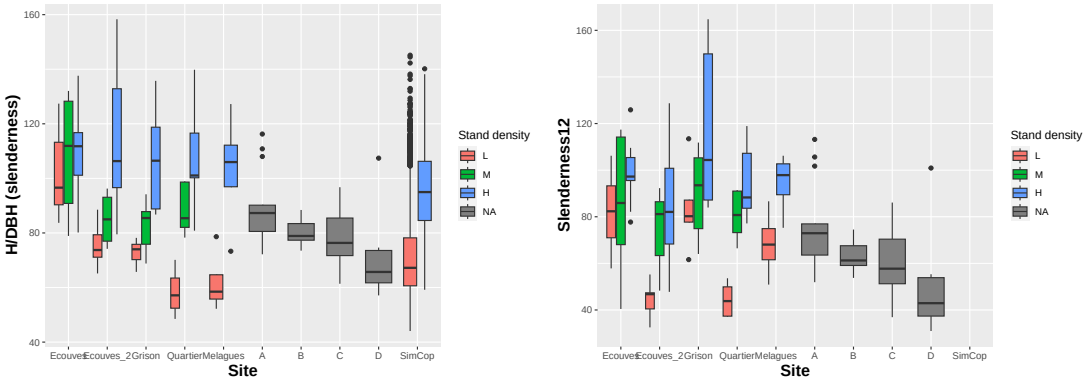

Figure A7.4: Variability of *slenderness*: Ratio of tree total height (H) to diameter at breast height (D_{BH}) (H/D_{BH}) (on the left) and $slenderness_{12}$ measured over the first 12 metres of the stem (on the right). H/D_{BH} was estimated from $slenderness_{12}$ for the **TreeTrace_Douglas** validation dataset (sites A, B, C and D) as explained in Appendix A6. $slenderness_{12}$ was not calculated for trees simulated with SimCop.

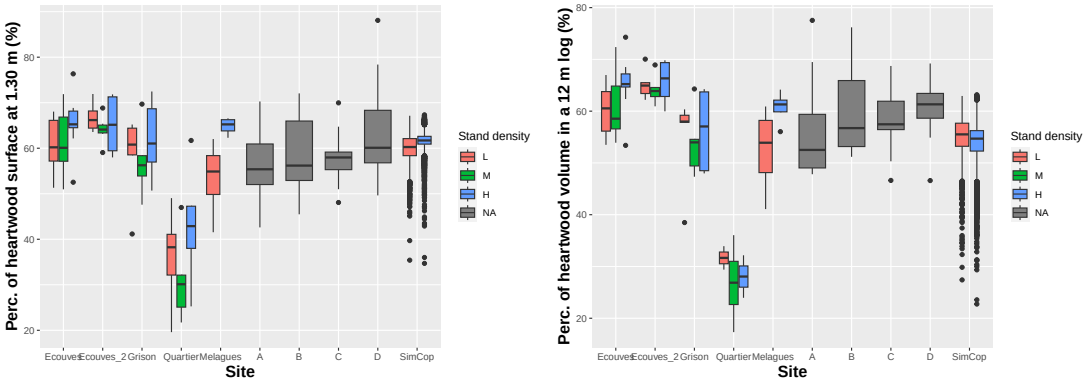

Figure A7.5: Variability of heartwood size: Percentage of heartwood surface at 1.30 m (on the left) and percentage of the volume of heartwood in relation to the total volume under-bark of a 12 m long log (on the right). A log length of 12 m from 0.30 m to 12.30 m high in the stem was chosen because this is what was available in the validation data.

APPENDIX A8

Simulations with SimCop

Two silvicultural scenarios were simulated using the SimCop simulator implemented in the Capsis platform. The initial density was set at 1111 stems/ha in both cases. In the "no intervention" treatment, no action was taken until the trees were harvested at 55 years of age. In the "with intervention" treatment, five thinning operations were simulated in order to maintain the RDI at around 0.45 before final harvesting at 55 years of age. Fifty repetitions of each scenario were simulated. Figure A8.1 shows the evolution over time of several stand variables in both cases. Figure A8.2 shows the volumes obtained during thinning and final cutting using the (D) model to predict the proportion of heartwood.

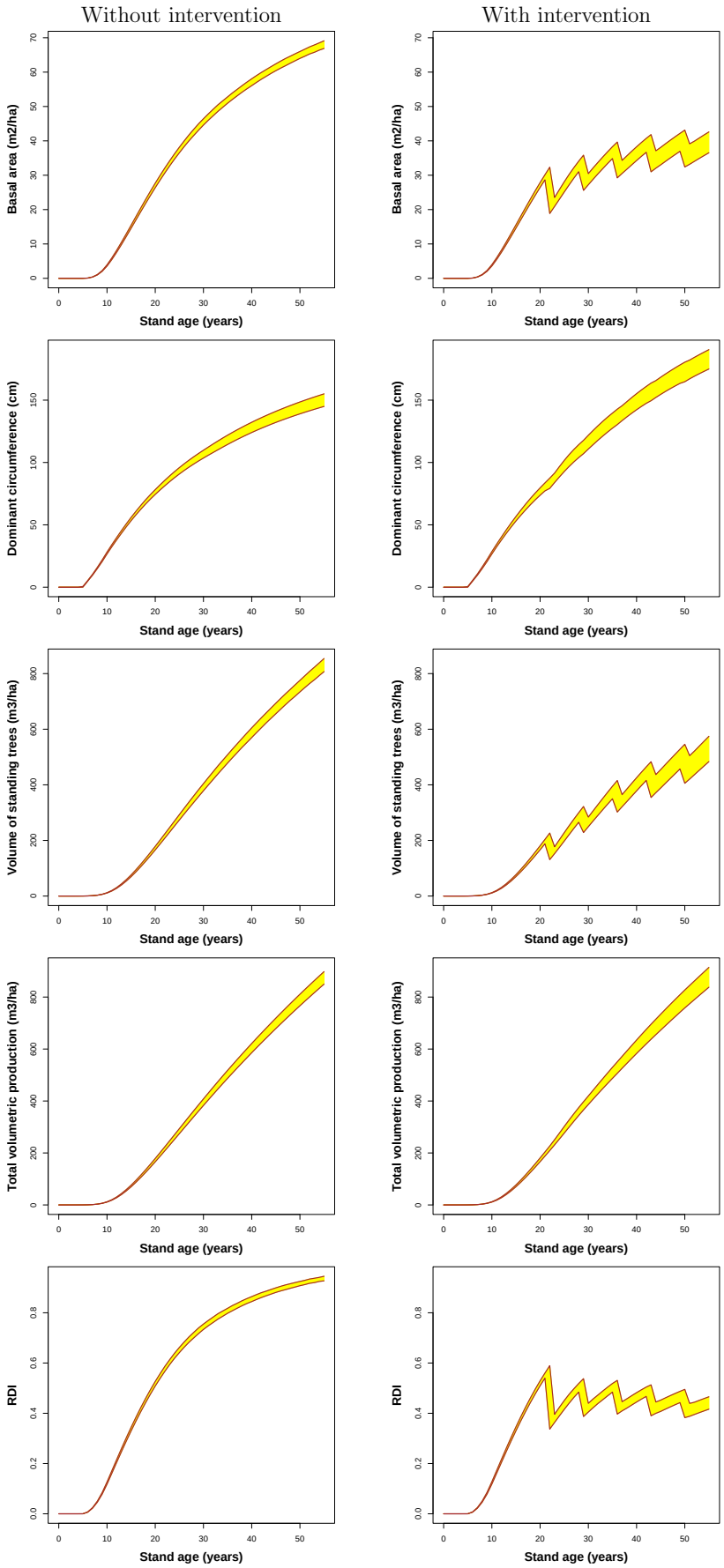

Figure A8.1: Evolution of basal area, dominant circumference, volume of standing trees, total volumetric production (volume of standing trees + cumulated volume of cut and dead trees) and *RDI* with time for both scenarios. The red lines show the maximal and minimal values obtained over 50 repetitions.

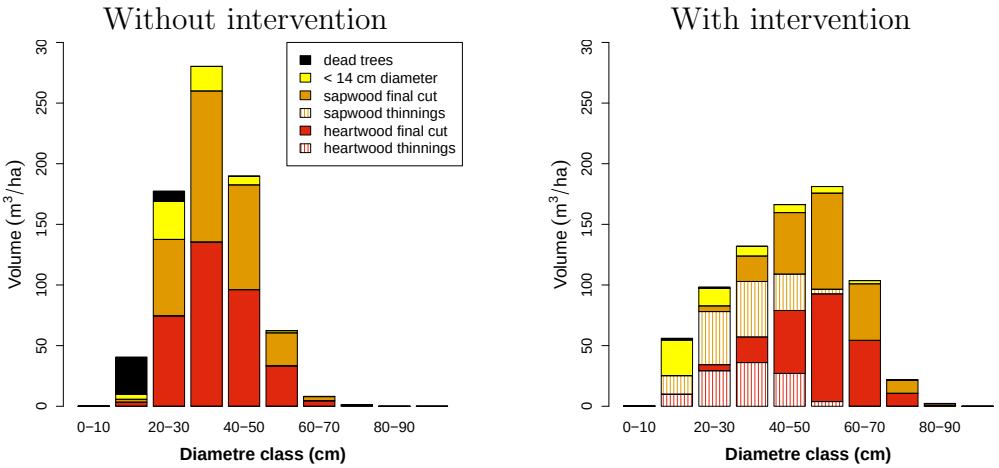

Figure A8.2: Heartwood/sapwood volumes predicted by the model (C) from growth simulations by diameter classes for the two studied scenarios: Volumes of sapwood (brown) and heartwood (red) collected during thinning operations (hatched lines) and final cut (plain colour) considering only the stem part above 14 cm in diameter, total above ground volume below 14 cm in diameter (yellow) and volume of dead trees (black).

APPENDIX A9

Heartwood radius as a function of under-bark stem radius for each tree of the calibration dataset

The following graphics show the relationship between heartwood radius (R_{HW}) and under-bark stem radius (R_{UB}) for each tree in the calibration dataset. The title of each page indicates the dataset (Écouves_2010, Écouves_2021, Grison, Quartier, Mélagues) and the density treatment (low, medium, high). Tree names are given in the top-left corner of each individual plot. The red lines correspond to the 4-parameter model (Equation (1)) fitted with tree random effects on parameters a, b and c and depending only on the under-bark stem radius. In this way it was possible to estimate tree specific values for a, b and c. Parameter s was let fixed for convergence problems. The blue lines correspond to the 9-parameter model (Model (D)) where parameters are predicted by using tree variables.

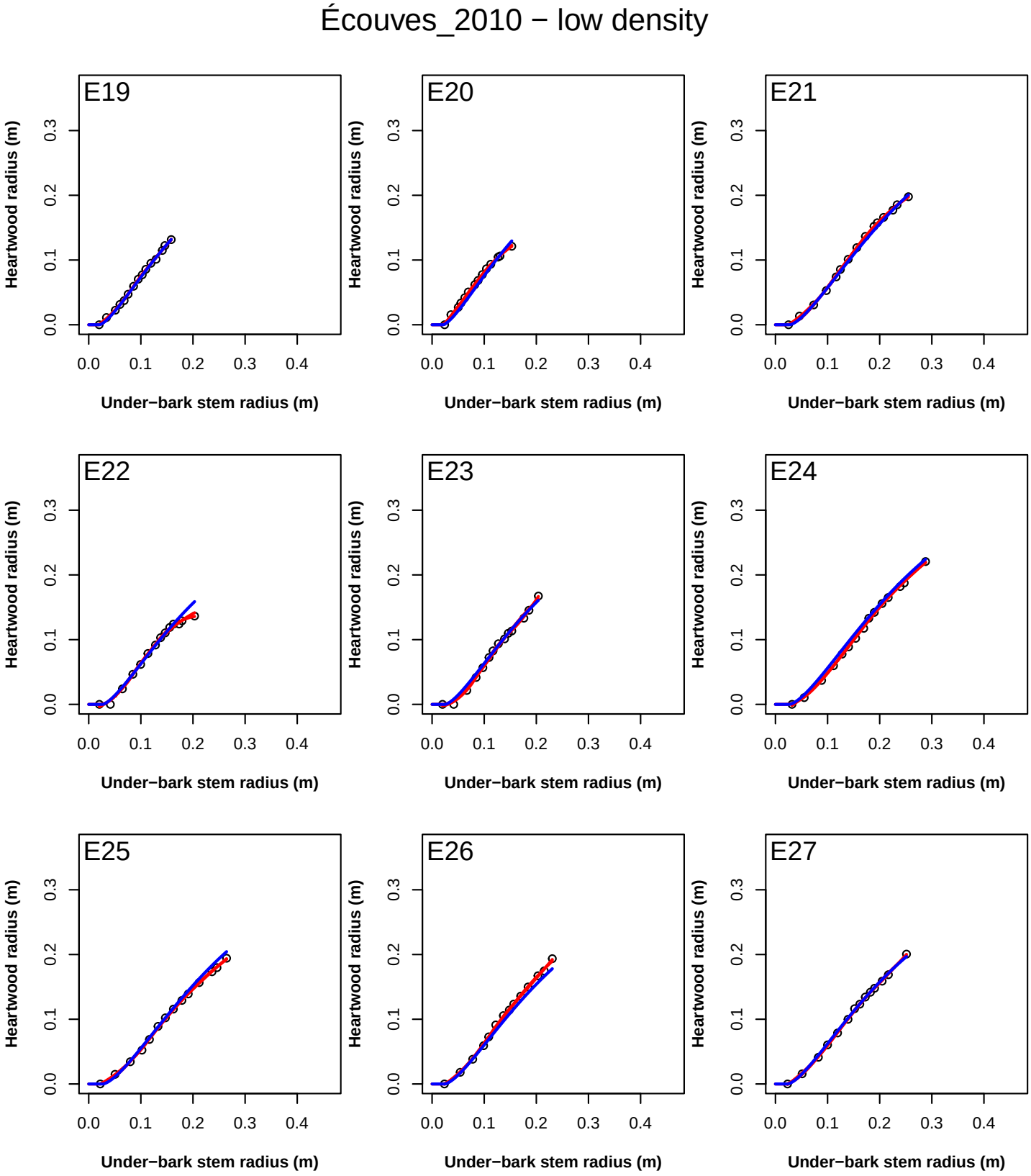

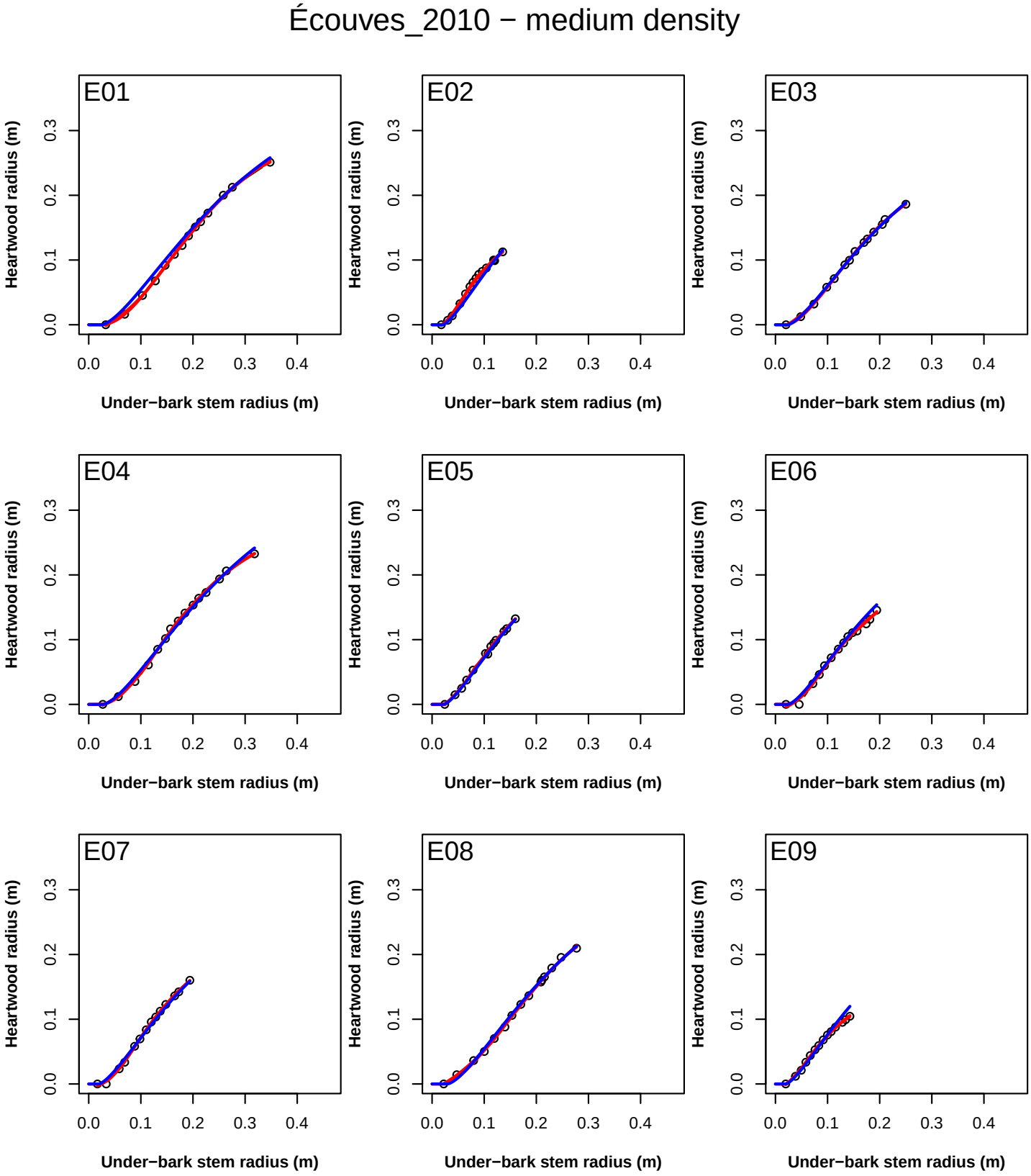

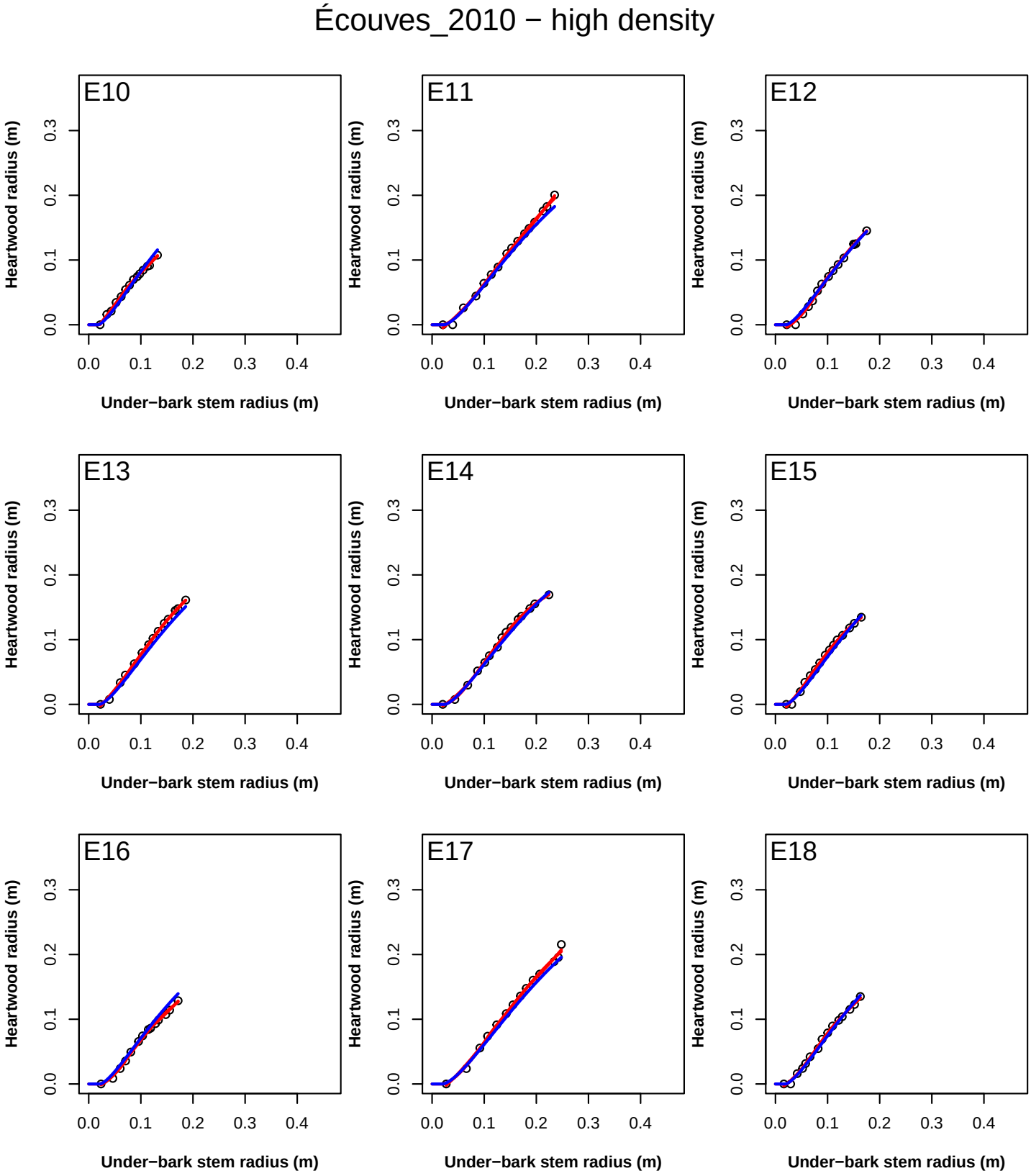

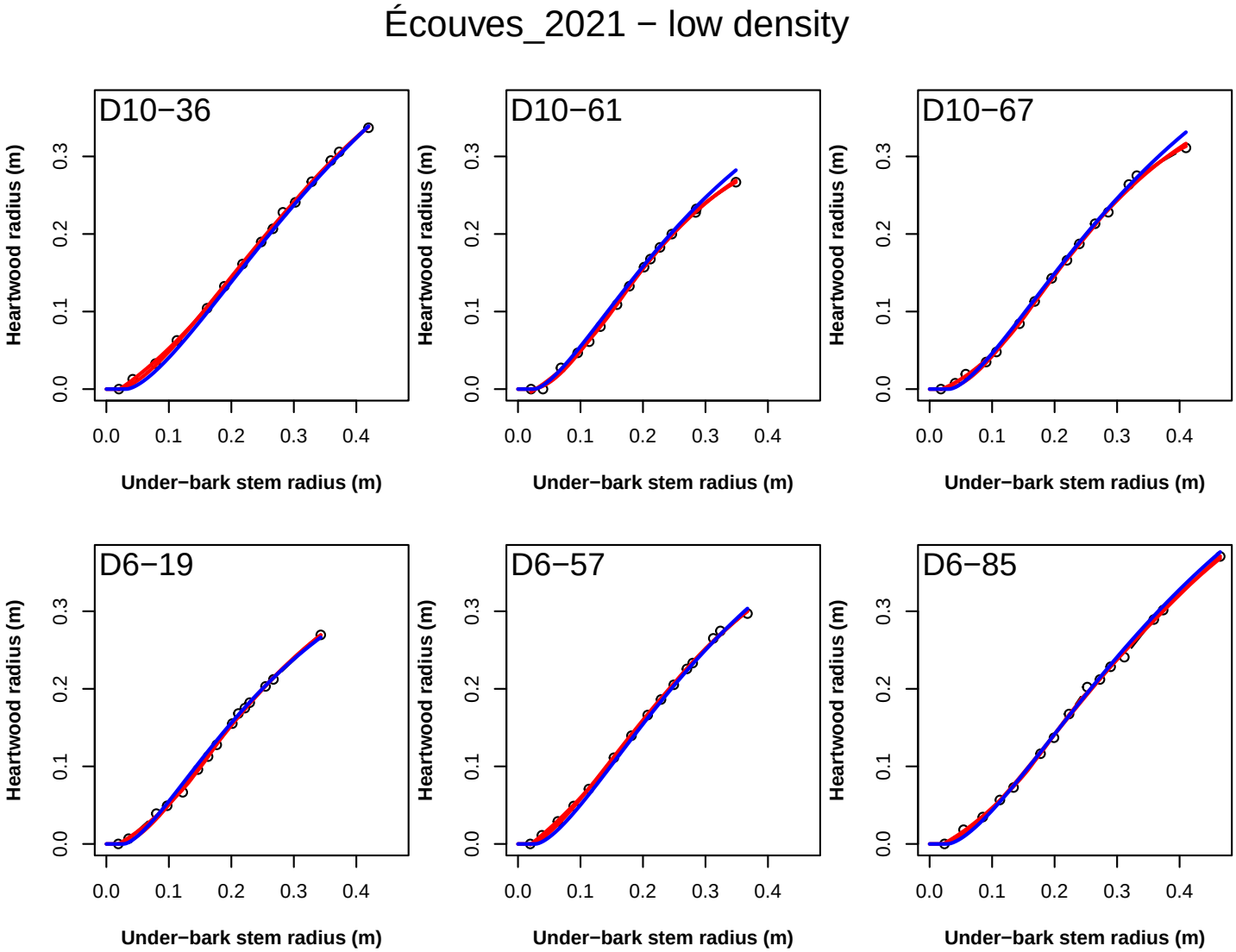

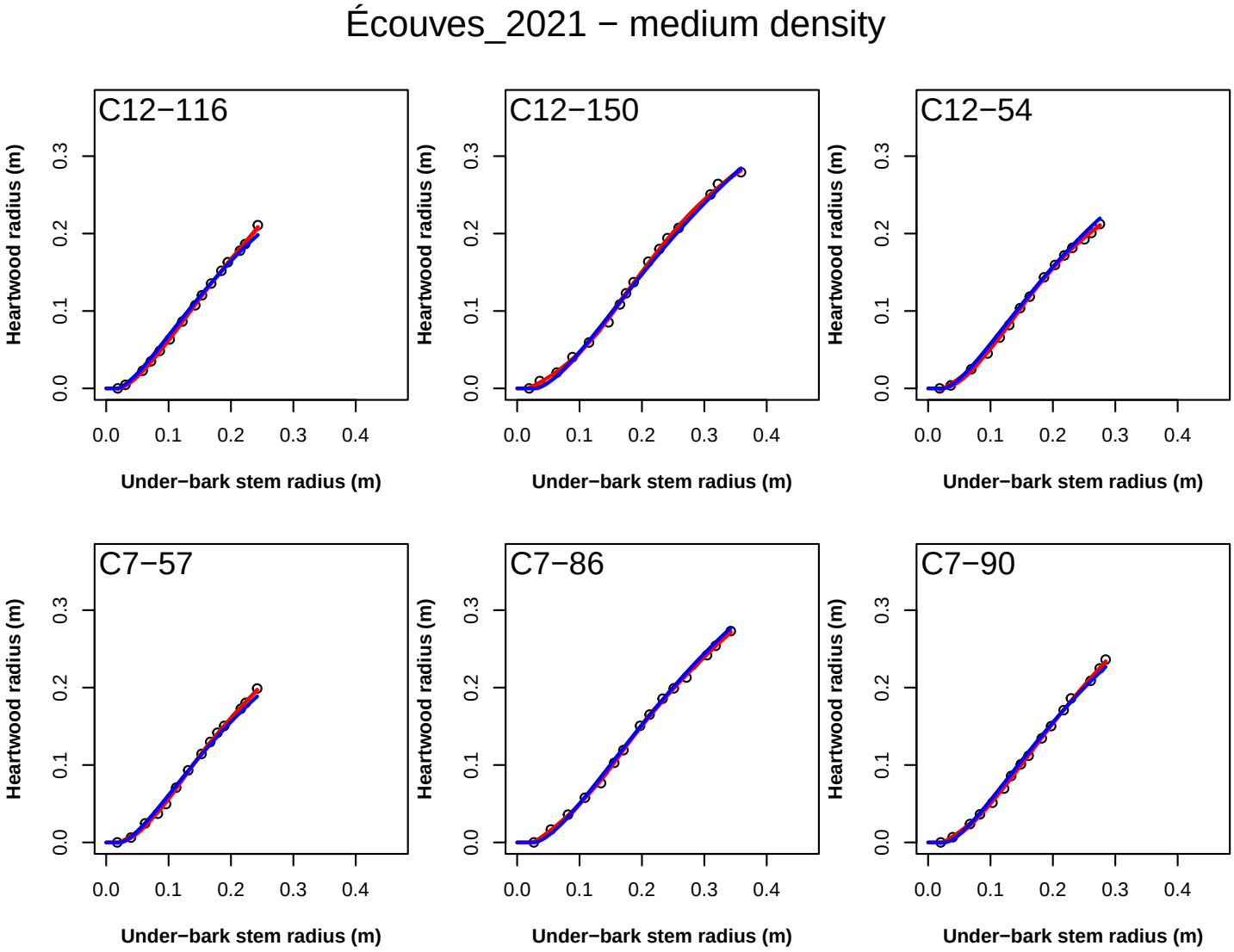

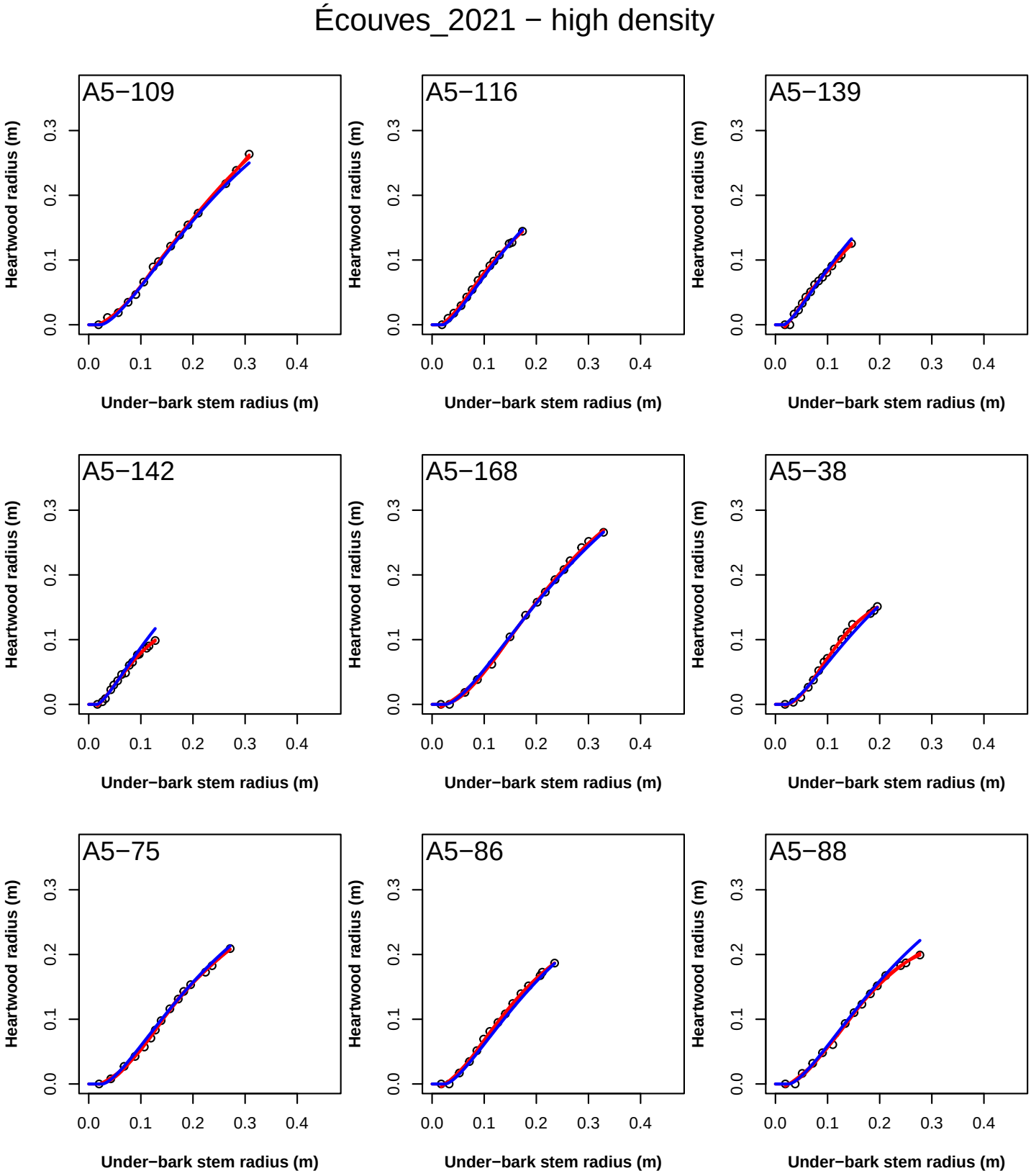

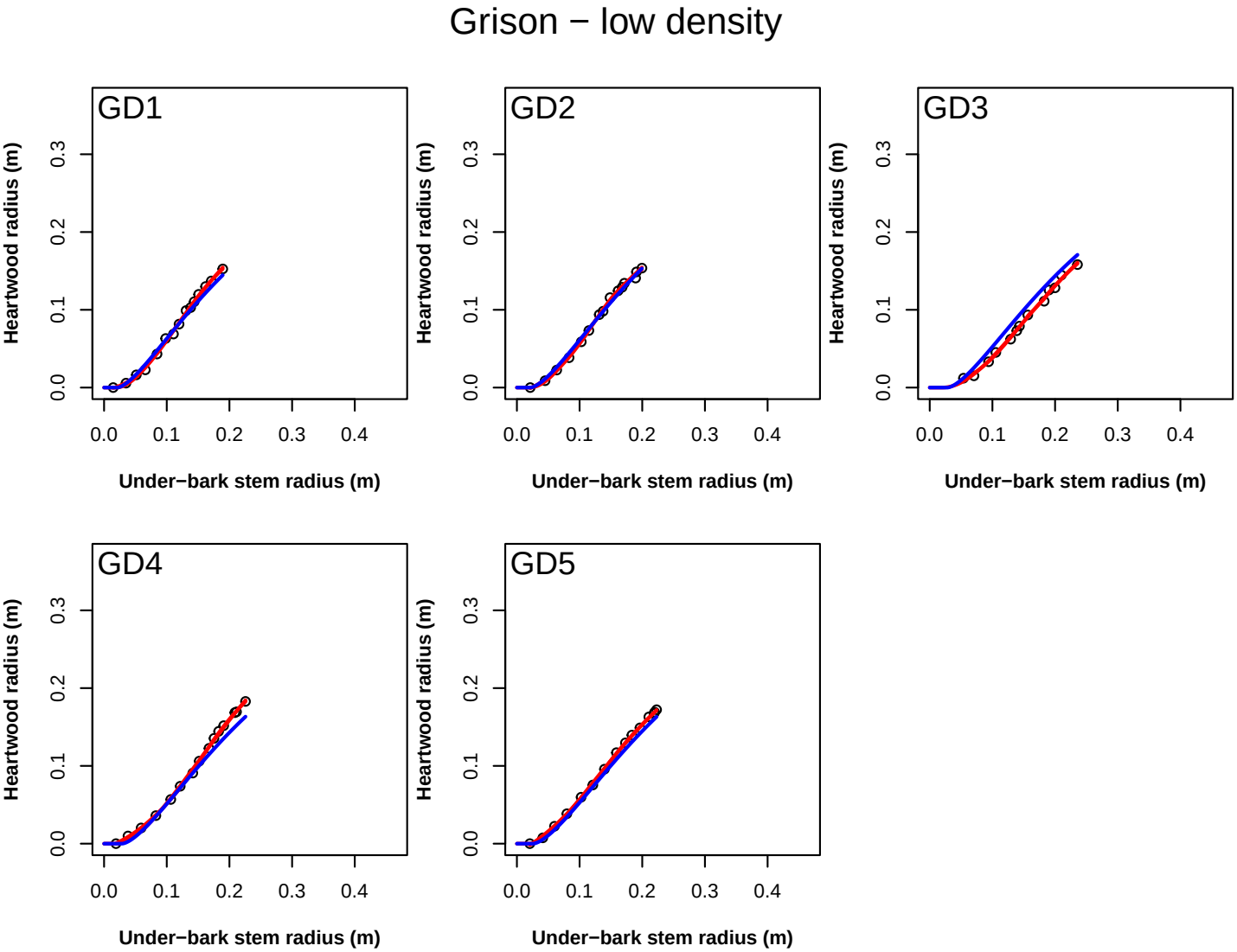

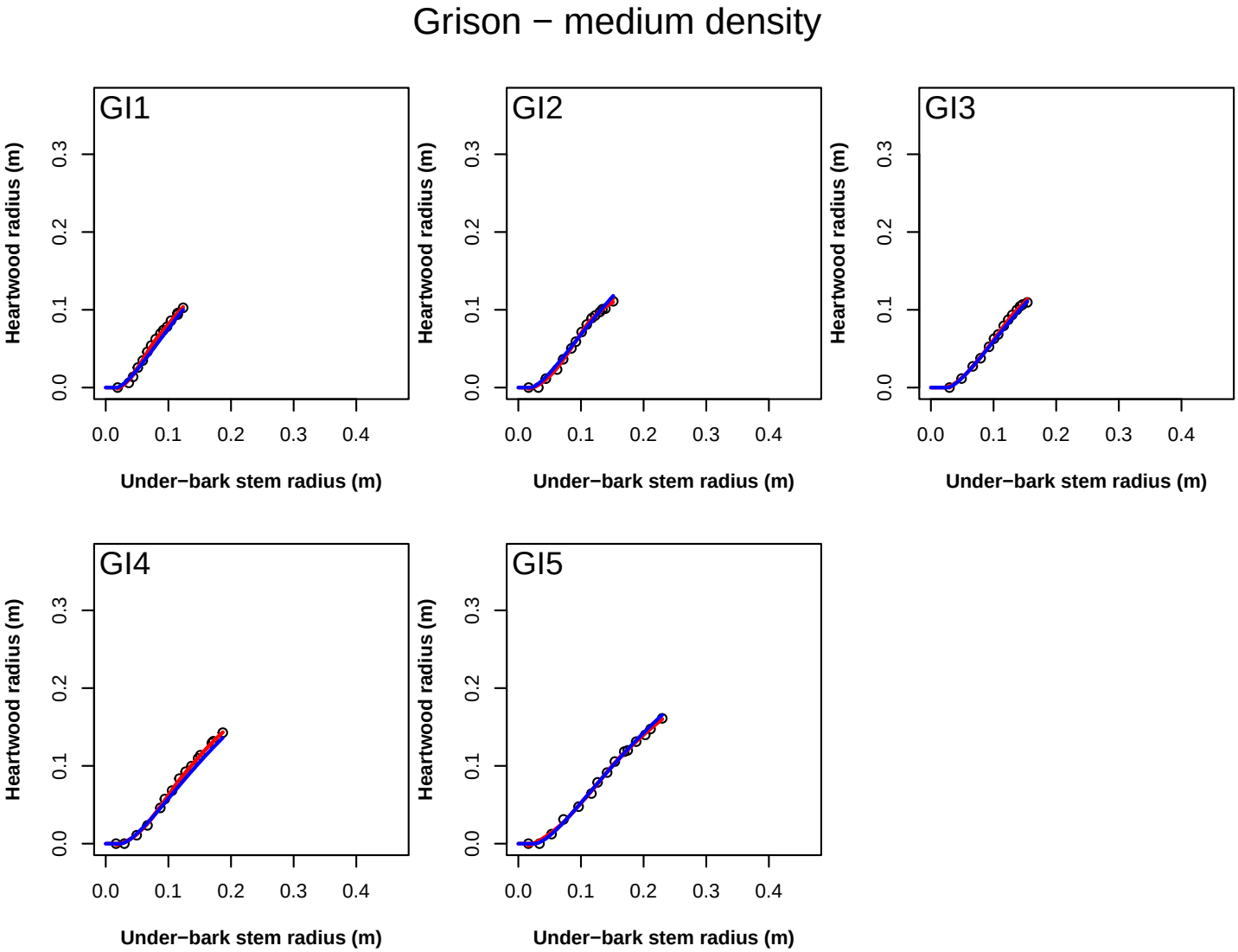

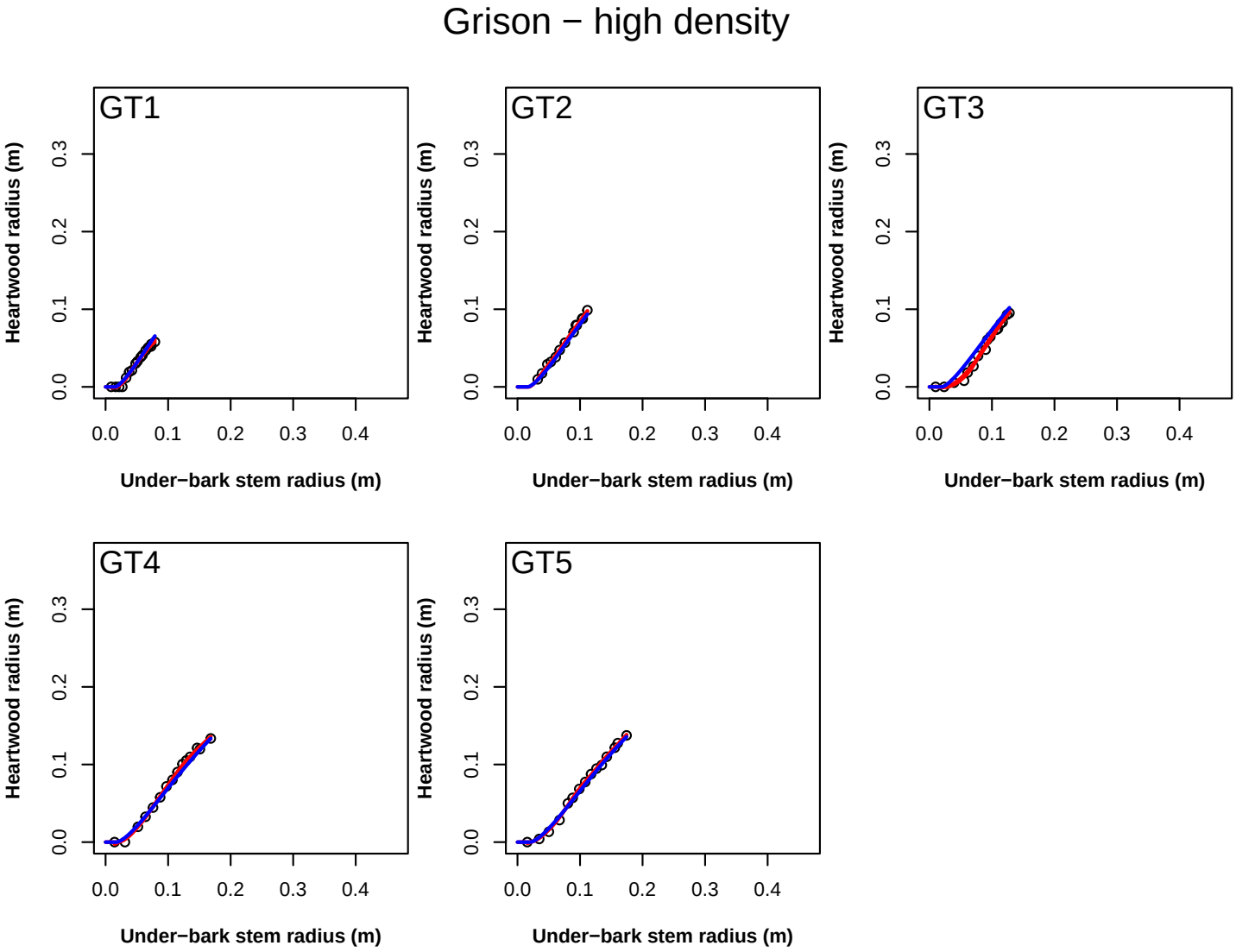

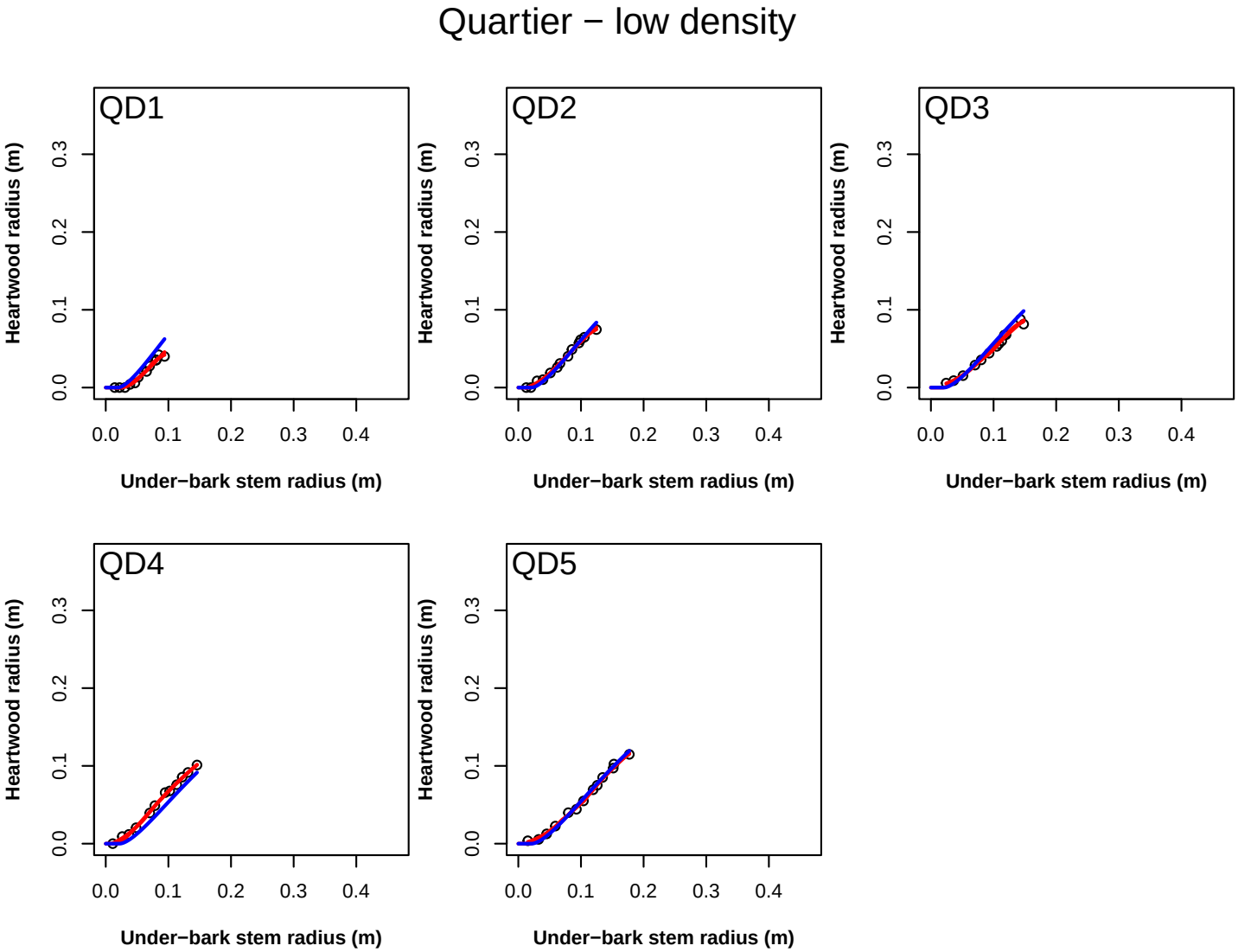

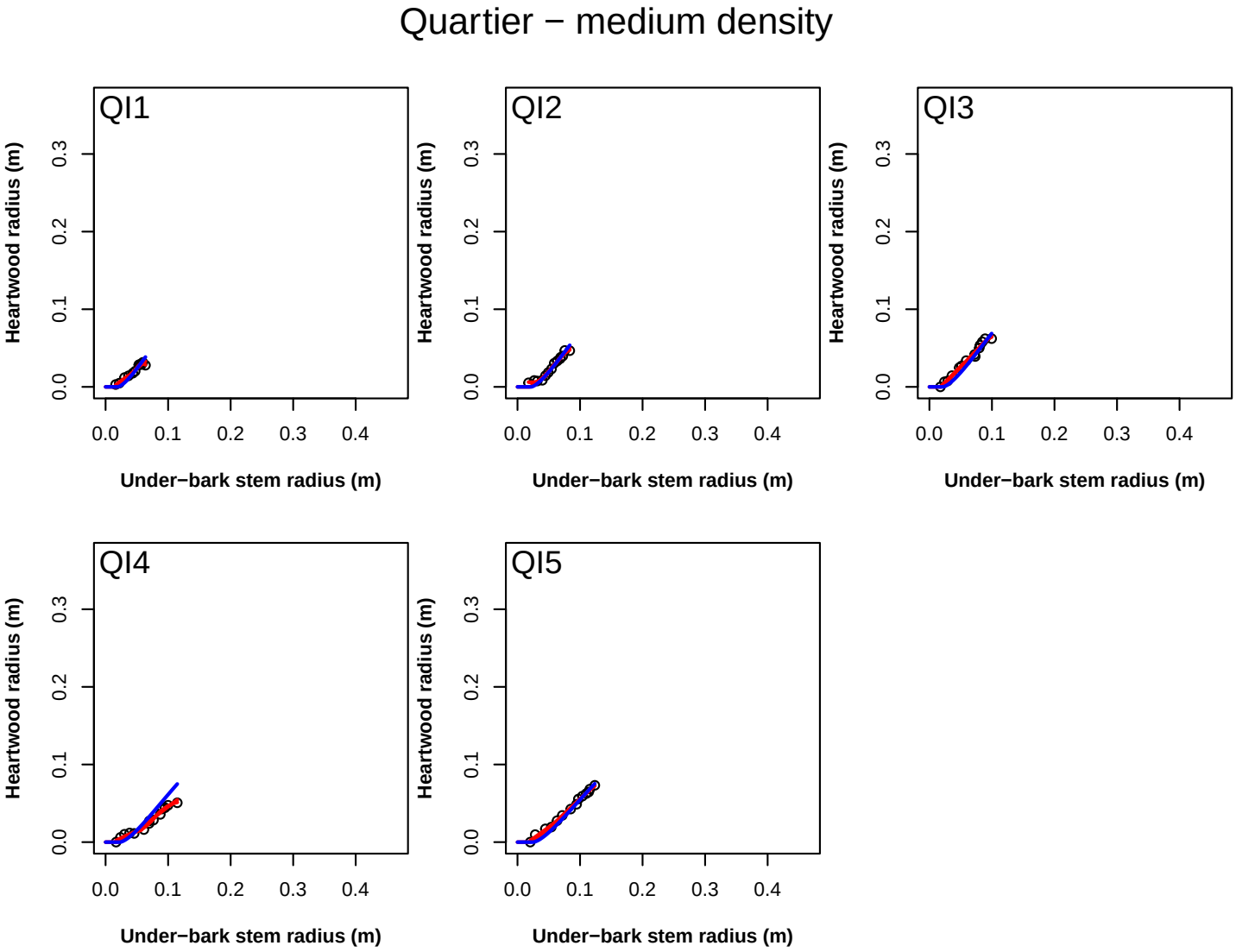

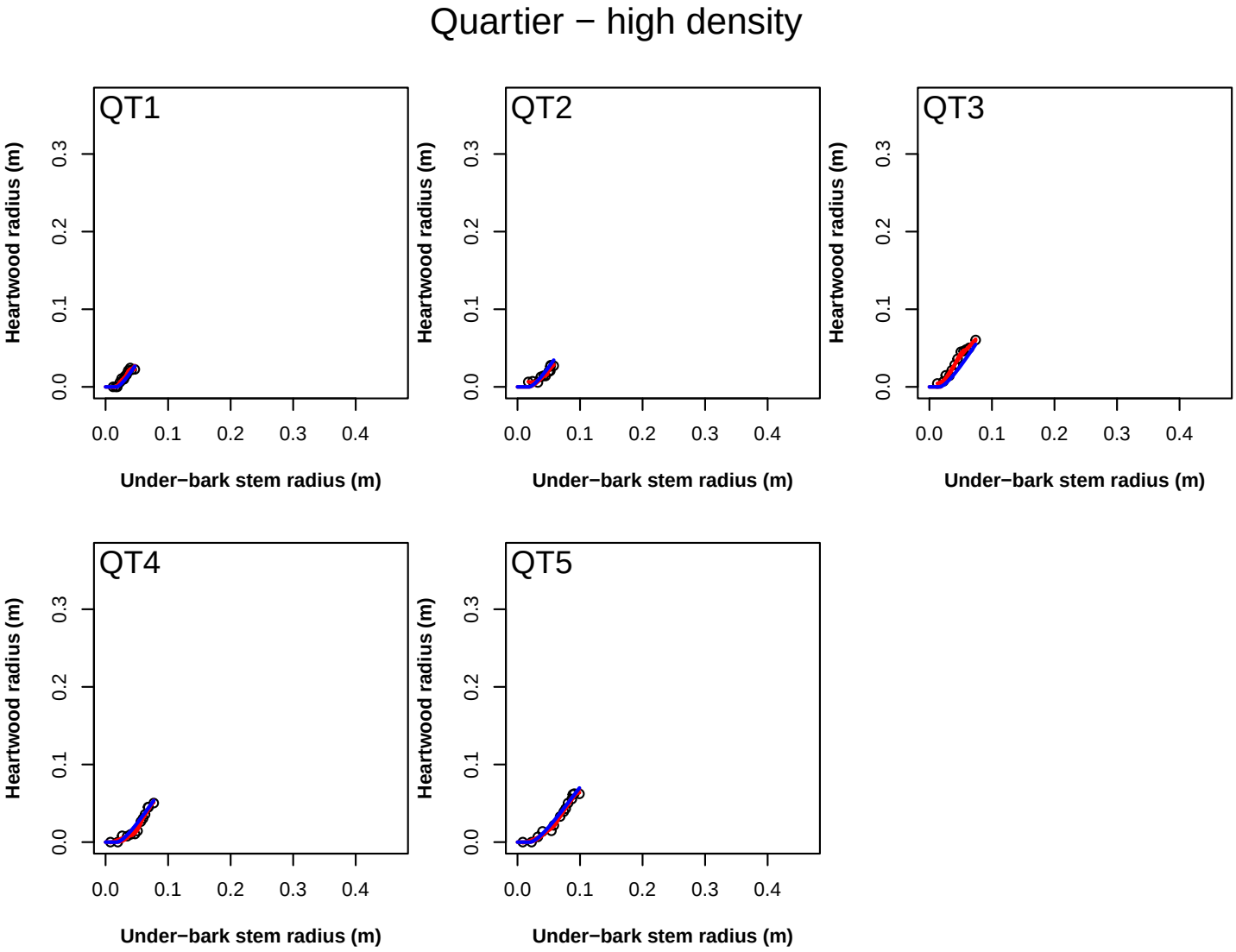

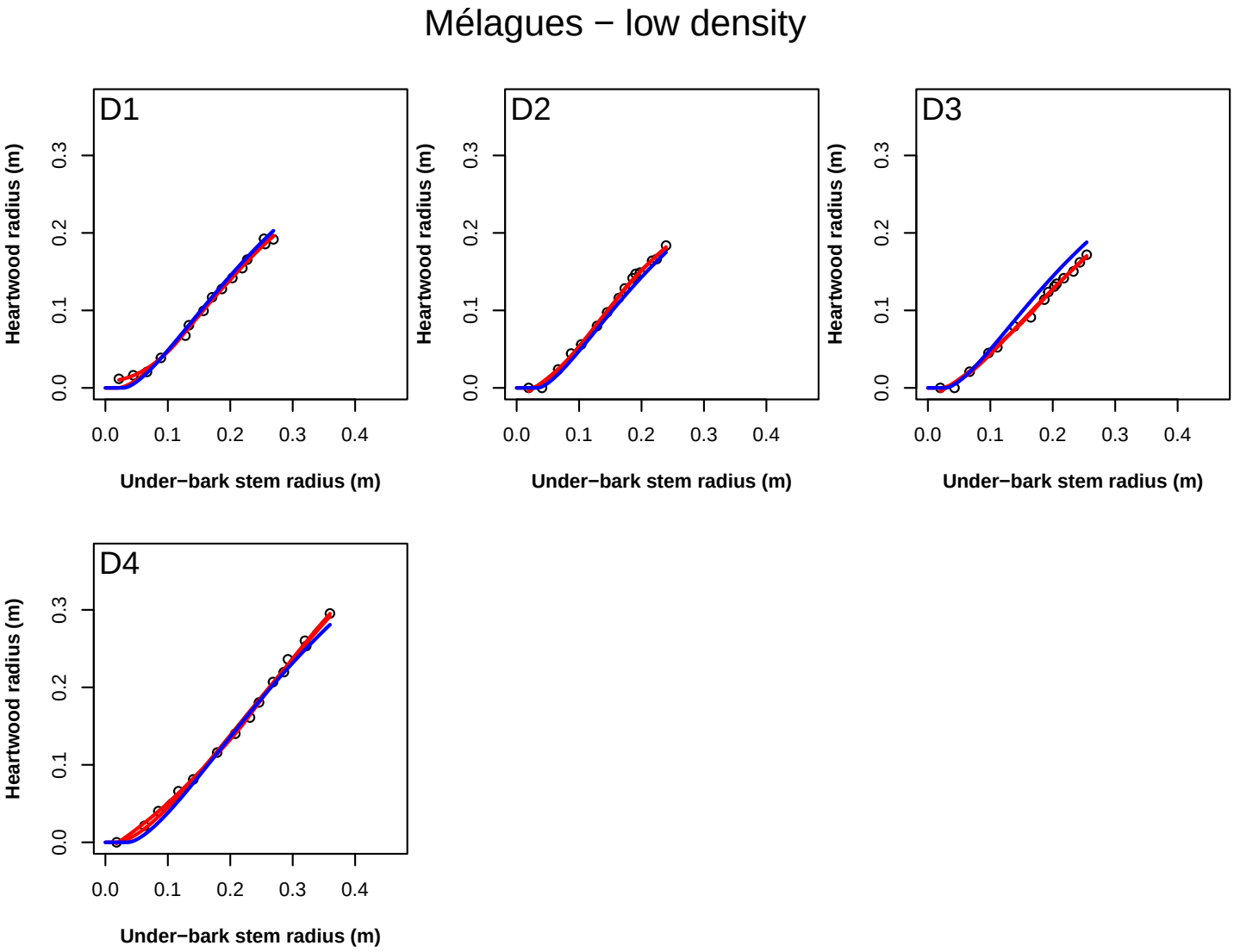

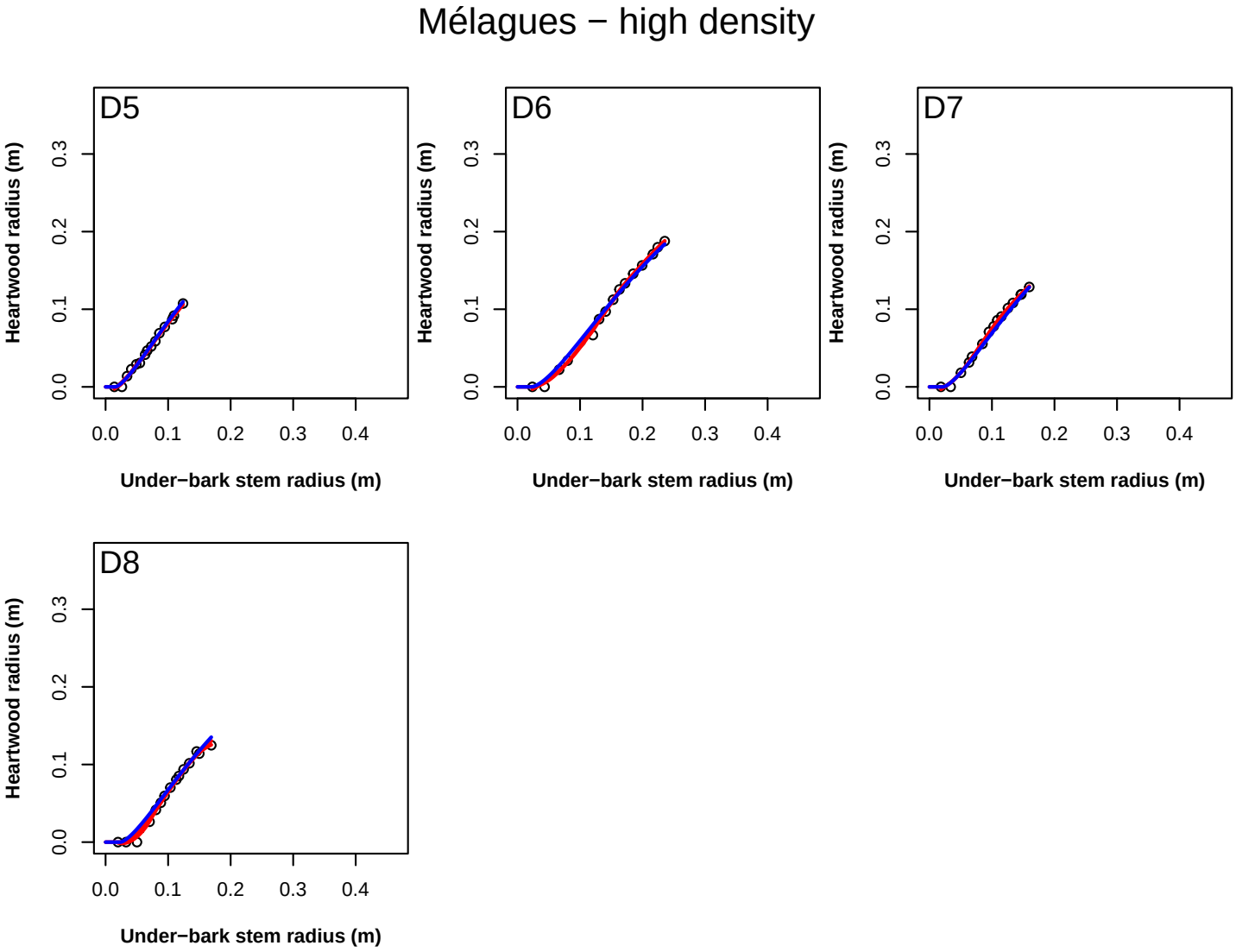

APPENDIX A10

Step-by-step construction of the model

A10.1 Step #1: Construction of Model (A)

After studying the plots of the relationships between parameters and candidate variables with the `pairs` function (Fig. A10.1), we chose to model parameter a as a function of D_{BH} (Fig. A10.2 on the left) since the correlation was the highest with 0.82. Then, the mixed model was fitted again after integrating this relationship between a and D_{BH} into the equation and the relationships between the parameters and candidate variables were again studied. This time the most interesting relationship was between parameter b and D_{BH} (Fig. A10.2 on the right). This new relationship was integrated into the equation to give Model (A). At each step we verified that the AIC has been reduced.

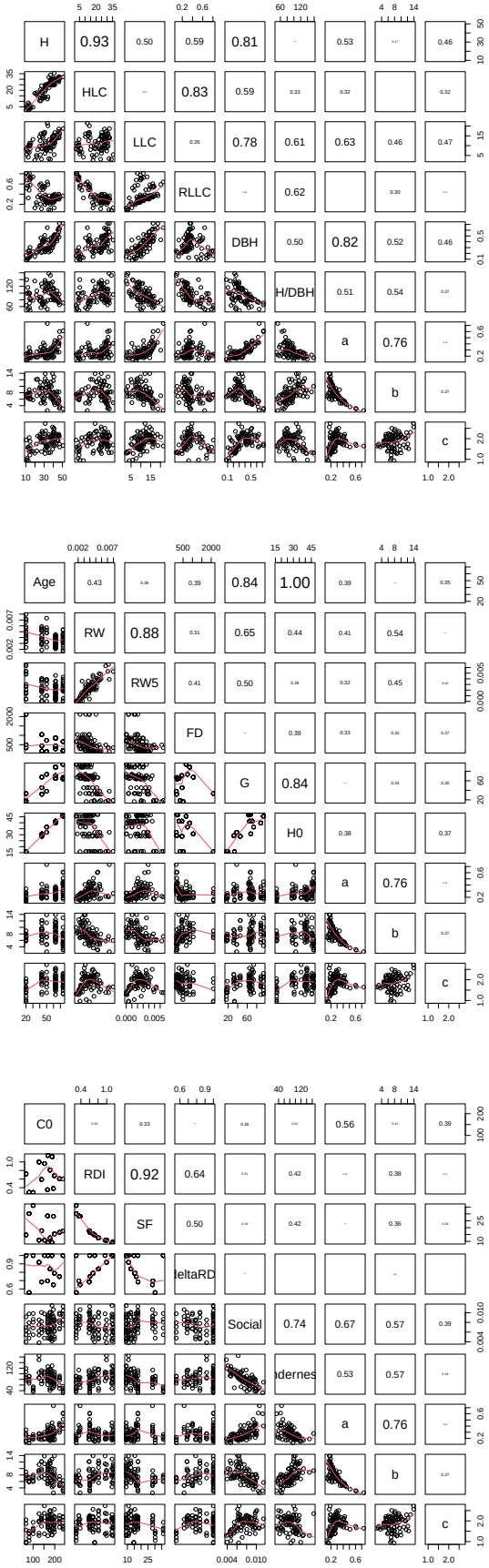

Figure A10.1: Relationships between the parameters of the mixed-effect model corresponding to Equation 1 and the candidate variables.

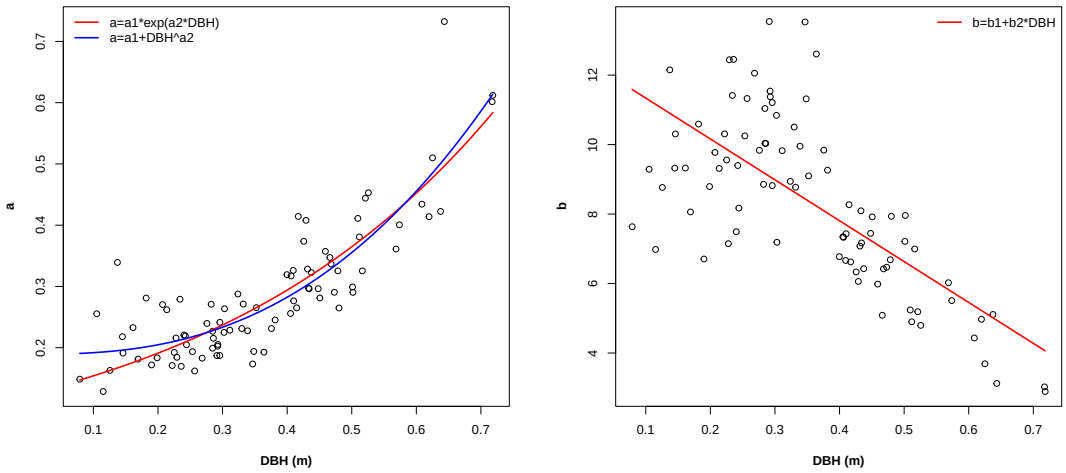

Figure A10.2: Relationships selected between parameters a and b on one side and the respective candidate variables on the other side for the construction of the Model (A).

A10.2 Step #2: Construction of Model (B)

We sought to further refine the model by adding new variables. At this stage, adding variables does not drastically improve the model but it allows trends to be highlighted and certain mechanisms to be understood. The new relationship given in Fig. A10.3 was integrated into the equation to give Model (B) and so the AIC has been further reduced.

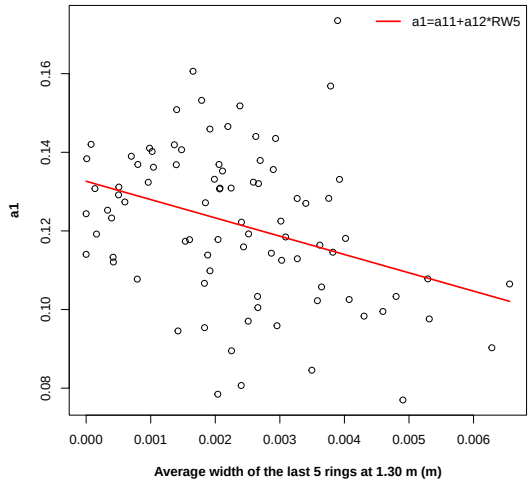

Figure A10.3: Relationship selected between the previous parameter $a1$ (as defined in Fig. A10.2 on the left) and the candidate variable RW_5 for the construction of the Model (B).

A10.3 Step #3: Construction of Model (C)

We continue the process by looking for the next variable of interest. The new relationship given in Fig. A10.4 was integrated into the equation to give Model (C) and so the AIC has been further reduced.

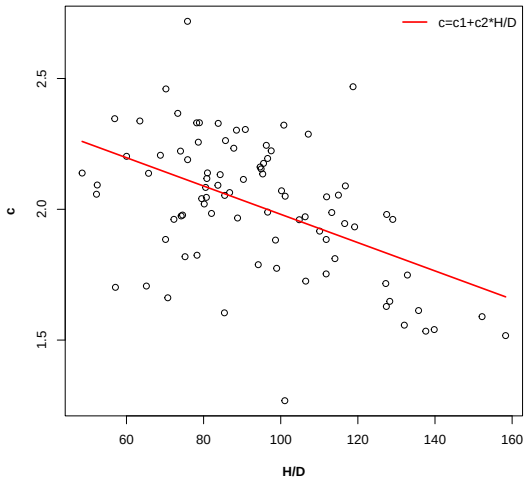

Figure A10.4: Relationship selected between parameter c and the candidate variable H/D_{BH} for the construction of the Model (C).

A10.4 Step #4: Construction of Model (D)

This last step enabled us to obtain the Model (D).

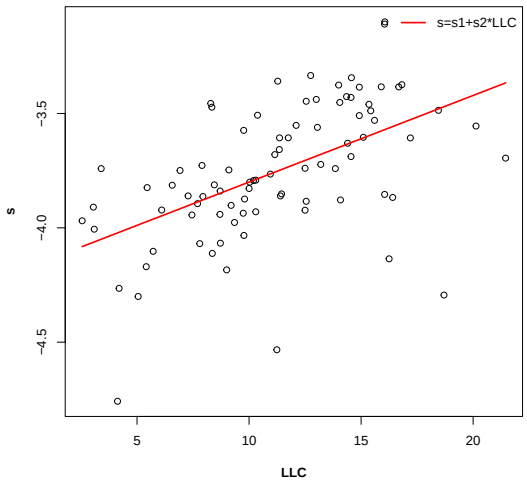

Figure A10.5: Relationship selected between parameter s and the candidate variable L_{LC} for the construction of the Model (D).

APPENDIX A11

Longitudinal variation in sapwood surface and sapwood width between 1.30 m and the base of the crown for the trees in the calibration dataset

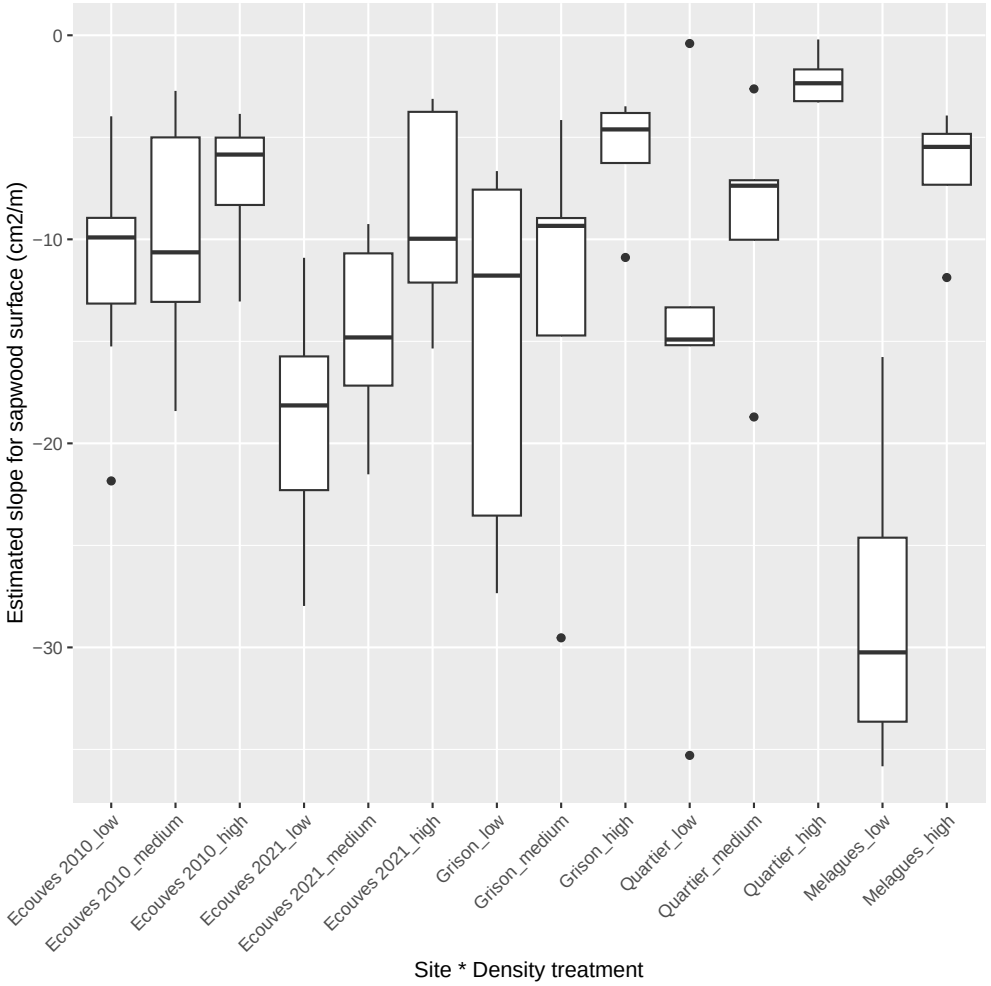

Figure A11.1: Boxplots illustrating the variability of estimated slopes for variations in sapwood surface between 1.30 m and the base of the crown by site and density treatment.

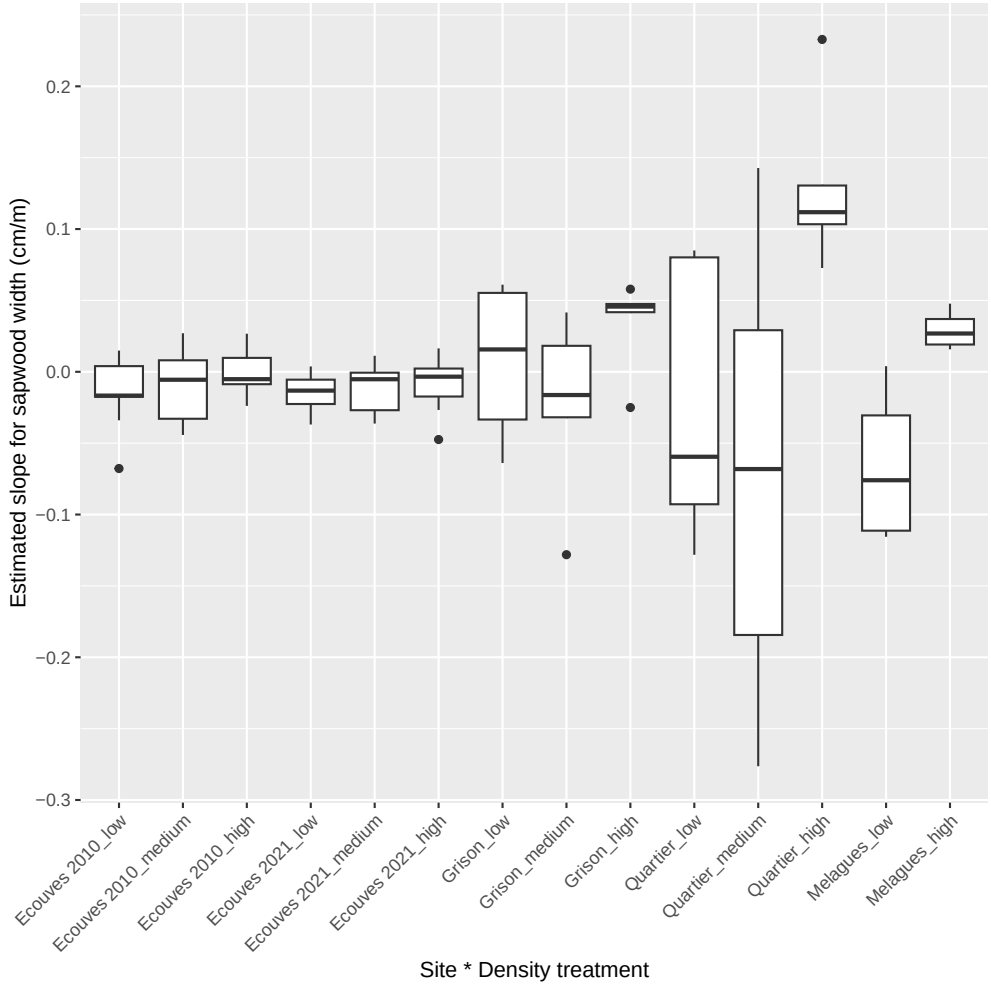

Figure A11.2: Boxplots illustrating the variability of estimated slopes for variations in sapwood width between 1.30 m and the base of the crown by site and density treatment.

APPENDIX A12

Validation on an independent dataset

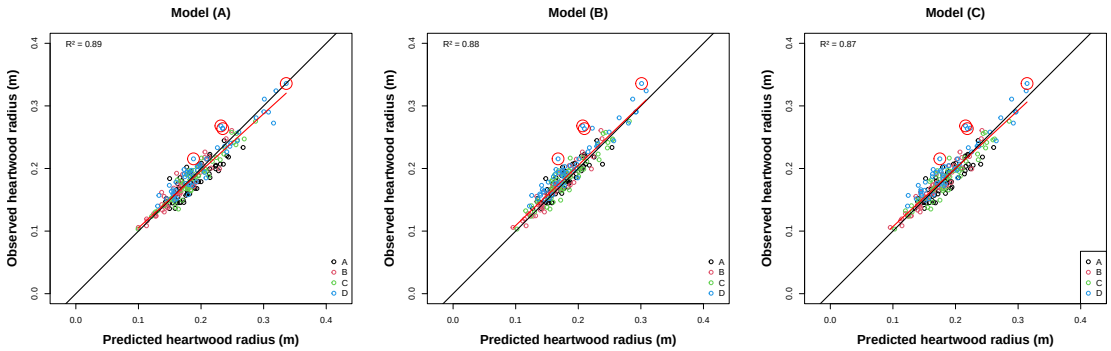

Figure A12.1: Observed values as a function of predicted values for the modelled heartwood radius. Models (A), (B) and (C) were applied to predict heartwood radius at four heights for each tree in the validation dataset. Consequently, one point represents one height level for a given tree. The $y = x$ line is shown in black and the linear regression of the scatter plot in red. The points circled in red represent the largest tree in the dataset ($D_{BH} = 0.81$ m) which is outside the validity limit of the model.

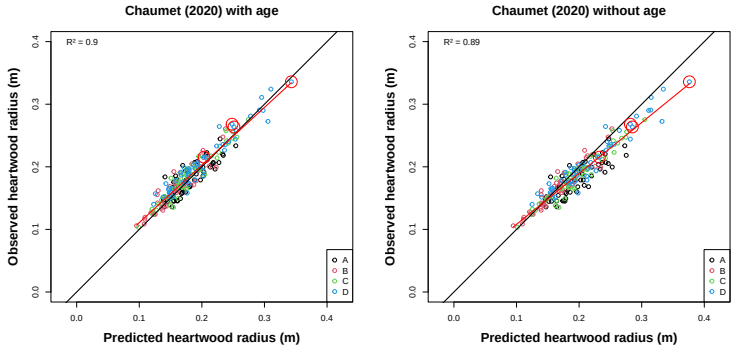

Figure A12.2: Observed values as a function of predicted values for the modelled heartwood radius. Models from Chaumet (2020b) (with and without age) were applied to predict heartwood radius at four heights for each tree in the validation dataset. Consequently, one point represents one height level for a given tree. The $y = x$ line is shown in black and the linear regression of the scatter plot in red. The points circled in red represent the largest tree in the dataset ($D_{BH} = 0.81$ m) which is outside the validity limit of the model.

APPENDIX A13

Effect of variations in input variables on the heartwood radius predicted by Models (C) and (D)

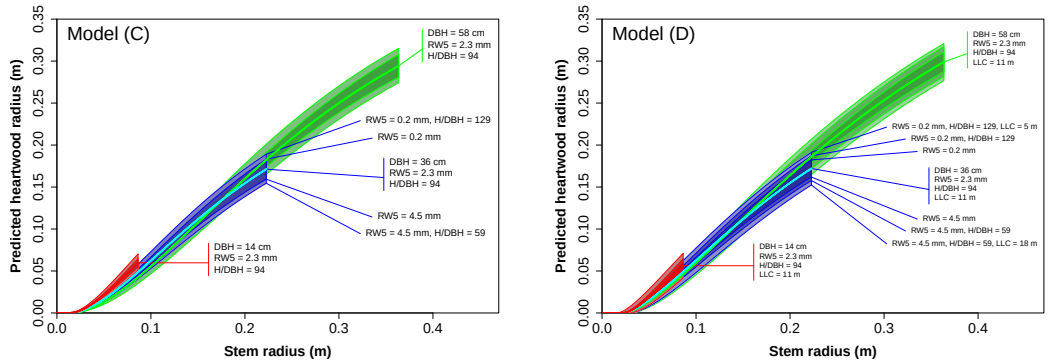

Figure A13.1: Graphs showing the effect of variations in input variables on the heartwood radius predicted by Models (C) and (D). The range of variation of each variable was set to the mean value ± 1.5 times the standard deviation. The mean values of D_{BH}, RW_5, H/D_{BH} and LLC measured on the calibration dataset were respectively: 36 cm, 2.3 mm, 94 and 11 m. The maximal disc radius (at ground level) was estimated by 1.25 times half of DBH.

APPENDIX A14

Model (C) input variables for SimCop simulated data as a function of diameter class at 1.30 m

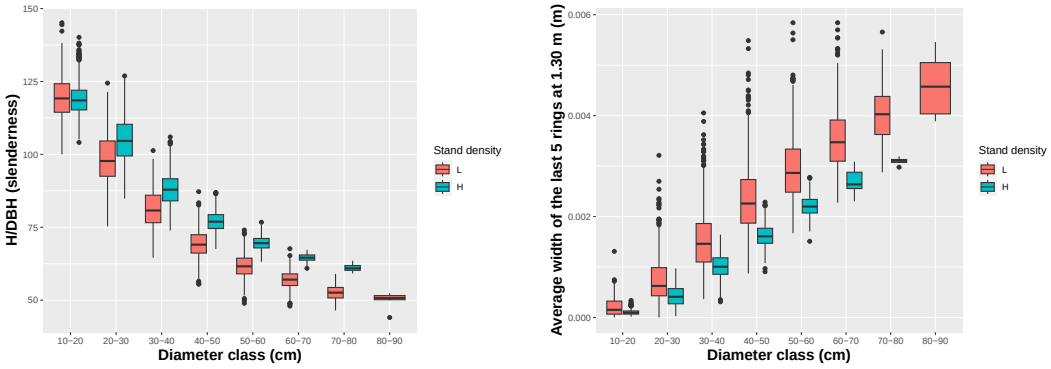

Figure A14.1: Variables H/D_{BH} (on the left) and average width of the last five rings, RW_5 (on the right) as a function of diameter class at 1.30 m for the two simulated scenarios.

APPENDIX A15

Determination of the sapwood/heartwood boundary

Figure A15.1 shows that the sapwood measured by colour difference is wider than the sapwood measured by X-ray scanner (i.e., water content, as the scans were performed in fresh state). These results are consistent with Rust (1999) findings on Scots pine, showing an additional sapwood zone for the staining method because the zone in question no longer conducts (i.e., it is less moist and therefore classified as heartwood by the X-ray scanner method) but is still chemically unaltered (i.e., it has not yet undergone duraminisation and is therefore classified as sapwood by the staining method). We can see that when plotting the line y = x, our points are close to this line but shifted upwards. This allows us to conclude that the methods are broadly equivalent. We observe a systematic average bias of 4.32 mm for the width of sapwood and therefore also for the radius of the heartwood. The surface area seems to give better results, but the scale is not the same, and for a given sapwood area at different heights in the stem, we do not have the same sapwood width since the diameter varies with height. The same sapwood area corresponds to a smaller width at the bottom than at the top of the stem.

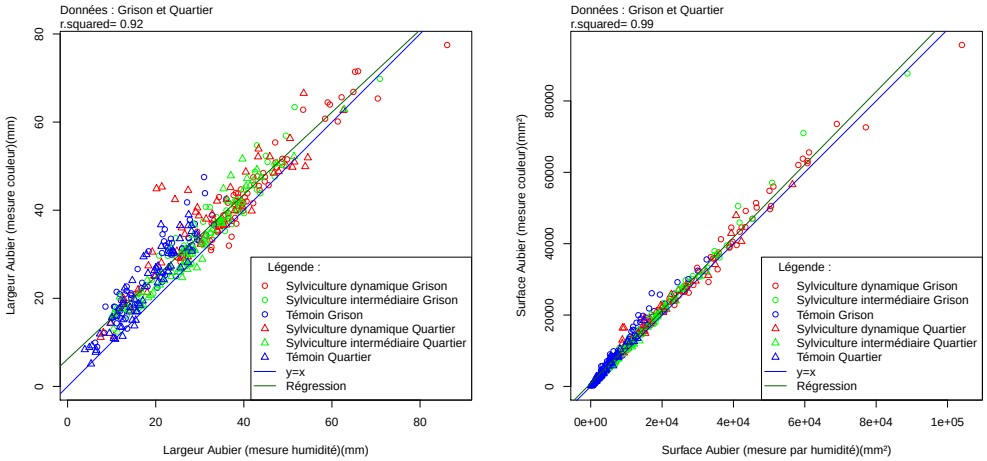

Figure A15.1: Relationship between sapwood width measured by colour (y-axis) and moisture content (X-ray scanner; x-axis) (on the left) and relationship between sapwood area measured by colour (y-axis) and moisture content (x-axis) (on the right).

APPENDIX A16

Behaviour of Model (A) when it is used in extrapolation for D_{BH} values to predict the amount of heartwood at 1.30 m

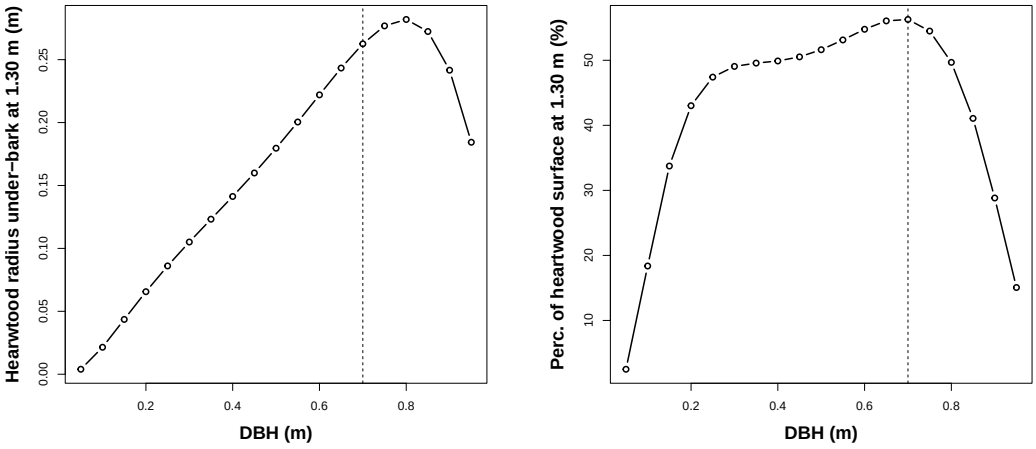

Figure A16.1: Heartwood radius under-bark (on the left) and percentage of heartwood surface (on the right) at 1.30 m as predicted by Model (A) as a function of D_{BH}. We assumed that the proportion of bark in surface at 1.30 m was 15% in order to estimate a bark thickness dependent on the D_{BH}. Here from point to point both the D_{BH} and the under-bark radius of the stem section at 1.30 m change. But the observed decrease can only be due to the effect of the D_{BH}, because when the trunk section increases, the heartwood radius can only increase. The dotted vertical line corresponds to a D_{BH} of 70 cm, which indicates approximately the limit of validity of the model in relation to the calibration data used to build it. A D_{BH} of up to 75 cm is considered reasonable, but not beyond.